(5) Thesis

Theory of the alkali-metal chemisorption on metal surfaces

(金属表面上のアルカリ原子吸着の理論)

石田 浩

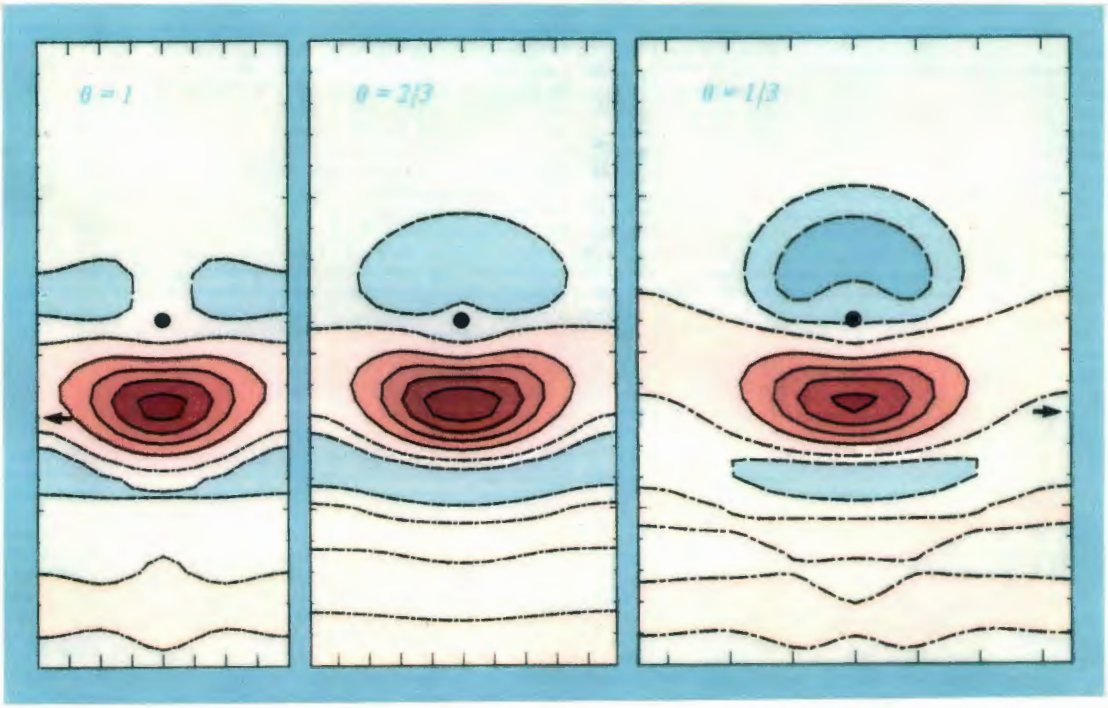

Electron charge redistribution caused by alkali-metal adsorped on a jellium metal. The increase and decrease of electron density are displayed with sepia and blue colors, respectively. See the text for detail.

Thesis

Theory of the alkali-metal chemisorption on metal surfaces

by

H. Ishida

Institute for Solid State Physics

University of Tokyo

1. Introduction

Alkali-metal adsorption on metal surfaces has been intensively studied for a long time because it provides a wide variety of electronic properties, which are attractive and important for those working not only in fundamental physics and chemistry but also in technological application. A pioneer work in this research field was done more than sixty years ago. In 1923, Kingdon and Langmuir [1] found that the electron emission rate of W, Ni and Mo filaments is greatly increased by the adsorption of a Cs layer. As the electron emission rate is governed by the work function of filaments, it follows that the work function is lowered by the Cs adsorption. Based on a classical picture - quantum mechanics was not developed at that time -, they explained this work function lowering as follows: since the ionization energy of Cs (I=3.89eV) is smaller than the work function of substrates (Φ~4.5eV), Cs adatoms become positive ions at the surface, and the resultant electric dipole layer formed by Cs^+ and its negative image charge lowers the potential barrier of an outgoing electron. Later, Langmuir and Kingdon [2] found that the electron emission rate of a cesiated W filament takes a maximum value at a certain coverage (θ) (fraction of the metal substrate covered with adatoms) and then decreases with further increasing θ, indicating the existence of a corresponding work function minimum. Taylor and Langmuir [3] studied the rate of atom, ion and electron emissions on a cesiated W surface as functions of θ and temperature in detail, and established that the work function takes a minimum value 1.7eV at about θ=0.7 before

reaching the full monolayer coverage (θ=1). After the pioneer works by Langmuir and his coworkers in 1920's and 1930's, the above-mentioned characteristic variation of the work function with θ, i.e., an initial rapid lowering proportional to θ which is follwed by a minimum and a subsequent small rise toward a saturation value, has been observed in vast numbers of chemisorption studies for all the alkali-metal adspecies (Li, Na, K, Rb and Cs) [4]. Because of the relevance to the cathode technology, most of the experiments performed so far employed transitiom metals as substrates, but exactly the same behaviour is observed on simple metals such as Be and Al [5-7]. It should be noted that this type of behaviour is observed even on semiconductor surfaces [8]. Fig.1 shows three examples of the measured work functions as a function of θ for Cs/Al(111) [7], Na/W(001) [9] and K/Cu(001) [10]. It is striking that three curves are similar to one another in spite of large difference in the electronic structures of the substrate metals: Al is a simple metal without d bands, while W and Cu have partially and completely filled d bands, respectively.

The work function lowering due to alkali-metal adatoms $\Delta\Phi(\theta)$ is evaluated as the dipole moment per an adatom $d(\theta)$ multiplied by $4\pi\theta$. Therefore the deviation of $\Delta\Phi(\theta)$ from its linear dependence on θ and the appearance of a maximum in $\Delta\Phi(\theta)$ indicate a rapid decrease of $d(\theta)$ with increasing θ. Topping [11] introduced a phenomenological parameter, Topping polarizability α_{eff} and assumed that the adatom dipole may be depolarized with increasing θ by the normal component of the electric field created

by the rest of adatoms ($\propto\theta^{3/2}$) as $d(\theta)=d(\theta=0)-\alpha_{eff}\theta^{3/2}$. However, the microscopic origin of α_{eff} was not discussed. In 1935, Gurney [12] presented the first quantum mechanical treatment of the alkali-metal chemisorption problem. He first pointed out that the alkali-metal valence s level (2s, 3s, 4s, 5s and 6s for Li, Na, K, Rb and Cs, respectively.) should suffer a lifetime broadening when an adatom approaches a substrate metal due to the mutual interaction, and thus even if the center of the s resonance is located high above the substrate Fermi level (E_F), its tail is partly occupied by electrons and the ionization of adatoms may not be complete. Provided that it is correct that alkali-metal adatoms are adsorbed essentially as positive ions and the dipole is formed by the positive ions and their negative images, the decrease of $d(\theta)$ may be interpreted as indicating a smaller adatom ionicity or neutralization of adatoms with increasing θ. Gurney gave a plausible explanation of the neutralization of adatoms with increasing θ by invoking a downward shift of the s resonance which may be caused by the lowering of the adatom potential relative to the substrate E_F due to the dipole fields of the other adatoms. The neutralization mechanism of alkali-metal adatoms originally proposed by Gurney [12] is schematically shown in Fig.2 It is proposed by Muscat and Newns [13] that the polarization of adatoms by the mixing of valence s and p_z (the z axis is the surface normal which points toward the vacuum region.) states should also contribute to Topping's α_{eff}, and developped a simplified model which incorporates both the downward shift of valence states and intraatomic polarization of adatoms. Since the work of Gurney

[12], the ionic-neutral (metallic) change of alkali-metal adatoms with increasing θ has been widely believed for more than half a century as a basic concept in the alkali-metal chemisorption problem for experimentalists when they interpret their data and for theorists when they set up simplified models.

Alkali-metal overlayers on metal surfaces once attracted a great deal of attention in connection with the insulator-metal transition of the two dimensional system. In 1969, MacRae *et al.* [14] studied the Cs adsorption on W(001) by the low energy electron diffraction (LEED) technique and electron energy loss spectroscopy (EELS). They discovered that an intense loss peak with energy ~2eV rapidly grows when θ exceeds a value corresponding to the work function minimum. The peak was interpreted as due to a plasmon localized in the Cs layer (overlayer plasmon) which appears at a high θ limit when the overlayer is metallized by the increased Cs-Cs interaction. Afterward, similar loss peaks were observed for a number of alkali-metal/metal surfaces at higher θ [15]. The loss energies were found to converge to the surface plasmon frequency of the bulk alkali-metals when adatoms form a multilayer film. Jostell [16] measured the plasmon dispersion, i.e., the two dimensional wave vector parallel to surface versus the loss energy, for Na, K and Rb monolayers on Ni(001). The measured plasmon energy starts from a finite value at the zero wave vector and has positive or negative linear dependence on the wave vector. Since the energy dispersion of the intraband plasmon characteristic of two dimensional metallic bands converges to zero in the long wavelength limit

[17], Jostell's work [16] discarded the direct relation between the appearance of a loss peak and overlayer metallization. In order to study the response of alkali-metal monolayers quantum mechanically, Newns [18] introduced a "box" model, in which electrons are assumed to move freely parallel to the layer while they are confined in the perpendicular direction within a region equal to adatom diameters by an infinite barrier potential on both sides. He pointed out that interband transitions from the partially filled lowest s-like band to the unoccupied p_z-like band become collective by their polarization field and thus may be associated with the loss peak. Nakayama *et al.* [19] developed a general theory of the interband overlayer plasmon and showed that its dispersion is quite sensitive to the symmetry of electron wave functions relevant to the excitation. However, it was not clarified why the interband overlayer plasmon becomes much more intensive than the intraband mode which is characteristic of two dimensional metals. Ishida and Tsukada [20] calculated the electron energy loss function of the alkali-metal monolayers on metal substrates by combining a tight-binding thin slab model with the random phase approximation (RPA). They showed that the intensity of the intraband overlayer plasmon becomes much weaker by the orbital hybridization between the adatom and substrate. The physical interpretation is as follows: when the overlayer and substrate states extend into the other side by the hybridization effect, charge densities of the overlayer plasmons are directly screened by the substrate surface plasmon; the monopole charge of the intraband mode is efficiently screened by the surface plasmon

which also has monopole character, whereas the dipole charge of the interband mode is hardly screened by the surface plasmon charge even if there is overlapping and its intensity remains essentially unchanged. Recently, Cousty *et al.* [9] investigated θ dependence of the energy of the alkali-metal induced loss peak for Na, K, Rb and Cs layers on W(001). The loss energy became appreciably larger with increasing θ for Na, while it remained almost constant for Cs. They argued that with the increasing adatom size the excitation character of the loss peak changes from collective to individual one and thus the origin of the peak for Cs may be individual excitations from Cs 6s to $6p_z$ states. Similar suggestion was also given by Hohlfeld *et al.* [7] for Cs/Al(111). All the theories of the overlayer plasmon advanced so far are phenomenoligocal ones which can not deal with difference in the electronic structure among different kinds of adatoms. None of them can answer to the above question on the excitation character at present.

Along with the work function lowering and spectroscopic quantities such as electron energy loss spectra, photoemission (inverse photoemission) spectra and core level shift, the structure of the alkali-metal overlayer has been extensively studied by LEED technique. With increasing θ, a sequence of various superstructures are observed in many alkali-metal adsorption systems. At lower θ, alkali-metal adatoms sit on an energetically favorable site on the substrate and form well-ordered structures at several coverages. For example, Cs adatoms form ordered $(\sqrt{3}\times\sqrt{3})R30^\circ$ and 2x2 structures at θ=1/3

and 1/4, respectively on Al(111) [7]. On the other hand, in most cases, the overlayer becomes a non-registered hexagonal lattice in high θ limit due to the increased cohesive interaction among adatoms. Aruga *et al.* [21] studied the structure of K overlayers on Cu(001) at a normal temperature and observed a disordered gas phase at low θ, two commensurate ordered structures at higher θ and an incommensurate hexagonal lattice in high θ limit. In the incommensurate phase, rotational epitaxy predicted for physisorbed rare-gas monolayers [22] was discovered, where the orientation angle between the substrate and overlayer lattices increased from 3.3 to 6.0 degrees with the contraction of the K interatomic distance. Besold *et al.* [23] studied the Cs layers on Rh(001) at a lower temperature $T\sim120K$ and observed several ordered structures in a gas phase at low θ. Rotational epitaxy was also observed in their case. On the theoretical side, the phase diagram of the overlayer structure has been studied by Monte Carlo calculations, where adatoms are approximated by classical dipoles which interact with one another through a r^{-3} repulsive potential [23,24]. Because of the long-range nature of the potential, the cut-off length of the potential often becomes a trouble in the actual calculation. Moreover, the model is not applicable at higher θ where direct interaction among adatoms due to orbital overlappings dominates the dipole-dipole interaction which diminishes with increasing θ by the depolarization of the adatom dipole. According to Aruga *et al.* [22], the structure transition at high θ is explained qualitatively by the competition of the two interactions, i.e., adatom-adatom and atatom-substrate ones:

the substrate potential stabilizes commensurate structures, while the cohesive interaction between adatoms favors the incommensurate hexagonal phase; the commensurate-incommensurate transition occurs when the latter exceeds the former. From a viewpoint of chemical bonding, it is expected that the strengthening of the adatom-adatom bond leads to the weaker adatom-substrate bond, since part of the bond charge between the adatom and substrate may move to the adatom-adatom bond. Experimentally, the decrease of the atomic binding energy with increasing θ had been already observed for Cs/W in the pioneer work of Taylor and Langmuir [3]: the measured desorption energy of Cs at low θ limit, 2.83eV decreased to 1.77eV when the Cs monolayer is completed.

Alkali-metal covered transition metal surfaces serve not only as the efficient electron emitters but also as promotors of catalytic reactions. It has been known for a long time that small amount of alkali-metal adatoms drastically changes reactivity of coadsorbed molecules and atoms. From the middle of 1970's, experimental studies making use of modern surface science techniques under ultra high vacuum condition have been intended for this reasearch area [25]. For example, Ertl *et al.* [26] found that dessociation rate of N_2 on Fe(001) is enhanced by two orders of magnitude by the dosage of 0.1 monolayer K atoms. Similarly, the presence of K strongly affects the adsorption energy and stretching frequency of coadsorbed CO on Fe and Pt surfaces [27,28]. These bahaviours also depend on the coverage of alkali-metal atoms. At low θ, the addition of H_2 increases the work function of cesiated Mo(110), while it lowers at higher θ

[29]. Theoretical approach on these problems remains still within the level of qualitative discussions. Feibelman and Hamann [30] argued that increase in the density of states (DOS) in surface regions by the adsorption of alklai-metal adatoms may enhance the interaction of the substrate and coadspecies. It is proposed by Lang *et al.* [31] that the local dipole field around alkali-metal adatoms will suppress or promote the charge transfer between the substrate metal and coadsorbed molecules and thus changing the reactivity of admolecules.

In the above, I have briefly reviewed highlights in the research activity of alkali-metal adsorption on metal surfaces from its pioneer work in 1920's to recent developments. In order to establish systematic and comprehensive understanding of various phenomena on alkali-metal/metal surfaces and especially of their θ dependence, it must be indispensable in the first step to clarify the electronic structure of adatoms and nature of chemical bonding between the substrate and adatom as a function of θ. As stated before, a simple picture originally proposed by Gurney [12], i.e., ionic-neutral (metallic) change of the overlayer with increasing θ by the downward shift of the s resonance, has been widely accepted and further developed to date, since it is intuitively appealing and gives a way to theorists to advance tractable models. Recently, there appear some works which cast a doubt upon the validity of this picture. Woratschek *et al.* [32] studied the K 4s resonance on Cu(110) by metastable-He deexcitation spectroscopy (MDS). The measured intensity of the H^* deexcitation spectra which is directly associated with the occupation of K 4s

level went up almost linearly with increasing θ up to 1/3 monolayer coverage, whereas the work function change $\Delta\Phi(\theta)$ started to deviate from its linear dependence on θ even at 1/10 monolayer coverage indicating a substantial decrease of $d(\theta)$. This observation suggests that the magnitude of the induced dipole is not directly related to ionicity of adatoms. Kono [33] measured the binding energy of the Cs 5p core orbital on Si(001) with the ultraviolet photoemission spectroscopy (UPS) as a function of Cs coverage. In spite of a large dipole field due to Cs adatoms, the measured Cs 5p level hardly shifted with θ, which implied that the potential lowering at adatom sites, which insures the downward shift of the valence s level, might be absent in real systems. On the theoretical side, Wimmer *et al.* [34] performed a first-principles electronic structure calculation of the cesiated W(001) surface within the local density functional (LDF) theory by the full-potential linearized augmented plane wave (FLAPW) method and discussed the mechanism of the work function lowering. It was shown that Cs-induced changes in the charge density were confined to regions outside surface W atoms, and particularly, build-up of charge responsible for the dipole occured in the interface of the Cs and W layers rather than around W atoms. It was found that energies of the W 5*d* surface states were lowered by 1eV due to hybridization with Cs 6s states. From these facts, it was concluded that origin of the induced dipole may be polarization of Cs atoms rather than ionization of Cs by the donation of 6s electrons onto W atoms: weakly bound and extended Cs 6s electrons hybridize strongly with localized W 5*d* electrons,

forming a *covalent* W-Cs bond which leads to an increase of the electron density in the interface and decrease in the vacuum side of a Cs. There are some weak points in their argument in criticizing the ionic adsorption picture. Firstly, the calculation was done only at a high θ limit assuming a c(2x2) structure (θ=1/2 in units of W layers) for Cs. In fact, even with Gurney's picture, the adatom-substrate bond should become covalent at higher θ when the center of the s resonence is shifted downward and located near the substrate E_F. Wimmer *et al.* felt necessity of further calculations at a p(2x2) coverage (θ=1/4) where the work function becomes minimum [35], but could not perform it because of the limit of computer capacity. Secondly, even if the Cs 6s resonance is located high above E_F, the positive Cs ion cores should be screened by metallic W electrons. In that case, the screening would be completed essentially outside the W surface, since the image plane of metals, i.e., center of gravity of the screening charge with respect to an external field is located by ~1Å outside the surface atoms [36]. Therefore it is of danger to infer the nature of a chemical bond solely from the charge resitribution.

The purpose of the present paper is to resolve the above-mentioned controvertial subject and reestablish a correct picture for the alkali-metal adsorption on metal surfaces. I will perform first-principles electronic structure calculations of alkali-metal covered metal surfaces with θ ranging from a high θ limit to a much lower one and clarify the nature of adatom-substrate bonding, adatom valence states and origin of the adatom

dipole as a function of θ. Electronic structure calculations of alkali-metal overlayers on metal and semiconductor surfaces have been restricted to date at high θ limit because the two dimensional periodicity of substrates hinders continuous change of θ and also the amount of labor required increases rapidly with decreasing θ [34,37-39]. In order to evade mainly the former difficulty, I first employ "jellium" as a substrate, where the discrete ion cores of the substrate is smeared out into a uniform positive background charge. By the use of jellium, θ as well as the structure of overlayers is completely at one's disposal. As stated before, various phenomena observed on alkali-metal covered metal surfaces are independent of detailed characters of the substrate such as the number of *d* electrons and geometry of surface atoms. Therefore the choice of the jellium as the substrate seems quite acceptable in order to extract the essence of the phenomena. One justification of approximating transition metal substrates by the jellium is sometimes explained in such a way that spacially extended orbitals of alkali-metal valence states may not interact strongly with localized *d* orbitals of substrates and the interaction may be dominated by *s* and *p* parts of the substrate states. There is a restriction in the lowest value of θ achieved in the present calculational scheme because of the limit of computer capacity. Nevertheless, chemisorption of a single alkali-metal atom on jellium surfaces was studied by Lang and Williams [40], which corresponds to the limit of $\theta \rightarrow 0$ in the present calculation. By comparing the calculated result with theirs, it is possible to check the accuracy of the present calculation at

low θ. Lang [41] once studied the alkali-metal adsorption on metal surfaces using the two step jellium model. In his model, not only the substrate but also the overlayer was modeled by a thin jellium slab whose density is proportinal to θ. However, as will be discussed later, the jellium approximation for the overlayer is entirely unphysical at lower θ and it is indispensable to keep discreteness of adatoms for the correct understanding of the adatom electronic structure. One drawback of approximating metal substrates by the jellium may exist in that it becomes somewhat ambiguous to examine the nature of chemical bonding between the adatom and substrate because of the lack of discrete atoms in the substrate. Therefore, in the next step, I retrieve discreteness of the substrate and clarify θ dependence of the electronic structure of alkali-metal adatoms, treating *both* the overlayer and substrate as discrete atoms. Al(001) is employed as the substrate. By virtue of the absence of localized *d* bands and owing to high symmetry, Al(001) is just fit for extending the calculation to a low θ regime. In this case, θ cannot be varied continuously and the calculations are done assuming three structures for the overlayers which correspond to θ=1/2, 1/4 and 1/8 in units of Al(001) monolayers. The result obtained in the present work is entirely contradictory with the widely accepted picture of Gurney [12]. No appreciable downward shift of alkali-metal valence states and θ dependence of the charge transfer to substrate states are found. On the contrary, it is shown that the adatom-substrate bond has strong *covalency* even at low θ. The adatom dipole should be interpreted as stemming from hybridization between the adatom

and substrate orbitals rather than ionization of adatoms in the whole θ regime. Consequently, oversimlified Gurney's picture which has been believed for more than half a century must be revised significantly.

The plan of the present paper is as follows. Before describing methods and results of the present calculation, I review in Section 2 theoretical models advanced so far for studiying the θ dependence of alkali-metal overlayers in some detail. One is Lang's two step jellium model [41] and its extended versions. Another approach utilizes the Newns-Anderson Hamiltonian [42,43] and incorporates the physical picture given by Gurney [12] in a quantitative way. This section is intended for disclosing unphysical or unreasonable assumptions involved in these phenomenological models and for making the reader recognize necessity of first-principles calculations which will be described in the subsequent Sections. Some general discussions of the adatom dipole moment are also given in this section, where the role of the covalent (off-diagonal) hybridization interaction of the substrate and adatom to the adatom dipole is emphasized. The present calculation is based on the local density approximation for exchange and correlation in the density functional theory, which is combined with the non-empirical norm-conserving pseudopotential. The detail of the calculational method and overlayer models are described in Section 3. Section 4 and 5 are the main parts of the present paper and devoted to the results and discussions of the present calculation. The results for the jellium and Al(001) substrates are presented in Section 4 and 5,

respectively. Finally, summary and conclusion are given in Section 6. Throughout the paper, the atomic units, m=1, e=1, $\hbar$=1 are used. The units of length and energy are 0.529Å and 27.2eV, respectively. At the end of this section, I comment that the present calculation is based on the first-principles and there are no adjustable parameters in it. The calculated results are exact within the calculational scheme. I hope the reader not to be preoccupied by Gurney's classical picture and to be openminded to accept the results and their interpretation presented in sebsequent sections.

2. Critical review of phenomenological models

This section is intended for reviewing two empirical theories which have been advanced to study alkali-metal overlayers on metal substrates and its θ dependence. The emphasis is laid on clarifying unphysical or unreliable assumptions as well as important effects ignored in them. Some general discussions of the induced dipole moment based on a simplified model will be also given in the latter half of this section for the sake of convenience in the later sections.

In 1971, Lang [41] presented a simplified model of the alkali-metal adsorption by extending the jellium calculation of metal surfaces by Lang and Kohn [44]. In his model, the alkali-metal ion cores were approximated by a uniform thin slab adsorbed on a substrate high-density jellium surface. The thickness of the slab was fixed to adatom diameters, whereas the increase in the number of ion cores was simulated by assuming the density of

the jellium slab to be proportional to θ. The rapid decrease of the work function at lower θ and subsequent appearance of a minimum was reproduced rather well by this "two-step jellium model". The essence of the model exists in taking the planar average of the adatom ion core potentials, by which the system is reduced essentially to one dimensional one and therefore numerical efforts required for the self-consistent calculation become independent of θ. The apparent success of the model as well as the great advantage in numerical calculations became impetus to the subsequent extention of the model. Serena *et al.* [45] changed not only the charge density but also the thickness of the jellium slab to adjust θ corresponding to the work function minimun to an experimental value. In order to examine the effect of the discrete lattice in the surface normal direction, Nicolaides and Andriotis [46] employed uniformly charged planes arrayed at interval of the lattice spacing instead of the jellium and studied the work function lowering. Serena and Garcia [47] studied the work function of the cesiated Al(111) using the empirical pseudopotential for Al and Cs ion cores. However, the ion core potentials were averaged parallel to the layer so as to make the calculation one dimensional one. Thus the work is nothing more than a minor refinement of Lang's model. Ning *et al.* [48] studied the cesiated W(001) treating the W substrate as discrete atoms while approximating the Cs layer by the jellium slab. The model requires a three dimensional calculation. But by virtue of the jellium approximation for Cs, the size of the unit cell becomes independent of θ and the numerical effort is greatly reduced.

The downward shift of the W surface states by cesiation predicted by Wimmer *et al.* [34] was again observed in their calculation, which apparently seemed to increase the credibility of the jellium approximation for the alkali-metal ion cores.

However, the success of the model in reproducing the rapid decrease of the work function does not necessarily mean that the physics involved in the model is correct, and the jellium approximation for the overlayer is completely meaningless at lower θ. To begin with, the idea of approximating the alkali-metal ion cores by the jellium is based on the observation that the *bulk* alkali-metal is one of the best examples in that the free-electron model works well. But one must recognize that the applicability of such a model is justified only when the orbital overlap between neighboring atoms is large enough to lead to a large valence band width. With decreasing θ, the overlayer just tends to be a set of isolated alkali-metal *atoms* with negligible interaction among them. In this limit, each electron is accommodated in the s orbital of an isolated ion core with binding energy 4-5eV. On the other hand, if the overlayer is represented by the jellium, or if the ion core potential is averaged over the plane direction, the atomic character of the alkali-metal atom is entirely lost and the binding energy of electrons tends to zero at low θ limit. In this case, it is not surprising that electrons in the overlayer flow to the substrate, forming a dipole layer which leads to the work function lowering. However, actually, the phenomenon which must be clarified by theory is the inducement of the dipole moment due to interaction of metal substrates with electrons with binding

energy 4-5eV, and *not* with those with *zero* binding energy. Therefore the apparent success of the model in explaining the work function lowering is not physically meaningfull. The unphysical nature of the model may be disclosed more clearly if one think of an experiment in which the substrate and adsorbate are interchanged, for instance, adsorption of Al atoms on a bulk alkali-metal surface. Since Al is also a good example of the free-electron metals, the jellium approximation for the Al overlayer would be no worse than for the alkali-metal overlayers. Then the model would again result in a rapid *decrease* of the work function at low Al θ. However, Al adatoms actually induces a negative dipole on the alkali-metal surfaces, which results in the *increase* of the work fuction [49]. Hence, the jellium model for the overlayer breaks down completely in this case. Eguiluz and Campbell [50] studied the electron energy loss function of the alkali-metal covered metal surfaces with the two-step jellium model. The calculated results failed in reproducing the observed alkali-metal induced energy loss peak for less than half monolayer coverage. This failure may reflect the absence of the atomic structure in the model, which should play a crucial role for the electronic properties of adatoms at lower θ.

The second model employs the Newns-Anderson Hamiltonian [42,43] and gives a quantitative expression for Gurney's classical picture [12]. The model Hamiltonian for an alkali-metal adatom on the metal substrate is written as [13,51-55],

$$H = \sum_{k,\sigma} \varepsilon_k C_{k\sigma}^{+} C_{k\sigma} + \varepsilon_s(\theta) \sum_{\sigma} C_{s\sigma}^{+} C_{s\sigma} + \sum_{k,\sigma} (V_{ks} C_{k\sigma}^{+} C_{s\sigma} + h.c.), \qquad (2.1)$$

where $C_{s\sigma}$ and $C_{k\sigma}$ denote the annihilation operators of the adatom valence s and substrate states with spin σ, respectively. The first two terms correspond to energy levels of substrate and adatom states, and the third is a mixing term between them by mutual interaction. For the sake of simpliclty, Coulomb repulsion energy of two electrons on the adatom site is neglected. The most important parameter in this model is the effective energy of the adatom s level,

$$\varepsilon_s(\theta) = -I + \frac{e^2}{4D} + \varepsilon_{dep}(\theta), \qquad (2.2)$$

where I is the first ionization energy of an isolated alkali-metal atom, and the latter two designate the level shifts due to the image effect and depolarization field created by the rest of adatoms. In previous treatments of this model, the adatom dipole is directly related with the occupancy of the s level. Thus in order to reproduce a large dipole at low θ, it is necessarily required that the s level is mostly empty and therefore $\varepsilon_s(\theta) \gg E_F$ of the substrate. Since the ionization energy of alkali-metal atoms are 5.39, 5.14, 4.34, 4.18 and 3.89eV for Li, Na, K, Rb and Cs, respectively, while the work function of metal substrates is typically ~4eV, ionization of an adatom is hardly expected from the comparison of these two parameters. In fact, the crucial assumption required for the adatom ionization is the upward shift of the s level by the image term $e^2/4D$. The effective reduction of the adatom ionization energy from I to $I-e^2/4D$ has its origin in relaxation of the surface after removal of one adatom electron due to virtual excitation of a substrate surface plasmon

which screens the positive adatom ion core. First, it should be noted that to express the relaxation energy by the image form $e^2/4D$ is appropriate only when the distance D between the adatom and image plane of the substrate is large. Based on a classical picture, the perpendicular distance between the adatom and outermost substrate layer is usually used as D. But, actually, the image plane of the substrate is located ~1Å outside the surface atom [36]. Furthermore, the surface plasmon charge density extends in the perpendicular direction over a region of ~π/(Fermi wavevector) thickness. Thus adatom orbitals at an equilibrium site completely overlap with the surface plasmon charge and the expression $e^2/4D$ is meaningless for estimating the relaxation energy. More serious problem is concerned with whether such a relaxation energy should be used in the chemisorption problem to renormalize the adatom level. It was shown by Hewson and Newns [56] that such an approximation is appropriate only in the case

$$\Delta(\varepsilon) \ll \omega_s, \tag{2.3}$$

$$\Delta(\varepsilon) = \pi \sum_k |V_{ks}|^2 \delta(\varepsilon-\varepsilon_k), \tag{2.4}$$

where ω_s is the surface plasmon frequency of the substrate. $\Delta(\varepsilon)^{-1}$ and ω_s^{-1} give the time scales of adatom screening by the direct electron transfer from the substrate to adatom and by virtual excitation of the surface plasmon, respectively. If $\Delta(\varepsilon)\sim\omega_s$, the use of eq.(2.2) would become much less clear. In most cases, the adatom is chemisorped at a position where its orbitals entirely overlap with substrate ones and the interaction

between them is strong. In fact, it was shown by the first-principles calculation of Lang and Williams [57] that screening of the adatom core hole is essentially caused by the direct electron transfer from the substrate to adatom empty orbitals rather than the surface plasmon excitation for a Na on the jellium. Therefore the trick used in the model calculation to shift up the adatom s level cannot be justified at all. Then there is no reason to believe that the alkali-metal adatom becomes ionic at low θ.

In the standard treatment of the model eq.(2.1), the decrease of the adatom dipole with increasing θ is attributed to the downward shift of the s level relative to E_F resulting in its gradual filling. The depolarization energy $\varepsilon_{dep}(\theta)$ which shifts down the s level is expressed as

$$\varepsilon_{dep}(\theta) = -\sum_i [r_i^{-1} - (r_i^2 + D^2)^{-1/2}] Q(\theta), \qquad (2.5)$$

where the summation is taken over all adatom sites excluding the one described in eq.(2.1) which is assumed to be at the origin, and $Q(\theta)$ is the charge transfer from the adatom to the substrate. Eq.(2.5) is entirely based on a classical picture that a point-charge $Q(\theta)$ is transfered from the center of adatoms to substrate surface atoms with perpendicular interval D. Eq.(2.5) includes only the Hatree potential change by the rest of adatoms. (However, the s level may be most sensitively affected by the adatom charge redistribution on the same site.) More importantly, in contrast to the classical picture, the increase and decrease of the electron density ocuur in real systems in the interface

and vacuum sides of an adatom site, respectively (See Figs. 7 and 19). In an extreme case where the incease and decrease of the charge is distributed perfectly symmetrically about the adatom site, the potential changes by the both sides exactly cancel with each other and there appears no depolarization shift. Therefore, in general, one cannot expect a large depolarization energy such as ~1eV which is required to neutrize adatoms at higher θ.

Even with the above-mentioned two mechanisms, i.e., the image effect and deplarization shift, the experimentary observed work function variation with increasing θ is often difficult to reproduce in the standard treatment of the Newns-Anderson model approach. In such a case, theorists working on the model further invoke additional mechanisms. Muscat and Batra [52] proposed that the appearance of the work function minimum means realization of a large outward relaxation of alkali-metal adatoms with increasing θ. Tsukada *et al.* [58] argued that clustering of adatoms at a critical coverage may correspond to the work function minimum.

Why is it then necessary to introduce the above-mentioned unreliable assumptions when working on the Newns-Anderson model? This is because the adatom induced dipole $d(\theta)$ is usually evaluated by the formula [13,51-55]

$$d(\theta) = D(1 - n_a(\theta)) = D(1 - \sum_{\sigma} \langle C_{s\sigma}^{+} C_{s\sigma} \rangle). \qquad (2.6)$$

Then in order to explain a large dipole at low θ and its rapid decrease with increasing θ, it is necessarily required that $n_a(\theta) \ll 1$ at low θ, while $n_a(\theta) \sim 1$ at higher θ. The shift up of the s level by the image effect and its subsequent downward shift

by the depolarization energy are quite convenient mechanisms which insure the above θ dependence of the s level occupancy. However, it is not correct to consider that eq.(2.6) alone contributes to the induced dipole moment. A more general expression for the dipole moment should be derived in order to make the situation clearer. First, I define the dipole density as

$$\mu(\theta,\varepsilon) = -\frac{1}{\pi}\int d^3r \; z \; ImG(r,r,\varepsilon+i\delta), \tag{2.7}$$

where $G(r,r,\varepsilon+i\delta)$ is the Green function $(\varepsilon+i\delta-H)^{-1}$ (δ is an infinitesimal positive number.). The z axis is the surface normal pointing to the vacuum region and and z=0 is understood to coincide with the adatom plane. The integration is done within the region where the charge redistribution takes place. $\mu(\theta,\varepsilon)$ is related to the induced dipole moment $d(\theta)$ by

$$d(\theta) = \frac{1}{N}\int_{\varepsilon\leq E_F} d\varepsilon \left(\mu(\theta,\varepsilon) - \mu(\theta=0,\varepsilon)\right), \tag{2.8}$$

where N is the number of adatoms. Unless the origin of the z axis is at the adatom plane, $\mu(\theta,\varepsilon)$ corresponding to isolated adatoms must be substracted from eq.(2.8) for evaluating the adatom induced dipole. Let us denote the base functions for the adatom s and substrate states as $\varphi_\alpha(r)$ and $\varphi_\beta(r)$, respectively. They are assumed to be normalized and orthogonal with one another. Then neglecting the mixing among adatom and substrate states, $\mu(\theta,\varepsilon)$ is written as

$$\mu(\theta,\varepsilon) = -\frac{1}{\pi}[\sum_\alpha \mu_{\alpha\alpha}\, ImG_{\alpha\alpha}(\varepsilon+i\delta) + \sum_\beta \mu_{\beta\beta}\, ImG_{\beta\beta}(\varepsilon+i\delta)$$

$$+ \sum_{\alpha\beta}(\mu_{\beta\alpha}\, ImG_{\alpha\beta}(\varepsilon+i\delta)+c.c.)\,], \tag{2.9}$$

where the dipole matrix element between the i and j states is defined as

$$\mu_{ij} = \int d^3r \, z \, \varphi_i^*(r)\varphi_j(r) \tag{2.10}$$

The first term in eq.(2.9) vanishes because $\mu_{\alpha\alpha}=0$ due to the symmetry of $\varphi_\alpha(r)$ about the plane z=0. The total density of states of the system $\rho(\theta,\varepsilon)$ is written in a similar way as

$$\rho(\theta,\varepsilon) = -\frac{1}{\pi}[\sum_\alpha ImG_{\alpha\alpha}(\varepsilon+i\delta) + \sum_\beta ImG_{\beta\beta}(\varepsilon+i\delta)], \tag{2.11}$$

Here the mixing term between adatom and substrate states does not appear because of the orthogonality of base functions. For the sake of simlicity, let us ignore β dependence of $\mu_{\beta\beta}$ and replace it by a single parameter D. Then from eqs.(2.9) and (2.11), $\mu(\theta,\varepsilon)$ is divided into two terms as

$$\mu(\theta,\varepsilon) = \mu_{ct}(\theta,\varepsilon) + \mu_{hyb}(\theta,\varepsilon), \tag{2.12}$$

where

$$\mu_{ct}(\theta,\varepsilon) = D\left(\rho(\theta,\varepsilon) + \frac{1}{\pi}\sum_\alpha ImG_{\alpha\alpha}(\varepsilon+i\delta)\right), \tag{2.13}$$

and

$$\mu_{hyb}(\theta,\varepsilon) = -\frac{1}{\pi}\sum_{\alpha\beta}\left(\mu_{\beta\alpha}\, ImG_{\alpha\beta}(\varepsilon+i\delta) + c.c.\right). \tag{2.14}$$

By using the relations

$$\int_{\varepsilon\le E_F} d\varepsilon \left(\rho(\theta,\varepsilon) - \rho(\theta=0,\varepsilon)\right) = N,$$

$$\int_{\varepsilon\le E_F} d\varepsilon \, -\frac{1}{\pi}\sum_\alpha ImG_{\alpha\alpha}(\varepsilon+i\delta) = N\, n_\alpha(\theta), \tag{2.15}$$

the induced dipole by eq.(2.13) is finally reduced to $D(1-n_\alpha(\theta))$,

which coincides with the familiar expression eq.(2.6) giving a contribution of the charge transfer. As is seen from the definition, it originates from the increase in the density of states of substrate states in the surface region by perturbation. There may be ambiguity in the definition of the concept "charge transfer". In the present paper, it is used in a narrow sence to denote the above-mentioned change in the occupation number of the overlayer orbitals and rigorously distinguished from the term "charge redistribution" which includes hybridization effects. On the other hand, the other one eq.(2.14) originates from the hybridization of the adatom s and substrate states, which was ignored completely in previous models based on the Newns-Anderson Hamiltonian. Its origin is the charge bulid-up in the interface (bond charge) and corresponding charge depletion in the vacuum side of the adatom or substrate regions. This term vanishes, for example, in case of homonuclear diatomic molecules. However, for alkali-metal adatoms on metals with a much lower symmetry, there is no reason to believe that this off-diagonal contribution to the dipole is dominated by the conventional diagonal charge transfer term. In fact, at a high θ limit, Wimmer *et al.* [34] demonstrated that the work function is lowered by the hybridization of the Cs 6s and W 5*d* for Cs/W(001). If the hybridization term is dominant even at low θ, the assumption of the almost empty s level at low θ may become unnecessary for explaining a large adatom dipole, and one may not have to resort anymore to unreliable assumptions about the image shift and depolarization energy.

In the first-priniples electronic structure calculations, it is impossible to divide in a definite way the calculated total dipole density into these two contributions, because the base functions for the substrate and adatom states cannot be chosen uniquely. Nevertheless, from the energy dependence of $\mu(\theta,\varepsilon)$, it seems possible to postulate the origin of the dipole density in a qualitative manner. From the definition, $\mu_{ct}(\theta,\varepsilon)$ has a positive sign as a function of energy. On the other hand, the dipole density due to the hybridization $\mu_{hyb}(\theta,\varepsilon)$ shows a characteristic energy dependence. The off-diagonal Green function $G_{\alpha\beta}(\varepsilon+i\delta)$ is given as [59]

$$G_{\alpha\beta}(\varepsilon+i\delta) = G_{\alpha\alpha}(\varepsilon+i\delta)V_{\alpha\beta}\frac{1}{\varepsilon+i\delta-\varepsilon_\beta} \tag{2.16}$$

where

$$G_{\alpha\alpha}(\varepsilon+i\delta) = \frac{1}{\varepsilon-\varepsilon_\alpha-\Delta_\alpha(\varepsilon)+i\Gamma_\alpha(\varepsilon)}. \tag{2.17}$$

Here ε_α, ε_β and $V_{\alpha\beta}$ are the diagonal and off-diagonal matrix elements of the Hamiltonian. If the interaction among neighboring adatom s orbitals is small, the energy shift $\Delta_\alpha(\varepsilon)$ and width $\Gamma_\alpha(\varepsilon)$ of the s resonance may be approximately given by

$$\Delta_\alpha(\varepsilon)-i\Gamma_\alpha(\varepsilon) = \sum_\beta \frac{|V_{\alpha\beta}|^2}{\varepsilon+i\delta-\varepsilon_\beta}. \tag{2.18}$$

From eqs.(2.14), (2.16) and (2.17), one yields

$$\mu_{hyb}(\theta,\varepsilon) = \sum_\alpha \frac{B_\alpha(\varepsilon)}{\pi}\,\frac{\varepsilon-\varepsilon_\alpha-\Delta_\alpha(\varepsilon)+(A_\alpha(\varepsilon)/B_\alpha(\varepsilon))\Gamma_\alpha(\varepsilon)}{(\varepsilon-\varepsilon_\alpha-\Delta_\alpha(\varepsilon))^2+\Gamma_\alpha(\varepsilon)^2}+c.c., \tag{2.19}$$

where $A_\alpha(\varepsilon)$ and $B_\alpha(\varepsilon)$ are defined as

$$A_\alpha(\varepsilon) = P\sum_\beta \frac{V_{\alpha\beta}\,\mu_{\beta\alpha}}{\varepsilon-\varepsilon_\beta} \tag{2.20}$$

$$B_\alpha(\varepsilon) = \pi \sum_\beta V_{\alpha\beta}\,\mu_{\beta\alpha}\;\;\delta(\varepsilon-\varepsilon_\beta). \tag{2.21}$$

Since the energy dependence of $\Delta_\alpha(\varepsilon)$, $\Gamma_\alpha(\varepsilon)$, $A_\alpha(\varepsilon)$ and $B_\alpha(\varepsilon)$ is not large unless substrate bands are narrow, they may be assumed energy-independent. Then eq.(2.19) shows that $\mu_{hyb}(\theta,\varepsilon)$ rapidly changes its sign at

$$\varepsilon = \varepsilon_\alpha + \Delta_\alpha - (A_\alpha/B_\alpha)\Gamma_\alpha. \tag{2.22}$$

This boundary is shifted from the center of the s resonance by the term $(A_\alpha/B_\alpha)\Gamma_\alpha$. If β dependence of the matrix elements $V_{\alpha\beta}\;\mu_{\beta\alpha}$ are neglected, and the substrate band is wide and has energy-independent density of states (DOS), A_α vanishes and the boundary coincides exactly with the resonance peak.

Another quantity closely related with $\mu_{hyb}(\theta,\varepsilon)$ is the bond order density defined by

$$\beta(\theta,\varepsilon) = \sum_n \psi_n(r_1)^*\psi_n(r_2)\;\delta(\varepsilon-\varepsilon_n) + c.c.$$

$$= -\frac{1}{\pi}\sum_{\alpha,\beta}\varphi_\beta(r_1)^*\varphi_\alpha(r_2)\;ImG_{\alpha\beta}(\varepsilon+i\delta) + c.c, \tag{2.23}$$

where ε_n and $\psi_n(r)$ are the energy and wave function of one electron states, and r_1 and r_2 are assumed in the substrate and adatom regions, respectively. It may be used as a measure of covalency in the adatom-substrate bond. $\beta(\theta,\varepsilon)$ is given by the same expression eq.(2.19) if $\mu_{\beta\alpha}$ is replaced by $\varphi_\beta(r_1)^*\varphi_\alpha(r_2)$ in evaluating $A_\alpha(\varepsilon)$ and $B_\alpha(\varepsilon)$ in eqs.(2.20) and (2.21). Thus $\mu_{hyb}(\theta,\varepsilon)$ and $\beta(\theta,\varepsilon)$ show a similar energy dependence. If the calculated total dipole density behaves similarly with the bond order density as a function of energy, one may infer that the

induced dipole comes mainly from the hybridization. The positive and negative parts of the bond order density correspond to the bonding and antibonding states, respectively. The bonding-antibonding boundary fairly coincides with the center of the resonance peak if $(A_\alpha/B_\alpha)\Gamma_\alpha$ is small. In fact, by the first-principles calculation of Lang and Williams [40] for single atom chemisorption on a high-density jellium surface, it was shown that the lower and upper halves of the adatom resonance state have bonding and antibonding characters, respectively. The charge accumulation (depletion) in the interface region in the bonding (antibonding) states is the origin of the hybridization induced dipole density and its rapid change of sign near the bonding-antibonding boundary around a center of the resonant peak.

The concept of the adatom polarization due to hybridization must be strictly distinguished from that of charge transfer. In Fig.3, the induced dipole moments due to the charge transfer $d_{ct}(\theta)$ and hybridization $d_{hyb}(\theta)$ are shown schematically as a function of E_F relative to the center of the s resonance. The charge transfer induced dipole disappears when E_F is located at the center of the s resonence, whereas the hybridization induced dipole becomes the largest by the maximum use of bonding states in this case. Since the work function of high-density metal substrates (Φ=4~5eV) is comparable with ionization energies of alkali-metal atoms, this might be surely the case in real systems. It has been clarified in this section that there are oversimplifications and unreliable assumptions in the

phenomenological treatments of the alkali-metal adsorption. Hence, first-principles studies are necessary to establish a correct picture of the alkali-metal adsorption and its θ dependence.

3. Calculational method and overlayer models

The ab initio calculation in the present work is based on the density functional theory of Hohenberg and Kohn [60]. In this formalism, the electronic energy of the interacting N electrons in an external field $V_{ex}(r)$ is expressed as

$$E[n] = T_0[n] + \int d^3r\, n(r)\, V_{ex}(r) + \frac{1}{2}\int d^3r d^3r' \frac{n(r)n(r')}{|r-r'|} + E_{xc}[n]. \qquad (3.1)$$

The first term is the kinetic energy of non-interacting electrons with the same density $n(r)$ and the last term is the exchange-correlation energy. The energy functional $E[n]$ becomes minimum for the true ground state electron density. Kohn and Sham [61] showed that the problem of finding the correct ground state denity for eq.(3.1) is reduced to solving a Schrödinger-like equation,

$$\left\{ -\frac{1}{2}\Delta + V_{ex}(r) + \int d^3r' \frac{n(r')}{|r-r'|} + \mu_{xc}[n] \right\}\psi_i(r) = \varepsilon_i \psi_i(r), \qquad (3.2)$$

$$n(r) = \sum_{i=1}^{N} |\psi_i(r)|^2, \qquad (3.3)$$

where effective exchange-correlation potential $\mu_{xc}[n]$ is given by $\delta E_{xc}[n]/\delta n$. In the local density approximation (LDA), $E_{xc}[n]$ is approximated by a simplified form

$$E_{xc}[n] = \int d^3r\, n(r)\, \varepsilon_{xc}(n(r)). \qquad (3.4)$$

Among numbers of suggested expressions for $\varepsilon_{ex}(n)$, the Wigner interpolation formula [62]

$$\varepsilon_{xc}(n) = -\frac{0.458}{r_s} - \frac{0.44}{r_s + 7.8}, \tag{3.5}$$

where $r_s=(3/4\pi n)^{1/3}$ is employed in the present work. Then the effective exchange-correlation potential is written as

$$\mu_{xc}(n) = -\frac{0.611}{r_s} - \frac{0.587 r_s + 3.432}{(r_s + 7.8)^2}. \tag{3.6}$$

The sources of the external field $V_{ex}(r)$ in eq.(3.1) are the jellium substrate and the ion cores of alkali-metal adatoms and also of Al for the case of the adsorption on Al(001). The potential due to the jellium substrate is given as

$$V_{jel}(r) = \int d^3r' \frac{n_{jel}(r')}{|r - r'|}, \tag{3.7}$$

where $n_{jel}(r)$ is the jellium density. In the present work, the ion cores are represented by the ab initio non-local norm-conserving pseudopotential of Bachelet, Hamann and Schlüter [63]. It is given in an analytical form as

$$V_{ion} = V_{core}(r) + \sum_l |l> V_l(r) <l|, \tag{3.8}$$

where the local core potential is

$$V_{core}(r) = -\frac{Z_v}{r}[\sum_{i=1}^{2} c_i \, erf(\beta_i^{1/2} r)], \tag{3.9}$$

while the l-th component of the non-local part is

$$V_l(r) = \sum_{i=1}^{3} (A_i^l + A_{i+3}^l r^2) \exp(-\alpha_i^l r^2). \tag{3.10}$$

Z_v is the valence charge. Various parameters for the core and

angular-momentum dependent parts are tabulated in ref.63. The norm-conserving pseudopotential can reproduce valence energy levels as well as their wave functions outside the core region. Eqs.(3.2) and (3.3) are solved by a standard iteration technique: (1) input a trial electron density; (2) solve the eigen equation eq.(3.2) with the input electron density; (3) construct the output electron density with eq.(3.3) using the wave functions obtained in (2); (4) set up the input electron density for the next iteration by mixing the input and output densities; (5) iterate the procedure (1)-(4) until the input and output densities coincide with each other within a given allowance. Once the eqs.(3.2) and (3.3) are solved, the total energy of the system consisting of the N electrons, jellium and ion cores is calculated by the equation

$$E_{total} = \sum_{i=1}^{N} \varepsilon_i - \frac{1}{2}\int d^3r d^3r' \cdot \frac{n(r)n(r')}{|r-r'|}$$

$$+ \int d^3r \, (\varepsilon_{xc}(n) - \mu_{xc}(n))n(r) + \frac{1}{2}\int d^3r d^3r' \cdot \frac{n_{jel}(r)n_{jel}(r')}{|r-r'|}$$

$$+ \sum_j \int d^3r \frac{Z_j \, n_{jel}(r)}{|R_j - r|} + \frac{1}{2}\sum_{i \neq j} \frac{Z_i Z_j}{|R_i - R_j|}, \qquad (3.11)$$

where R_j and Z_j denote the position vector and valence charge of the j-th ion core. The electrostatic energy terms coming from the jellium density in eq.(3.11) should be omitted in case of the Al(001) substrate. Eq.(3.11) is evaluated by the momentum space formalism of Ihm, Zunger and Cohen [64].

In the present work, the surface electronic structure calculation is done by utilizing the conventional repeating slab

geometry, in which the semi-infinite surface is replaced by a thin slab and the slab geometry is repeated periodically in the surface normal direction. The vacuum region between neighboring slabs should be large enough to prevent their mutual interaction. In the present case, it must be larger than is commonly used in order to evaluate the contribution of a surface dipole layer to the work function accurately (For discussing the work function change of an order of 0.1eV, a vacuum spacing more than 20a.u. is necessary.). By virtue of the repeating slab geometry, various numerical techniques developed for three dimensional systems become available without any rectifications, which is of great advantage in the present case in order to perform very large calculations at lower θ with high accuracy and reliability. Above all, it becomes possible to expand the wave function $\psi_i(r)$ in eq.(3.2) by plane wave bases as

$$\psi_{n,k}(r) = \frac{1}{V^{1/2}} \sum_G A_{n,k}(G) \exp\left(i(k+G)\, r\right), \tag{3.12}$$

where n and k are the suffices for the energy band and wave vector, and V and G denote the volume of the system and reciprocal lattice vector, respectively. The work function is quite sensitive to a minute change of the electron density. Therefore its accurate evaluation of an order of 0.1eV necessiates adopting highly flexible base functions for $\psi_{n,k}(r)$. The plane wave base set is one of the few examples appropriate for such a purpose. It should be noted that the LCAO (linear combination of atomic orbitals) bases without sufficiently large number of excited orbitals cannot evaluate the work function even with accuracy of an order of 1eV.

By inserting eq.(3.12) into eq.(3.2), the secular equation is reduced to a matrix form

$$\left\{\frac{|k+G|^2}{2}\delta_{G,G'} + V_{jel}(G-G') + V_{ion}(k+G,k+G')\right.$$

$$\left. + \frac{4\pi\,\rho(G-G')}{|G-G'|^2} + \mu_{xc}(G-G')\right\}A_{n,k}(G') = \varepsilon_{n,k}\,A_{n,k}(G). \qquad (3.13)$$

In the above, the matrix elements of the jellium, Hartree and exchange-correlation potentials are local, while that of ion cores includes the non local angular dependent part. The Fourier component of the charge density $\rho(G)$ is calculated by

$$\rho(G) = \sum_n \int_{\varepsilon_{n,k}\le E_F} \frac{d^3k}{(2\pi)^3} \sum_{G'} A_{n,k}(G+G')A_{n,k}(G')^*, \qquad (3.14)$$

where E_F is the Fermi energy, which is determined by the condition $\rho(G=0)=N/V$. The k-space integration in eq.(3.14) is performed by the tetrahedron method of Lehmann and Taut [65]. The matrix element of the ion core potential is analytically calculated from eqs.(3.8)-(3.10), while the evaluation of the exchange-correlation part necessiates potential calculations at meshed sampling points in the unit cell and a subsequent Fourier transformation to the k-space. The matrix element of the jellium substrate is given by

$$V_{jel}(G) = \frac{8\pi\, n_{jel}}{A_z\, G_z^3}\,\sin\left(\frac{D_{jel}G_z}{2}\right), \qquad (3.15)$$

where D_{jel} and n_{jel} denote the thickness and density of the jellium slab, and A_z is the period in the surface normal (z) direction. Eq.(3.13) is diagonalized by a standard numerical program in the independent mesh points in the Brillouin zone, and then the charge density is constructed by eq.(3.14). Because of the negligible

interaction between the neighboring slabs for the occupied states, diagonalization of the matrix is necessary only in the two dimensional Brillouin zone where k_z=0. For the case of the Al(001) substrate, the two dimensional square Brillouin zone is divided into 8x8, 6x6 and 4x4 meshes for θ=1/2, 1/4 and 1/8, respectively. Similar mesh density is used in the case of the jellium substrate. The initial input charge for the iteration is the superposed density of the bare substrate and unsupported overlayer. Mixing rate of input and output charge densities for the next iteration is typically ~5%. The iteration procedure is continued until the self-consistent condition is achieved. The self-consistency is assumed when the difference between the input and output surface dipole layers converges less than 0.1eV. The calculated total energy converges much faster than the potential energy and the convergence less than 1meV is easily attained. The cut-off energy for the plane wave bases E_{cut}, i.e., the maximum of $|k+G|^2/2$ is 6.5Ry in all of the present calculations, which is sufficiently large for the alkali-metals, Al and jellium substrate. An additional calulation with E_{cut}=10Ry was performed at θ=1/2 for the Al substrate to demonstrate the convergence of the calculation. The inversion symmetry of the system is utilized to make the matrix real, while by virtue of the mirror symmetry with respect to the center plane of substrate slabs, the plane waves can be classified into even and odd bases and separatively diagonalized. The choice of Al(001) as a realistic metal substrate satisfies these conditions and is quite appropriate for the calculation at low θ. On the other hand, the lowest θ would

be severely limited, for example, with Al(111) due to the lack of the mirror symmetry. The number of the plane wave bases exceeds 4500 in the largest system in the present calculation. No perturbative approaches are used and all the bases are diagonalized exactly.

Fig.4 shows the model geometry used for the study of the alkali-metal adsorption on the jellium surface. The alkali-metal atoms are adsorbed on both sides of the substrate to preserve the symmetry. Most of the calculations are done employing Na as the adsorbate. But the effect of different alkali-metal adspecies will be also examined. So as to simulate the adsorption on high density metal substrates, the jellium density is chosen as n_{jel}=0.00267a.u. (r_s=2.1a.u.), which corresponds to the bulk electron density of Al. Lang and Williams [40] used the jellium with r_s=2.0a.u. in their study of the single atom chemisorption. The small difference in the jellium density changes the calculated results little, and their results may correctly give the limit of $\theta \rightarrow 0$ in the present calculation. D_{jel} and A_z are set equal to 16a.u. and 48a.u., respectively, by which the work function of the semi-infinite jellium 3.8eV [44] is reproduced. The two dimensional structure of the overlayer is entirely at one's disposal as far as the translational symmetry is held. In the present work, the overlayers are assumed to form a square lattice with a lattice constant $a_{//}$ and θ is controled by changing the one parameter $a_{//}$. Because of the extended nature of the s orbital as well as due to the lack of p electrons which may result in polarized sp orbitals, the different choice of the overlayer

structure would not change calculated results qualitatively. Another important parameter is the distance between the substrate and overlayer D_{as}. Wimmer *et al.* [34] treated D_{as} as an adjustable parameter and examined D_{as} dependence of the work function for Cs/W(001) (θ=1/2). They showed that the work function is sensitive to D_{as}. In the present calculation, D_{as} is determined from the minimization of the calculated total energy eq.(3.11) for higher θ. It will be shown that relaxtion of D_{as} is not so large and of an order of 0.1a.u. Within the variation of D_{as} in this order, the change of the electron charge density and work function is rather small. Thus D_{as} is fixed for lower θ in order to save the computational work.

In the case of the alkali-metal adsorption on Al(001), the Al(001) substrate is represented by a unrelaxed five layer Al slab with the nearest Al-Al distance equal to the corresponding bulk value 5.42a.u. Na is chosen as the alkali-metal because only Na/Al(001) has been studied experimentally. Porteus [66] studied the Na adsorption on Al(001) and Al(111) by the low energy electron diffraction (LEED) technique and observed a c(2x2) structure on Na/Al(001) at θ=1/2 in units of Al(001) layers. Van Hove *et al.* [67] analyzed the LEED intensity corresponding to the c(2x2) coverage, and came to the conclusion that Na adatoms sit on the four-fold hollow site where the perpendicular distance between Na and top-layer Al atoms was determined as 3.87a.u. The conclusion was further established by the similar LEED analysis of Hutchins *et al.* [68]. In the present work, the electronic structures of Na/Al(001) are calculated for three coverages. The structure

corresponding to the highest θ is the experimentally observed c(2x2) structure (θ=1/2). For lower coverages, p(2x2) (θ=1/4) and $(\sqrt{8}x\sqrt{8})R45^{\circ}$ (θ=1/8) are assumed, where Na atoms sit on the same four-fold site and form a square lattice. The latter two are not experimentally observed but may be meaningful to investigate the distant adatom-adatom interaction. The lattice constants $a_{//}$ are 7.66, 10.83 and 15.32a.u., for θ=1/2, 1/4 and 1/8, respectively. The overlayer structures for three coverages are depicted in Fig.5. The perpendicular relaxation of Na is not considered, since it will be shown for the jellium substrate that its effect is rather small.

4. Results and discussions for the jellium substrate

The electronic structure calculations of the Na overlayers on the high-density jellium (r_s=2.1a.u.) surface are done for five coverages assuming a square lattice for Na. The lattice constant $a_{//}$ for the highest θ is chosen as 8.0a.u. Just for the sake of convenience, this coverage is defined as θ=1 in this section. But it is not necessarily meant that θ=1 corresponds to the full coverage in experimental systems. Since the nearest Na-Na distance is 6.6a.u. in the bulk Na, θ=1 may roughly correspond to 60~70% of the full coverage. The units of the coverage in this section is different from that in the next section for the Al(001) substrate, where θ is measured in units of Al(001) layers. θ=1 in this section corresponds to θ=0.46 in units of Al(001) layers. The other calculations are done for θ=3/4, 1/2, 1/3 and 1/5, where $a_{//}$= 9.238, 11.314, 13.856 and 17.888a.u., respectively. They

would correspond to θ=0.34, 0.23, 0.15 and 0.09 if θ was measured in units of Al(001) layers.

The total energy minimization was done in determining the adatom-jellium distance D_{as} for θ=1/2, 3/4 and 1. The calculated energy minimum points are D_{as}=2.9, 3.0 and 3.1a.u. for θ=1/2, 3/4 and 1, respectively. The vibrational frequency of the stretching motion of Na in the surface normal direction is estimated as ~17meV from the curveture of the total energy curve as a function of D_{as} at the minimum point. The frequency is found to decrease slightly with increasing θ. Because the number of sampling points for D_{as} was not taken so densely, though quite interesting, I will not discuss the θ dependence of vibrational properties of the overlayer in more detail in the present work. Within the variation of D_{as} of an order of 0.1a.u., the resultant work function change is only of an order of 0.01eV. Thus in order to save the computational efforts, D_{as} are assumed 2.9a.u. for θ=1/5 and 1/3. The small outward relaxation of Na with increasing θ reflects the weakening of the Na-jellium bond with increasing θ as will be discussed later. Muscat and Batra [52] proposed that the outward relaxation of the overlayer with increasing θ is essential in reproducing the observed work function variation. They required a large D_{as} relaxation of ~1a.u. for fitting their results to experimental work function curves. However, such a value seems somewhat too large even with different choices of substrates and adatoms, and the disagreement with experiments should be ascribed to their use of a simplified model based on the Newns-Anderson model in Section.2.

4.1 Charge density and difference charge

The upper panels of Fig.6 show the calculated electron charge densities on a vertical cut plane passing Na atoms at every interval of $a_{//}$ for θ=1 and 1/3. The Na atoms and jellium edges are shown by the filled circles and arrows, respectively. Because of the pseudopotential calculation, the charge density takes a minimum at Na sites. The ample magnitude of the electron density in the midregion of the neighboring Na atoms at θ=1 indicates that the Na layer has a metallic character at this coverage. However, it is not meant that the overlayer is a two dimensional metal, since the Na valence states strongly hybridize with the jellium bands in the present case. With decreasing θ, the electron density at the Na-Na bond region becomes smaller, and the adatom electronic structure approaches that of an isolated adatom.

The lower panels of Fig.6 show the corresponding difference charge defined by

$$\delta\rho(\mathbf{r},\theta) = \rho(\mathbf{r},\theta) - \{ \rho_{jel}(\mathbf{r}) + \rho_{alk}(\mathbf{r},\theta) \}, \qquad (4.1)$$

where $\rho(\mathbf{r},\theta)$, $\rho_{jel}(\mathbf{r})$ and $\rho_{alk}(\mathbf{r},\theta)$ denote the electron charge densities of the Na covered jellium, isolated jellium and unsupported Na layer, respectivety. The definition is quite natural in elucidating the charge redistribution caused by the mutual interaction between the overlayer and substrate. By the definition, $\delta\rho(\mathbf{r},\theta)$ satifies the condition

$$\int d^3\mathbf{r}\, \delta\rho(\mathbf{r},\theta) = 0. \qquad (4.2)$$

The characteristic features in $\delta\rho(\mathbf{r},\theta)$ common to all the coverages are the build-up of the electron density in the interface of the

jellium and Na layer and the correponding charge depletions in the jellium and Na sides. The θ dependence of the charge redistribution is discussed in detail in the following.

Fig.7 shows the contour maps of the difference charges for the five Na coverages on the same vertical cut plane as in Fig.6. The shaded and hatched areas designate the regions where $\delta\rho(r,\theta)\geq 0.001 a.u.$ (accumulation of the electron density) and $\delta\rho(r,\theta)\leq -0.0005 a.u.$ (depletion of the electron density), respectively. The dash-dotted curves correspond to $\delta\rho(r,\theta)=0$. The charge map for $\theta=1/5$ bears a close resemlance to that of a Li/jellium given by Lang and Williams [40] for a single atom chemisorption, suggesting that the direct interaction among adatoms is negligibly small at $\theta=1/5$. Hence, Fig.7 traces the θ dependence of the difference charge in the whole regime during the monolayer formation. The most striking feature discovered in the present work is that the bond charge is formed between the jellium and adatom irrespective of θ, and that its contour (shaded area) and amplitude are almost unchanged throughout the monolayer formation. Slight expansion (contraction) of the bond charge contour vertical (parallel) to the surface with increasing θ is the only noticeable minor change. The bond charge contour which is almost independent of θ may be interpreted as indicating that the nature of the adatom-substrate bonding remains essentially unchanged during the monolayer formation, which is in contrast with Gurney's classical picture [12] where the adatom- substrate bonding changes rapidly from ionic to covalent. On the other hand, a striking θ dependence exists in the hatched areas from which

electrons flow into the bond region. The kidney-shaped charge depletion on the vacuum side of Na becomes smaller with increasing θ, and the center of gravity of the depletion region on the Na side moves from the outside of Na to the Na-Na bond region. At θ=1, the major depletion area in the Na side appears between neighboring Na adatoms at the expense of some bonding charge between Na-Na metallic bonds. On the other hand, θ dependence of the depletion region on the jellium side is not so drastic. However, it should be noted that the depletion in the substrate side is not small. Actually, as is seen from Fig.6, the deepest charge depletion appears in the jellium side rather than the Na side at θ=1. The above θ dependence of the charge redistribution is far from the point-charge transfer picture assumed in the standard model analyses based on the Newns-Anderson Hamiltonian. It is manifest that the simple treatment cannot take account of the bond charge at the interface which is unchanged during the monolayer formation and the charge depletion on the jellium side.

The increase and decrease of the electron density in realistic calculations occur in the interface and vacuum sides of an adatom, respectively. Therefore, the depolarization field at adatom sites evaluated based on a classical point-charge transfer picture, eq.(2.5) is not appropriate. Fig.8 shows the change in the electrostatic potential $\delta\varphi_{ele}(r,\theta)$ due to $\delta\rho(r,\theta)$, i.e.,

$$\delta\varphi_{ele}(r,\theta) = \int dr'^{3}\ \frac{\delta\rho(r',\theta)}{|r-r'|} \tag{4.3}$$

for θ=1/5, 1/3, 1/2 and 1 on the same vertical cut plane as in Figs. 6 and 7. Accumulation and depletion of the electron density

in the interface and vacuum sides of a Na lead to the corresponding rise and lowering in $\delta\varphi_{ele}(r,\theta)$ in each part. However, at the Na site, both contributions mostly cancel with each other. The calculated $\delta\varphi_{ele}(r,\theta)$ at Na sites as measured from the interior of the jellium are -0.40, -0.15, -0.14 and -0.24eV for θ=1/5, 1/3, 1/2 and 1, respectively, showing no appreciable downward shift with increasing θ. Therefore one cannot expect a large depolarization shift of the adatom s level, which is typically assumed more than 1eV in order to reproduce the θ dependence of the adatom dipole moment. As will be shown later, the depolarization shift of the adatom valence states below E_F is indeed absent in the present calculation.

Fig.9 shows the similar difference charge contour maps of the Li/jellium systems at θ=1, 3/4 and 1/2. D_{as} is determined from the calculated total energy as 2.4, 2.5 and 2.6a.u. for θ=1/2, 3/4 and 1, respectively. It is seen that qualitative features of the charge redistribution are independent of the alkali-metal adspecies.

4.2 Work function change and adatom dipole moment

The work function of metal surfaces is defined as a minimum energy to remove electrons in metals to the vacuum. Within the local density fuctional theory, the potential barrier confining electrons in metals consists of the surface dipole layer (contribution of the electrostatic potential) and the exchange-correlation potential. The work function change $\Delta\Phi(\theta)$ of metals due to the alkali-metal adsorption originates from the change of the former due to the charge redistribution $\delta\rho(r,\theta)$. From Fig.8,

one sees that the electrostatic potential change is almost constant in the vacuum region and interior of the jellium. $\delta\varphi_{ele}(r,\theta)$ in the former is lower than that in the latter, indicating that the electrostatic potential barrier is reduced by the alkali-metal adsorption. The difference in $\delta\varphi_{ele}(r,\theta)$ between the vacuum and interior of the jellium gives the work function change $\Delta\Phi(\theta)$. Equally, $\Delta\Phi(\theta)$ is expressed as

$$\Delta\Phi(\theta) = 4\pi \int_0^{A_z/2} dz\, z\, \delta\rho_{ave}(z,\theta), \tag{4.4}$$

where $\delta\rho_{ave}(z,\theta)$ denotes the planar average of the difference charge eq.(4.1). The work function of the system is also directly obtained as the vacuum level measured from the Fermi energy E_F. The two expressions should give the same value if the system is semi-infinite. Because of the use of the finite jellium slab, there is a small discrepancy between the two valus. However, it is at most 0.05eV and causes no problem in discussing the work function change of an order of 0.1eV. The results given in the following are based on eq.(4.4). The induced dipole moment per an adatom $d(\theta)$ is related with the work function change by

$$d(\theta) = \frac{\Delta\Phi(\theta)\, a^2}{4\pi}. \tag{4.5}$$

The calculated work function and adatom dipole are shown as a function of θ in Fig.10 for the Na covered high-density jellium surfaces. The outward dipole which reduces the work function monotonically decreases with increasing θ. The origin of the outward dipole is the build-up of the electron density (bond charge) in the interface and the corresponding major depletion

area on the vacuum side of Na shown in Fig.7. Its monotonical decrease reflects the inward shift of the center of gravity of the depletion area on the Na side as well as the relative increase of the weight of the depletion area on the jellium side when θ is increased. On account of the rapid decrease of the adatom dipole, the calculated work function deviates from its linear dependence on θ, takes a minimum at about θ=1/2 and begins to rise toward a saturation value. The work function at θ=1, 2.8eV is close to that of Na(001), 2.9eV, which is calculated with a five layer slab model following the same calculational scheme. The present jellium substrate might be the best to simulate the most closely packed Al(111) surface. For Al(111), Hohlfeld *et al.* [7] measured the work function as a function of Cs coverage. The atomic density corresponding to the minimum point was 0.2×10^{15} atoms/cm^2, which is somewhat smaller than the present value 0.28×10^{15} atoms/cm^2 at θ=1/2. The difference may be attributed to a larger atomic size of Cs as compared with Na, since it leads to a larger adatom-adatom interaction at lower θ. The above result shows that the widely observed characteristic variation of the work function with increasing θ can be reproduced very well as far as the charge redistribution by the adatom-substrate interaction is described realistically by a first-principles method. Large relaxation of D_{as} [52] and/or clustering among adatoms [58] are not essential for the appearance of the work function minimum.

In order to shed light on the origin of the rapid decrease of $d(\theta)$ with increasing θ, the calculated planar average of the charge redistribution $\delta\rho_{ave}(z,\theta)$ is shown as a function of θ in

Fig.11. Its asymmetry about the center plane of the bond charge in the Na-jellium interface is the origin of the outward dipole layer. It is seen that $\delta\rho_{ave}(z,\theta)$ is quite different from a classical point-charge transfer picture assumed in the Newns-Anderson model analysis. For the sake of quantitative discussions, let us define the effective dipole length $D_{eff}(\theta)$ as

$$D_{eff}(\theta) = 2\int dz\ z\ \delta\rho_{ave}(z,\theta) \Big/ \int dz\ |\delta\rho_{ave}(z,\theta)|. \qquad (4.6)$$

For a classical dipole made of two positive and negative point charges, $D_{eff}(\theta)$ just gives the distance between the two charges. In the standard model analysis, $D_{eff}(\theta)$ is assumed constant and all of θ dependence of the adatom dipole is attributed to a decrease in the transferred charge $Q(\theta)$ with increasing θ. However, $D_{eff}(\theta)$ actually depends significantly on θ. The calculated $D_{eff}(\theta)$ are 2.4, 2.0, 1.8 and 1.5a.u. for θ=1/5, 1/3, 1/2 and 1, respectively. As explained before, this rapid contraction of $D_{eff}(\theta)$ comes from the inward shift of the depletion region on the Na side and the relative increase of the depletion on the jellium side. It plays a crucial role in reproducing the rapid decrease of the adatom dipole necessary for the appearance of the work function minimum. The above argument implies that it is of danger to use the single parameter expression eq.(2.6) in evaluating the work function change, because the difference charge density has infinite degrees of freedom in three dimensional space.

4.3 Adatom valence states

Discrete energy levels of an isolated alkali-metal atom are

strongly modified by the interaction with the high-density metal substrate. The key point to be clarified is whether there is a large θ dependence in the alkali-metal valence levels. For this purpose, I calculate the adatom induced density of states (DOS) $\rho_a(\varepsilon,\theta)$ defined by

$$\rho_a(\varepsilon,\theta) = \int_R dr^3 \sum_i |\psi_i^{\theta}(r)|^2 \delta(\varepsilon-\varepsilon_i^{\theta}) - \int_R dr^3 \sum_i |\psi_i^{\theta=0}(r)|^2 \delta(\varepsilon-\varepsilon_i^{\theta=0}), \quad (4.7)$$

where ε_i^{θ} and $\psi_i^{\theta}(r)$ are the energy and wave function of one electron state at coverage θ, and the integration is done within a sphere of radius R (~atomic radius of alkali-metal atoms) centered at an adatom site. The above definition coincides with that of Lang and Williams [40] used in the study of a single atom chemisorption on the jellium surface if R is sufficiently large. In the present study, the maximum of R is limited by the condition that two spheres at neighboring adatom sites do not overlap. The calculated $\rho_a(\varepsilon,\theta)$ is shown in Fig.12 as a function of θ. The origin of the energy is adjusted to E_F and the sphere radius R is chosen as 3.83a.u. The qualitative aspect of the results is insensitive to the small difference of R. Due to the slab approximation for the jellium substrate, the continuum energy spectrum of a semi-infinite jellium in the surface normal direction is replaced by discrete energy levels in the present case. As a result, the calculated $\rho_a(\varepsilon,\theta)$ is somewhat modified even at low θ limit from that of a single Na on the semi-infinite jellium given by Lang and Williams [40,57]. Especially, the interaction of the discrete jellium and adatom levels results in sharp spiky peaks at low θ, which would disappear with

semi-infinite substrates. Nevertheless, from the comparison of $\rho_a(\varepsilon,\theta)$ at θ=1/5 and that for a single Na on a semi-infinite jellium, one finds that they are essentially the same once the sharp peaks in $\rho_a(\varepsilon,\theta)$ at θ=1/5 are smeared out around the peak energies.

With increasing θ, discrete energy levels of an isolated Na becomes broad bands by the overlap of neighboring adatom orbitals. Consequently, sharp peaks in $\rho_a(\varepsilon,\theta)$ at lower θ become broad structures. It may be surprising for those who believe Gurney's classical picture [12] that there occurs no noticeable changes in $\rho_a(\varepsilon,\theta)$ with increasing θ except for the above-mentioned broadening of sharp peaks. In fact, no downward shift of the adatom valence states was observed below E_F in the present calculation. In Fig.12(d), $\rho_a(\varepsilon,\theta)$ at θ=1 is shown by dashed lines for the sake of comparison with that at θ=1/5. The adatom dipole at θ=1/5 is more than three times larger than that at θ=1. However, the corresponding change in the occupancy of adatom states is almost negligible, which is consistent with the fact that $\delta\varphi_{ele}(r,\theta)$ at adatom sites is almost independent of θ. Let us define the occupancy of adatom valence states in the sphere $n_a^R(\theta)$ by

$$n_a^R(\theta) = \int_{\varepsilon \le E_F} d\varepsilon\, \rho_a(\varepsilon,\theta). \qquad (4.8)$$

The calculated $n_a^R(\theta)$ (R=3.83a.u.) are 0.63, 0.62, 0.68, 0.61 and 0.65 electrons for θ=1/5, 1/3, 1/2, 3/4 and 1, respectively. It may be concluded that $n_a^R(\theta)$ is independent of θ within small numerical errors. The rather small θ dependence of the occupancy

of the adatom valence states as compared with the induced dipole is in good accord with the recent MDS experiment of Woratschek *et al*. [32]. Moreover, $n_a^R(\theta)$ is ~0.01 electrons larger than the number of electrons within the same sphere calculated for the corresponding isolated Na monolayers ($n_{iso}^R(\theta)$) regardless of θ, implying that the adatom region is essentially neutral even at low θ.

One possible mechanism which accounts for the increase and decrease of the electron density in the interface and vacuum sides of Na atoms is the polarization of a Na by the mixing of the Na 3s and $3p_z$ states. In order to examine this effect, I next study partial DOS of Na adatoms as a function of θ. For this purpose, the wave function $\psi_i^\theta(r)$ is expanded within the sphere centered at an adatom into s, p and higher angular-momentum components. With the present calculational scheme, this is easily done by expanding plane wave bases into spherical Bessel functions. Then the partial DOS of the l-th (l=s,p_x,p_z,...) component of the adatom valence state is defined as

$$\rho_a(\varepsilon,l,\theta) = \int_R dr^3 \sum_i |\psi_{i,l}^{\theta}(r)|^2 \delta(\varepsilon-\varepsilon_i^{\theta}) - \int_R dr^3 \sum_i |\psi_{i,l}^{\theta=0}(r)|^2 \delta(\varepsilon-\varepsilon_i^{\theta=0}), \quad (4.9)$$

where $\psi_{i,l}^{\theta}(r)$ denotes the l-th component of $\psi_i^{\theta}(r)$ in the sphere. The calculated s, $p_x(p_y)$ and p_z partial DOS of a Na adatom are shown in Fig.13, 14 and 15 as a function of θ, respectively. The sphere radius R=3.83a.u. is the same as in Fig.12. The thick and dashed curves indicate the first and second terms of the right hand side

of eq.(4.9), and thus the l-th partial DOS induced by the Na adsorption is given by the difference of the thick and dashed curves. The spiky sharp peaks in the partial DOS grow into broad band sructures with increasing θ by the overlap of neighboring adatom orbitals. The important fact is that the Na induced states below E_F mostly come from the 3s component of a Na. It is seen from Figs.14 and 15 that p_x (p_y) and p_z components of the Na valence states are essentially located above E_F. ($\rho_a(\varepsilon,p_x,\theta)$ is more broadened than $\rho_a(\varepsilon,p_z,\theta)$ on account of the larger interaction with substrate states.) This clearly shows that the redistribution of the electron density around a Na, and therefore the adatom dipole is *not* caused by the mixing of the Na 3s and $3p_z$ states. On the other hand, Na 3s and $3p_z$ states hybridize strongly above E_F and give rise to outward polarized states which have an antibonding character against the substrate, as will be discussed later.

In many of EELS experiments, an intensive loss peak characteristic of the adsorbed alkali-metal has been observed at higher θ [7,9,10,14-20]. The valence structure of alkali-metal adatoms given in the above may suggest that the observed peak may be interpreted as due to excitations from the partially filled s-like states to the essentially unoccupied p_z-like states. The excitation satisfies the dipolar scattering condition [69] and thus should have a strong intensity. The mode has a dipole character and is consistent with the conclusion in the model calculation of Ishida and Tsukada [20]. However, at present, the question of whether the excitation is collective or individual cannot be

answered, since one must compute the energy loss functions so as to estimate the strength of the polarization field by the excitation.

In the calculation of Lang and Williams [40] for semi-infinite surfaces, the sharp peaks in $\rho_a(\varepsilon,\theta)$ above E_F were smoothed out, and as a result, $\rho_a(\varepsilon,\theta)$ appeared as if it formed a single peak structure with its center located ~2eV above E_F. Lang and Williams interpreted this single peak above E_F as due to the alkali-metal s state and judged that alkali-metal s resonance is mostly empty on the jellium surface. However, the above partial DOS analysis of the alkali-metal valence states clarified that Na induced states above E_F are contributed dominantly by the Na 3p states partially hybridized with Na 3s rather than the pure Na 3s states.

4.4 Bond order density

Above analysis of the adatom valence state, which is found to show only a minor change as a function of θ, is contradictory with Gurney's classical picture [12] in which the adatom-substrate bond is assumed to change drastically from ionic to covalent one with increasing θ. In order to clarify the nature of the adatom-substrate bonding more directly, I study the bond order density defined by

$$\beta_{as}(\varepsilon,\theta) = \sum_i \psi_i^{\theta}(r_1)^* \psi_i^{\theta}(r_2)\, \delta(\varepsilon-\varepsilon_i) + c.c., \qquad (4.10)$$

where r_1 and r_2 are taken at some point in the interior of the jellium and at the Na site, respectively. Fig.16 shows the calculated $\beta_{as}(\varepsilon,\theta)$ of the Na covered jellium surfaces as a

function of θ. Here $r_{\parallel}$ is chosen at a point on a vertical axis passing through a Na and 2a.u. inside the jellium edge. The calculated results are insensitive to the position of $r_{\parallel}$ unless it is too far from the bond region. The positive and negative parts of $\beta_{as}(\varepsilon,\theta)$ correspond to the bonding and antbonding states, respectively. Qualitative features of $\beta_{as}(\varepsilon,\theta)$ are understood from eq.(2.19), especially for the region below E_F. Its rapid change of sign at the bonding-antibonding boundary near E_F may be interpreted as being characteristic of the off-diagonal Green function. However, it was assumed in the discussion in Section 2 that the overlayer states originate only from the alkali-metal s orbital. The calculated $\beta_{as}(\varepsilon,\theta)$ above E_F is modified from eq.(2.17) because of the existence of higher orbitals such as Na 3p which dominate the alkali-metal induced states above E_F as well as continuum states above the vacuum level. There is a strong antibonding peak slightly above E_F which becomes sharper with decreasing θ. The origin of the peak is the outward polarized orbital made by strong hybridization of the Na 3s and $3p_z$ orbitals.

At θ=1/5, the bonding-antibonding boundary is very close to E_F, indicating strong *covalency* in the adatom-substrate bond by the maximum use of the bonding states. The build-up of the electron density at the interface of the jellium and Na shown in Fig.7 is a natural consequence of this covalency. With increasing θ, E_F slightly moves into the antibonding region. The bond order of the adatom-substrate bond is defined by

$$B_{as}(\theta) = \int_{\varepsilon \leq E_F} d\varepsilon \, \beta_{as}(\varepsilon, \theta). \qquad (4.11)$$

The calculated $B_{as}(\theta)$ are 2.1×10^{-3}, 2.0×10^{-3}, 1.8×10^{-3} and 1.6×10^{-3}a.u. for θ=1/5, 1/2, 3/4 and 1, respectively. The decrease of $B_{as}(\theta)$ with increasing θ implies weakening of the adatom-substrate bond, which is in accord with the small outward relaxation and decrease in a stretching frequency of a Na with increasing θ. The weakening of the adatom-substrate bond is more directly demonstrated from adatom binding energies. The adsorption energies of a Na calculated as the total energy of the Na/jellium minus those of the bare jellium and unsupported Na layer are 1.5, 1.3, 1.1, 0.9 and 0.7eV for θ=1/5, 1/3, 1/2, 3/4 and 1, respectively. It is seen that the θ dependence of $B_{as}(\theta)$ is smaller than that of the Na binding energy. The definition of $\beta_{as}(\varepsilon, \theta)$ includes only the amplitude of one electron wave functions at a particular point $r_{\parallel}$ in the jellium, and takes no account of θ dependence of the bond region. Since the bond area per a Na diminishes as θ^{-1} with increasing θ, it may be natural that $B_{as}(\theta)$ underestimates the weakening of the adatom-substrate bond.

The above result for the bond order density contradicts with Gurney's classical picture in the following points: (i) if the s resonance is primarily located above E_F at low θ, E_F should be located inside the bonding region in $\beta_{as}(\varepsilon, \theta)$, since the lower and upper halves of the s resonance roughly correspond to the bonding and antibonding regions, respectively; however, in the present calculation, the bonding-antibonding boundary coincides

with E_F even at θ=1/5: (ii) if the adatom-substrate bonding changes from ionic to covalent one, the bond order $B_{as}(\theta)$ which is the measure of covalency should increase with increasing θ, while $B_{as}(\theta)$ decreases with θ in the present calculation.

The weakening of the adatom-substrate bond with increasing θ is partly due to the corresponding strengthening of the neighboring Na-Na bonds. Fig.17 shows the calculated bond order density of the nearest Na-Na bond $\beta_{aa}(\varepsilon,\theta)$ as a function of θ, which is computed by eq.(4.10) with r_1 and r_2 taken at neighboring Na sites. By the indirect interaction of neighboring Na atoms through the substrate, $\beta_{aa}(\varepsilon,\theta)$ shows oscillatory behaviors as a function of ε for lower θ. The Na-Na bond orders defined in the same way as eq.(4.11) are 8.0×10^{-6}, 8.1×10^{-5}, 1.2×10^{-4} and 1.8×10^{-4}a.u. for θ=1/5, 1/2, 3/4 and 1, respectively. The calculated bond orders for the adatom-substrate and adatom-adatom bonds qualitatively explain the observed commensurate-incommensurate transition of the overlayer structure [21-23] at higher θ well.

The increase of the Na-Na bond order reflects larger adatom-adatom interaction with increasing θ by the direct overlap of neighboring adatom orbitals. At θ=1, the direct interaction among adatoms surpasses the indirect one, and the calculated $\beta_{aa}(\varepsilon,\theta)$ at θ=1 keeps a positive sign (bonding states) in most of the region below E_F. An important observation is that its bonding-antibonding boundary coincides fairly well with E_F just as in the case of an isolated Na layer with a *half* filled s band. Even for $\beta_{aa}(\varepsilon,\theta)$ at lower θ, one notices a rapid change of its sign

near E_F. This implies that the Na 3s band is *half* filled even on a high-density jellium surface, which is consistent with the result that the adatom region is essentially neutral irrespective of θ.

4.5 Dipole density

Now let us proceed to the important problem about the origin of the adatom dipole. It is seen from Fig.7 that the major charge redistribution region due to the alkali-metal adsorption is localized around adatoms. If one takes a sphere with radius R centered at an adatom site, the dipole density within the sphere mainly comes from the cross term of the s and p_z components of one electron wave functions. Therefore the dipole density within the sphere $\mu(\varepsilon,\theta)$ is calculated as

$$\mu(\varepsilon;\theta) = \sum_i \int_R d^3r\, z\, \psi_{i,s}^{\theta\,*}(r)\psi_{i,p_z}^{\theta}(r)\, \delta(\varepsilon-\varepsilon_i^{\theta}) + c.c. \qquad (4.12)$$

Fig.18 shows the calculated $\mu(\varepsilon,\theta)$ of the Na covered jellium surfaces as a function of θ, where the sphere radius R is 3.83a.u. Its positive sign corresponds to the inward polarization of the one electron wave function (outward dipole). The dashed curves in the figure represent $\mu(\varepsilon,\theta)$ at θ=0 calculated within the same sphere for the bare jellium surface. Therefore the difference between the full and dashed curves contributes to the alkali-metal induced dipole which lowers the work function (see eq.(2.8)). The induced dipoles within the sphere calculated by integrating the difference up to E_F are 0.34, 0.30, 0.18 and 0.12a.u. for θ=1/5, 1/2, 3/4 and 1, respectively, which reproduces the rapid decrease of the adatom dipole with increasing θ. Although the

induced dipole within the sphere is less than half of the total adatom dipole shown in Fig.10, one can obtain larger absolute values by increasing the sphere radius.

There is a qualitative difference in $\mu(\varepsilon,\theta)$ between finite and zero θ. The positive sign of $\mu(\varepsilon,\theta)$ at θ=0 below the vacuum level (the work function of the jellium 3.8eV) means attenuation of one electron wave functions into the vacuum region, which is seen as its inward polarization within the sphere. Its sudden drop at the vacuum level comes from the corresponding change of the dipole matrix elements. On the other hand, $\mu(\varepsilon,\theta)$ for a finite θ shows quite different behaviors as a function of ε. Its sign changes rapidly near the Fermi level E_F. It is seen from the definition eq.(4.12) that the negative sharp peaks above E_F indicates the strong mixing of the s and p_z componemts of wave functions. As is shown before, these correspond to outward polarized antibonding states mainly contributed by the Na 3s and $3p_z$ orbitals. The positive part in $\mu(\varepsilon,\theta)$ below E_F designates the inward plarization of the one electron states, which thus results in the build-up of the electron density in the interface (bond charge) shown in Fig.7. By comparing Figs.16 and 18, one finds a close similarity between the bond order and dipole densities. The small deviation of the positive-negative boundary from E_F as well as broadening of the peaks above E_F with increasing θ are common characteristic features observed both in the dipole and bond order densities.

In the present first-principles calculation, there are no base functions for the overlayer and substrate states as used in

the discussions of Section 2. So the adatom induced dipole cannot be uniquely divided into the charge transfer and hybridization terms. However, as discussed in Section 2, the close similarity between the dipole and bond order densities as well as its characteristic energy dependence strongly suggests that the adatom induced dipole dominantly originates from the hybridization rather than the charge transfer. The fact that the build-up of the electron density which is responsible for the adatom dipole appears at the interface as a *covalent* bond charge supports the crucial role of the adatom-substrate hybridization term to the induced dipole. It was shown in the analysis of the partial DOS that the Na induced p_z states are primarily located above E_F. Therefore, from the definition eq.(4.12), (eq.(4.12) extracts the dipole density coming from hybridization of the s and p_z components of wave functions.), it may be quite natural to interpret that the adatom induced dipole is caused by the hybridization of the partially filled Na 3s states and the p_z components of the substrate wave functions within the sphere.

4.6 On the θ dependence of the adatom dipole

Negligibly small depolarization shifts of adatom valence states below E_F as well as the above analysis of bond order and dipole densities distinctly demonstrates that the adatom dipole cannot be explained in terms of the conventional θ dependent diagonal charge transfer. The adatom dipole should be rather attributed to the off-diagonal hybridization term reflecting the strong covalent interaction of the adatom and substrate metal (see eq.(2.14).). Then how should one interpret a rapid decrease of

the dipole moment with increasing θ which is correctly reproduced in the present calculation? One reason is the weakening of the adatom-substrate bond as exemplified by $B_{as}(\theta)$ as well as adatom binding energies. The Na binding energy at θ=1 is ~50% of the corresponding one at θ=1/5. Secondly, the dipole matrix element $\mu_{\beta\alpha}$ in eq.(2.14) may become significantly smaller with increasing θ by the following reason: with increasing θ, the weight of $|\varphi_\alpha(r)|^2$ in the Na-Na bond region becomes larger at the expence of that in vacuum sides, and as a result, the major depletion area in the hybridization density $\sum_{\alpha,\beta}\langle C_\alpha^+ C_\beta\rangle \varphi_\alpha^*(r)\varphi_\beta(r)$+c.c. moves from the outside of a Na to the Na-Na bond region. This effect appears as a rapid decrease of the effective dipole distance $D_{eff}(\theta)$. The calculated $D_{eff}(\theta)$ at θ=1 is ~60% of that at θ=1/5. If the above two effects are naively multiplied, the adatom dipole at θ=1 is estimated as ~30% (0.5x0.6) of that at θ=1/5, which is in agreement with the calculated ones.

5. *Results and discussions for the Al(001) substrate*

Calculated results for the Na covered Al(001) surfaces are presented in a parallel way to those for the jellium substrate. The main interest here concerns whether conclusions on the alkali-metal adatom electronic structure obtained for the jellium substrate should be qualitatively revised or not when the jellium is replaced by a realistic metal substrate made of discrete atoms. As described in Section 3, the Al(001) substrate is represented by an unrelaxed five-layer slab. Na adatoms sit on four fold hollow sites, where the perpendicular distance between nearest Na

and Al atoms is fixed to a value determined by LEED [67,68]. The calculated work function of Al(001), 4.7eV is in fair agreement with an experimental value 4.41±0.03eV of Grepstad *et al.* [70]. Wimmer *et al.* [71] obtained a better theoretical value 4.53eV in their FLAPW calculation by increasing the Al(001) layer number from five to nine.

Before describing the calculated results, I should refer to a previous theoretical work on Na/Al(001) by Benesh *et al.* [39], who studied the electronic structure of a Na covered Al(001) surface by the LAPW method (the non-spherical part of the potential within muffin-tin spheres was neglected in their calculation.). Al(001) was modeled by a three layer slab, and the Na overlayer was assumed to form an experimentally observed c(2x2) (θ=1/2 in units of Al(001) layers) structure. The work function lowering by the Na adlayer was reproduced by their model. The calculated work functions were 5.45 and 2.46eV for the bare and Na covered Al(001) surfaces, respectively. The three-layer slab approximation for Al(001) was insufficient and the work function for Al(001) is overestimated by more than 1eV. By comparing the local DOS within Na muffin-tin spheres with that of an isolated Na on the jellium given by Lang and Williams [40], they concluded that Na adatoms are ionic even at θ=1/2. However, if Gurney's picture is correct, the local DOS of a Na at θ=1/2 should be considerably different from that at low θ limit, since the adatom dipole is much smaller at θ=1/2. Thus, in principle, they should have had a doubt on the direct relationship between the induced dipole and the location of adatom valence states.

5.1 Difference charge

First, I discuss the charge redistribution due to the interaction between the adatom and substrate which leads to the work function lowering. Fig.19 shows the calculated difference charge of the Na covered Al(001) surfaces for (a) c(2x2) (θ=1/2) (b) p(2x2) (θ=1/4) and (c) $(\sqrt{8}x\sqrt{8})R45^{\circ}$ (θ=1/8) coverages on a vertical cut plane which includes a Na and two of its nearest neighbor Al atoms. The shaded and hatched areas designate the regions where $\delta\rho(r,\theta)\geqq 0.001 a.u.$ (accumulation of the electron density) and $\delta\rho(r,\theta)\leqq -0.0005 a.u.$ (depletion of the electron density), respectively. The dash-dotted curves correspond to $\delta\rho(r,\theta)=0$. Na and Al atoms are shown by filled circles. Apart from the counter-polarization of core orbitals which is absent in the present pseudopotential calculation, $\delta\rho(r,\theta)$ at θ=1/2 is very similar to that of Cs/W(001) at c(2x2) coverage given by Wimmer *et al.* [34] and also to that of Cs/Mo(001) by Chubb *et al.* [38]. The effect, if treated by all electron calculations, would be smaller in the present case because of the deeper energy level and smaller orbital extention of Na $2p_z$ as compared with Cs $5p_z$. For lower coverages, kidney-shaped charge depletions appear on the vacuum side of a Na as in the case of alkali-metal/jellium surfaces.

In the case of jellium substrates, there was a little ambiguity in whether the build-up of the electron density occurs in the substrate region or at the interface of the adatom and substrate because of the absence of discrete atoms in the substrate side. Fig.19 clearly answers to the question. The maximum in

the build-up of the electron density appears at the midpoint between the nearest neighbor Na and Al atoms, while the electron density decreases in the area around Al atoms. As will be discussed later, the charge accumulation at the interface should be again regarded as a bond charge due to a strong covalent interaction of the adatom and substrate rather than the charge transfer.

Although the essential features seen in $\delta\rho(r,\theta)$ are common to jellium and Al(001) substrates, there is some differences in its detail. For the jellium substrate, there is one to one correspondence between the adatom and bond charge, whereas, for Al(001), the bond charge contour has four maxima around a given Na, each for one of the four nearest neighbor Al-Na bonds. It was found for the jellium that the bond charge contour map is almost independent of θ from θ=1/5 to 1. On the other hand, for Al(001), the contour map at θ=1/2 looks considerably different from those for lower θ. For θ=1/4 and 1/8, Al atoms around a Na contribute to only one Na-Al bond, while they make two Na-Al bonds at θ=1/2. This difference in the local atomic structure around an Al leads to the modification of bond charge contours.

5.2 Work function change and adatom dipole moment

The calculated work function and adatom dipole are shown as a function of θ in Fig.20. The adatom dipole becomes rapidly smaller with increasing θ. Correspondingly, the work function takes a minium for the p(2x2) structure (θ=1/4) as observed for Cs/W(001) [35]. Porteus [66] measured the work function change of Na covered Al(001) and Al(111) surfaces as a function of θ. He

found a saturation in the work function lowering at higher θ as in many other systems, but did not observed an absolute minimum point for both Al(001) and Al(111). However, in recent experiments of the alkali-metal adsorption on Al(111) [6,7], a minimum in the work function was clearly observed. Therefore a successive experiment is necessay in order to examine whether the work function does not really take a minimum for the Al(001) substrate. In the present calculation, p(2x2) was assumed for θ=1/4. This structure corresponds to a strong atomic correlation limit in the sense that all the nearest adatoms of a given Na sit on the 3rd nearest hollow sites, with the 1st and 2nd hollow sites being unoccupied. If the atomic correlation is weaker in a real Na/Al(001) at θ=1/4, part of adatoms would occupy the neighboring hollow sites. It might happen that adatoms form a small domain of the c(2x2) structure. In such a case, due to increasead interaction among adatoms, the averaged induced dipole per an adatom may become smaller than that of an ideal p(2x2) structure. Hence, although it is not so clear at present whether the work function does not take a minimum value on Na/Al(001), the prsent result certainly emphasizes the work function minimum somewhat too much.

5.3 On the origin of the work function minimum

Among various electronic properties observed in alkali-metal adsorption systems, the existence of a minimum in the measured work function has especially attracted much attention of theorists. In fact, being so generally observed, it may be natural to believe in some special reason of the minimum which could be understood

with a *qualitative* argument based on simplified models and thus indifferent to *quantitative* aspects such as the detail of the electron density profile. The work function change $\Delta\Phi(\theta)$ due to the alkali-metal adsorption is proportiol to $\theta d(\theta)$. Therefore, the appearance of an extreme in $\Delta\Phi(\theta)$ requires that the adatom dipole $d(\theta)$ becomes smaller at least faster than θ^{-1}. Nevertheless, the condition alone does not insure that $\Delta\Phi(\theta)$ becomes a maximum before the monolayer coverage. Since $\Delta\Phi(\theta)$ is governed only by one scalar $d(\theta)$, one may tend to think that it is feasible to derive an approximate expression of $d(\theta)$ analytically. In fact, in the previous Newns-Anderson model aporoach, the adatom dipole $d(\theta)$ is directly related with one parameter, the occupancy of the s resonance $\langle C_s^{+}C_s \rangle$ whose analytical expression is easy to derive. Thus theorists have advanced seemingly plausible arguments with respect to the work function minimum so far. However, actually, the scalar quantity $d(\theta)$ is calculated only through the full knoledge of $\delta\rho(r,\theta)$ which has infinite degrees of freedom in the three dimensional space.

Fig.21 shows the planar average of the difference charge $\delta\rho_{ave}(z,\theta)$ at θ=1/2 (dashed lines) and θ=1/4 (full lines), which is related with the work function change by eq.(4.4). Its amplitude both in the Na-Al bond region and in the depletion area in the vacuum side of a Na is larger for the c(2x2) coverage. This seems to imply that $\Delta\Phi(\theta)$ at θ=1/2 would exceed that at θ=1/4 if the change in the profile of $\delta\rho_{ave}(z,\theta)$ with increasing θ could be ignored. However, the calculated work function change becomes

a maximum at θ=1/4. How should one explain it? See the tail region of $\delta\rho_{ave}(z,\theta)$ in the vacuum side. Although its maximum amplitude in the depletion area at θ=1/4 is smaller than the corresponding one at θ=1/2, $\delta\rho_{ave}(z,\theta)$ at θ=1/4 has a longer tail into the vacuum than that at θ=1/2. This longer tail in $\delta\rho_{ave}(z,\theta)$ then results in a larger dipole at θ=1/4 and finally the work function minimum at the p(2x2) structure. The shrinkage of the vacuum tail in $\delta\rho_{ave}(z,\theta)$ is quantitatively estimated from the effective dipole distance $D_{eff}(\theta)$. The calculated $D_{eff}(\theta)$ are 2.3 and 1.6a.u. at θ=1/4 and 1/2, respectively. Fig.22 shows calculated planar averages of the local part of the effective one electron potential for θ=1/2 (full lines) and θ=1/4 (dashed lines). Reflecting the longer tail of $\delta\rho_{ave}(z,\theta)$ at θ=1/4, the two potentials are inverted *far* (~10a.u.) outside the adatom, which then leads to the 0.4eV smaller work function at θ=1/4. The above argument demonstrates to what a delicate problem the appearance of the work function minimum actually belongs. The change in the work function of an order of 0.1eV is connected with that in the electron density of an order of 0.0001a.u. In other words, qualitative arguments based on an simplified view are inappropriate.

5.4 adatom valence states

The adatom induced density of states $\rho_a(\varepsilon,\theta)$ defined by eq.(4.7) is plotted in Fig.23 for the three Na coverages. The origin of the energy is E_F and the sphere radius R is chosen as 3.3a.u. The dashed curve in Fig.23(a) shows the result calculated with the plane wave cut-off energy E_{cut}=10Ry, which confirms the

convergence of the present calculation. As in the case of the jellium substrate, the spiky sharp peaks at θ=1/8 change to broad structures at θ=1/2 by the overlap of neighboring adatom orbitals. There is again no appreciable downward shift of the adatom states with increasing θ for occupied states. This behavior is understood from the change in the electrostatic potential $\delta\varphi_{ele}(r,\theta)$ defined by eq.(4.3). The calculated $\delta\varphi_{ele}(r,\theta)$ for three coverages is drawn in Fig.24 on the same vertical cut plane as in Fig.21. $\delta\varphi_{ele}(r,\theta)$ at a Na site as measured from the interior of Al(001) are -0.25, -0.40 and -0.37eV for θ=1/8, 1/4 and 1/2, respectively, which is consistent with the negligibly small depolarization shift of the adatom valence states below E_F. The calculated $n_a^R(\theta)$ are 0.39, 0.40 and 0.45 electrons for θ=1/8, 1/4 and 1/2, respectively. The smaller $n_a^R(\theta)$ as compared with those for the jellium in the last section merely stems from the smaller choice of R and does not mean that adatoms are more ionic. In fact, $n_a^R(\theta)$ increases to 0.46, 0.48 and 0.53 electrons for each θ by the choice of R=3.5a.u. $n_a^R(\theta)$ becomes larger with increasing θ by ~0.05 electrons. However, this does not imply a larger ionicity for lower θ, since $n_a^R(\theta)$ is always larger than the corresponding $n_{iso}^R(\theta)$. For example, $n_a^R(\theta$=1/8)=0.39, 0.46 and 0.64 electrons for R=3.3, 3.5 and 4.0a.u., respectively, while corresponding $n_{iso}^R(\theta$=1/8)=0.36, 0.41 and 0.55 electrons for each R. The adatom region is essentially neutral irrespective of θ once the electron density is integrated within the sphere.

Figs.25-27 show the s, p_x (p_y) and p_z partial DOS of a Na

adatom defined by eq.(4.9) for three coverages, respectively. The sphere radius 3.3a.u. is the same as in Fig.23. The thick and dashed curves indicate the first and second terms of the right hand side of eq.(4.9), and thus the l-th partial DOS induced by a Na is given by the difference of the thick and dashed curves. Qualitative aspects of the results are the same as those for the jellium substrate in the last section, except that Na induced states below E_F is contributed by the Na $3p_x$ and $3p_y$ components besides Na 3s with a larger weight as compared with that for the jellium substrate. It is considered that the four fold symmetry of a Na site on Al(001) leads to larger interaction of the substrate and Na $3p_x$ (p_y) orbitals, which then results in its larger filling. On the other hand, Na $3p_z$ state is primarily located above E_F irrespective of θ, indicating that the adatom dipole is *not* caused by the mixing of the Na 3s and $3p_z$ states. The onset of the Na $3p_z$ peak shifts downward with increasing θ, which is partly due to the increase in the Na $3p_z$ band width. At the same time, in contrast to the case of Na 3s, there might be some lowering in the $3p_z$ level by the following reason: as will be shown later, Na $3p_z$ is partially hybridized with Na 3s and results in an outward polarized orbital with its larger weight on the vacuum side of a Na rather than the interface side; in this case, the orbital feels a potential lowering on the vacuum side due to the charge redistribution and might shift downward to some degree. If the observed characteristic loss peak in EELS experiments [7,9,10,14-20] is due to the excitation from the partially filled Na 3s to unoccupied $3p_z$ states as discussed in

the last section, the downward shift of the onset of the Na $3p_z$ band may lead to decrease in the loss energy with increasing θ. Such tendency was really observed in previous experiments [9,10]. Aruga *et al.* [9] measured the energy of the K induced loss peak on Cu(001) as a function of θ. The loss energy decreased for lower θ, while it turns to increase at higher θ where the interaction among adatoms becomes large. The increase in the loss energy at higer θ may be interpreted as due to a plasmon effect rather than the increase in the individual excitation energy.

5.5 *Bond order and dipole densities*

In order to clarify the nature of the Al-Na bonding directly, the bond order density defined by eq.(4.10) is calculated by choosing r_1 and r_2 at the nearest neighbor Na and Al sites. The caclulated $\beta_{as}(\varepsilon,\theta)$ for three coverages are shown in Fig.28. The positive and negative parts correspond to the bonding and antibonding states, respectively. As in the case of the jellium substrate, qualitative features of $\beta_{as}(\varepsilon,\theta)$ are characteristic of the off-diagonall Green function eq.(2.17). The strong antibonding peak slightly above E_F which is sharpened with decreasing θ originates from Na $3p_z$ partially admixed with Na 3s. The bonding-antibonding boundary coincides almost perfectly with E_F at θ=1/8, indicating strong covalency in the Na-Al bond by the maximum use of the bonding states. The Na-Al bond should be regarded as *covalent* rather than *ionic* one. The build-up of the electron density in the midpoint between the neighboring Al-Na atoms shown in Fig.19 is a natural consequence of this covalency. With increasing θ, E_F slightly moves into the antibonding regions,

and consequently the bond order $B_{as}(\theta)$ defined by eq.(4.11) decreases by ~15%, indicating weakening of the Na-Al bond. The adsorption energies of a Na calculated as the total energy of Na/Al(001) minus those of the bare Al(001) and isolated Na layer are 2.9, 2.5 and 2.2eV for θ=1/8, 1/4 and 1/2, respectively. As described in Introduction, such weakening of the adatom-substrate bond with increasing θ was observed in many experiments since the pioneer work of Taylor and Langmuir [3,21,23]. The calculated adsorption energies at lower θ are comparable with typical experimental values, for instance, 2.83eV for Cs/W [3], 2.6eV for Na/W(110) and 2.8eV for K/W(110) [72]. On the other hand, the calculated adsorption energies for the jellium substrate in the last section were considerably smaller than them. It may be concluded that by recovering the discreteness in the substrate, adatoms can make more localized and firmer covalent bonds with neighboring substrate atoms, which results in larger adatom binding energies.

Fig.28 shows the calculated dipole densities defined by eq.(4.12) for three Na coverages in the same sphere as in Fig.25. As in the case of the jellium substrate, the most important is the close similarity between the bond order density in Fig.26 and dipole density in Fig.27. The dipole density rapidly changes its sign near E_F, and the boundary shifts slightly into the bonding states with increasing θ. This similarity indicates that the origin of the outward (inward) dipole density below (above) E_F is the accumulation (depletion) of the electron density in the bond region which reflects bonding (antibonding) character of one

electron wave functions. Hence the adatom dipole which lowers the work function should be again interpreted as a result of the strong covalent interaction of the adatom and substrate rather than ionization of adatoms.

6. Summary and conclusion

Alkali-metal adsorption on metal surfaces has been studied intensively for more than sixty years as one of the simplest chemisorption systems showing a variety of electronic properties. They include, for example, characteristic work function variation with adatom coverage θ and appearance of overlayer plasmon peaks in electron energy loss spectra at higher θ. In 1935, Gurney proposed a simple picture which explains a large adatom induced dipole at low θ and its rapid decrease with increasing θ. He attributed the adatom dipole to ionicity of adatoms, and its subsequent decrease to adatom neutralization due to the downward shift of the adatom s resonance caused by the depolarization field. This simple and physically appealing picture has been widely accepted for more than half a century as a basic concept in the alkali-metal adsorption on metal surfaces. While divergent number of experimental studies concentrated on this system because of its importance in practical applications such as cathode technology and catalytic reactions, theoretical works remained within the level of phenomenological approaches based on Gurney's classical picture. Recently, there appeared several works which threw a doubt on this oversimplified view from both experimental and theoretical sides. The purpose of the present study was to

elucidate the electronic structure of adatoms as well as nature of the adatom-substrate bonding as a function of θ by a first-principles calculation, and to reestablish a correct picture for the alkali-metal adsorption.

The present calculation was based on the local density approximation within the density functional theory combined with the ab initio norm-conserving pseudopotential. In previous theoretical works, two dimensional periodicity of substrates unabled arbitrary choice of the adatom coverage and structure. This severe restriction is removed in the present work by using the "jellium" as the metal substrate. In the latter half of the present study, I retrieved its discreteness by employing Al(001). It was confirmed that important conclusions obtained with the jellium substrate suffer no rectifications even with discrete substrate atoms.

As Gurney's view seems too much generally accepted at present, I reviewed in Section 2 previous phenomenological approaches and showed how their apparent success was based on unreliable and unphysical assumptions. Ionization of an adatom by the image effect and its subsequent neutralization by the depolarization field are surely attractive devices to explain the observed θ dependence of the adatom dipole. However, it is unfortunate that theorists did not dare to check that they are surely the case in *real* materials, having no recognition that it is the most important process that material scientists should attack. In the latter half of Section 2, I gave general discussions of the adatom dipole using a tight-binding model, and

pointed out that the off-diagonal hybridization term, which is a measure of covalency in the adatom-substrate bonding, should also contribute to the induced dipole moment besides the conventional diagonal charge transfer one. The charge transfer induced dipole disappears when the Fermi level E_F coincides with the center of the adatom s resonance, whereas the hybridization induced dipole becomes maximum in such a case by the maximum use of bonding states. The origin of the latter is build-up of the electron density in the interface region (bond charge).

The calculated results for the jellium substrate was presented in Section 4. A jellium slab with r_s=2.1a.u. was chosen so as to simulate high-density metal substrates, and alkali-metal adatoms were assumed to form a square lattice whose lattice constant diminishes as $\theta^{-1/2}$ with increasing θ. The calculated work function reproduced the observed rapid lowering at initial θ and subsequent minimum very well. However, it was shown that the charge redistribution by the interaction of the adatom and substrate and its θ dependence are far from the point-charge transfer picture assumed in previous theories. Consequently, the change in the electrostatic potential at adatom sites was found almost independent of θ. From the standpoint of Gurney's picture, this result is fatally serious, since θ dependence of the adatom dipole is wholly attributed to the depolarization energy. I further calculated the adatom density of states (DOS) as a function of θ, and demonstrated that there is little θ dependence in it for occupied states. The adatom region was found essentially neutral irrespective of θ. In order to clarify the nature of the

adatom-substrate bond and adatom dipole more directly, the bond order and dipole densities were calculated. It was shown that the adatom-substrate bond has strong covalency even at low θ by the maximum use of bonding states. The bonding-antibonding boundary coincided fairly well with the Fermi level at lower θ, which was contradictory with the ionic adsorption picture. The calculated dipole density showed a close similarity to the corresponding bond order density, which, together with the discussion in Section 2, implied that the adatom dipole results from strong hybridization of the adatom and substrate states rather than charge transfer. The θ dependence of the adatom dipole was attributed to a weakening of covalency in the adatom-substrate bond with increasing θ as well as a significant decrease in the dipole matrix elements.

The results for the Al(001) substrate was given in Section 5 in a parallel way to those for the jellium. The calculation was done for three coverages assuming (i) c(2x2) (θ=1/2) (ii) p(2x2) (θ=1/4) and (iii) ($\sqrt{8}$x$\sqrt{8}$)R45° (θ=1/8) structures for Na overlayers. The calculated charge redistribution, adatom density of states, bond order density as well as the dipole density confirmed that all the conclusions drawn for the jellium substrate hold true even if the jellium is replaced by a realistic metal substrate. Moreover, it was shown that the too much smaller binding energies of adatoms on the jellium were improved to values comparable with experiments by recovering discrete substrate atoms.

The discussions on the dipole in Section 2 might give the

reader an impression that which of the hybridization and charge transfer is dominant in the total adatom dipole is not physically so meaningful, since to divide the dipole into the two contributions depends on the base functions for adatom and substrate states. However, it should be noted that the concept such as the adatom s resonance and its bonding-antibonding boundary is a complete physical entity, which has nothing to do with a specific choice of the base functions. As far as the base functions are chosen so that they may be physically meaningful (for example, a s-orbital located artificially in the vaccum side of an adatom should not be called as the *alkali-metal* s orbital.), I believe that my assignment of the adatom dipole to the adatom-substrate hybridization rather than the adatom ionization is a unique one that can explain all of the calculated results in a consistent way. In this regard, it should be emphasized that the present calculation is exact within the local density functional theory and thus the results themselves are completely free from the problem of interpretation. The new picture for the alkali-metal adsorption presented in the present work is further supported by recent experimental works which threw a doubt on the essence of Gurney's classical picture such as the direct relationship between the adatom dipole and ionicity, and depolarization shift of adatom levels with increasing θ.

Most of the previous experimental studies on the alkali-metal adsorption employed transition metals with localized d bands as metal substrates. As stated in Introduction, there are no qualitative differences in various observed phenomena between

transition and simple metal substrates. Therefore it is expected that the conclusions in the present work may be also applicable to transition metal substrates. At least, at a high θ limit, the calculation of Wimmer *et al.* for Cs/W(001) lead to the same conclusion as for the origin of the adatom dipole. However, it may be important to check if the localized d bands of transition metals may not affect the conclusion with respect to the adatom dipole even at lower θ.

The initial motivation with which I began to work on the alkali-metal/jellium system was to clarify systematically the θ and adatom dependence of the observed alkali-metal induced peak in electron enegy loss spectra rather than ground state properties such as the work function lowering. The tight-binding Hamiltonian combined with the random phase approximation (RPA), which I had worked on until then, could not describe the detailed electronic structure of the overlayer. The alkali-metal/jellium system was introduced as the simplest one fit for the purpose. I had no doubt on Gurney's picture at that time, but subsequent studies until now have changed my view on the alkali-metal adsorption. In the next step, I would like to clarify the nature of the alkali-metal overlayer plasmons microscopically by calculating electron energy loss functions using electron energy bands and wave functions obtained in the present work.

Acknoledgment

I am grateful to Professor K. Terakura for many discussions and critical reading of the manuscript. The numerical calculations were done at the computer centers of University of Tokyo and Institute for Molecular Science. This work is partially supported by a Grand-in-Aid for Scientific Research on Priority Areas by the Ministry of the Education, Science and Culture.

References

[1] K.H. Kingdon and I. Langmuir, Phys. Rev. 21, 380(1923).

[2] I. Langmuir and K.H. Kingdon, Proc. Roy. Soc. (London) A107, 61(1925).

[3] J.B. Taylor and I. Langmuir, Phys. Rev. 44, 423(1933).

[4] For example, J.P. Muscat and D.M. Newns, Prog. Surf. Sci. 9, 1(1978); N.D. Lang, in *Theory of the inhomogeneous electron gas* edited by S. Lundqvist and N.H. March (Plenum Press, New York, 1983).

[5] G.S. Tompa, M. Seidl, W.C. Ermler and W.E. Carr, Surf. Sci. 185, L453(1987).

[6] D. Heskett, K.-H. Frank, E.E. Koch and H.-J. Freund, Phys. Rev. B36, 1276(1987).

[7] A. Hohlfeld, M. Sunjic and K. Horn, J. Vac. Sci. Technol. A5, 679(1987).

[8] H. Tochihara, Surf. Sci. 126, 523(1983); T. Aruga, H. Tochihara and Y. Murata, Phys. Rev. Lett. 53, 372(1984); E.M. Oellig and R. Miranda, Surf. Sci. 177, L947(1986).

[9] T. Aruga, H. Tochihara and Y. Murata, Phys. Rev. B34, 8237(1986).

[10] J. Cousty, R. Riwan and P. Soukiassian, J. Phisique (Paris) 46, 1693(1985).

[11] J. Topping, Proc. Roy. Soc. (London), A114, 67(1927).

[12] R.W. Gurney, Phys. Rev. 47, 479(1935).

[13] J.M. Muscat and D.M. Newns, J. Phys. C7, 2630(1974).

[14] A.U. MacRae, K. Müller, J.J. Lander, J. Morrison and J.C. Phillips, Phys. Rev. Lett. 22, 1048(1969).

[15] S. Thomas and T.W. Haas, Solid. State. Commun. 11, 193(1972); S. Andersson and U. Jostell, Surf. Sci. 46, 625(1974); S.A. Lindgren and L. Walldén, Phys. Rev. B22, 5969(1980).

[16] U. Jostell, Surf. Sci. 82, 333(1979).

[17] F. Stern, Phys. Rev. Lett. 18, 546(1967).

[18] D.M. Newns, Phys. Lett. 39A, 341(1972).

[19] M. Nakayama, T. kato and K. Ohtomi, Solid. State. Commun. 50, 409(1984).

[20] H. Ishida and M. Tsukada, Surf. Sci. 169, 225(1986).

[21] T. Aruga, H. Tochihara and Y. Murata, Surf. Sci. 158, 490(1985).

[22] A.D. Novaco and J.P. McTague, Phys. Rev. Lett. 38, 1286(1977).

[23] G. Besold, Th. Schaffroth, K. Heinz, G. Schmidt and K. Müller, Surf. Sci. 189/190, 252(1987).

[24] L.D. Roelofs and D.L. Kriebel, J. Phys. C20, 2937(1987).

[25] H.P. Bonzel, J. Vac. Sci. Technol. A2, 866(1984).

[26] G. Ertl, M. Weiss and S.B. Lee, Chem. Phys. Lett. 60, 391(1979).

[27] U. Seip, I.C. Basignana, J. Küppers and G. Ertl, Surf. Sci. 160, 400(1985).

[28] E.L. Garfunkel, J.E. Crowell and G.A. Somorjai, J. Phys. Chem. 86, 310(1982).

[29] M.-L. Ernst-vidalis, M. Kamaratos and C. Papageorgopoulos, Surf. Sci. 189/190, 276(1987).

[30] P.J. Feibelman and D.R. Hamann, Phys. Rev. Lett. 52,

61(1984); Surf. Sci. 149, 48(1985).

[31] N.D. Lang, S. Holloway and J.K. Nørskov, Surf. Sci. 150, 24(1985).

[32] B. Woratschek, W. Sesselmann, J. Küppers and G. Ertl, Phys. Rev. Lett. 55, 1231(1985).

[33] S.Kono, private communication.

[34] E. Wimmer, A.J. Freeman, J.R. Hiskes and A.M. Karo, Phys. Rev. B28, 3074(1983).

[35] C.A. Papageorgopoulos and J.M. Chen, Surf. Sci. 39, 283(1973).

[36] J.E. Inglesfield, Surf. Sci. 188, L701(1987).

[37] H. Ishida, N. Shima and M. Tsukada, Phys. Rev. B32, 6246(1985); H. Ishida, K. Terakura and M.Tsukada, Solid Commun. 59, 365(1986).

[38] S.R. Chubb, E. Wimmer, A.J. Freeman, J.R. Hiskes and A.M. Karo, Phys. Rev. B36, 4112(1987).

[39] G.A. Benesh, H. Krakauer, U.E. Ellis and M. Posternak, Surf. Sci. 104, 599(1981).

[40] N.D. Lang and A.R. Williams, Phys. Rev. B18, 616(1978).

[41] N.D. Lang, Phys. Rev. B4, 4234(1971).

[42] P.W. Anderson, Phys. Rev. 124, 41(1961).

[43] D.M. Newns, Phys. Rev. 178, 1123(1969).

[44] N.D. Lang and W. Kohn, Phys. Rev. B1, 4555(1970).

[45] P.A. Serena, J.M. Soler, N. Garcia and I.P. Batra, Phys. Rev. B36, 3452(1987).

[46] C.A. Nicolaides and A.N. Andriotis, Int. J. Quantum Chem. 23, 561(1983).

[47] P.A. Serena and N. Garcia, Surf. Sci. 189/190, 232(1987).

[48] W. Ning, C. Kailai and W. Dingsheng, Phys. Rev. Lett. 56, 2759(1986).

[49] This observation is based on my first-principles electronic structure calculation for Al/Na(001) at θ=1/2 (in units of Na(001) layers), where the distance between nearest neighbor Al adatoms is 10.8a.u. The calculated work function 2.9eV of the five-layer Na(001) film increased to 4.1eV by the Al adsorption.

[50] A.G. Eguiluz and A. Campbell, Phys. Rev. B31, 7572(1985).

[51] J.P. Muscat and D.M. Newns, Solid State Commun. 11, 737(1972).

[52] J.P. Muscat and I.P. Batra, Phys. Rev. B34, 2889(1986).

[53] L.D. Schmidt and R.J. Gomer, J. Chem. Phys. 45, 1605(1966).

[54] A.J. Benett, J. Chem. Phys. 49, 1340(1968).

[55] J.W. Gadzuk, Surf. Sci. 6, 133(1967).

[56] A.C. Hewson and D.M. Newns, Jpn. J. Appl. Phys. Suppl. Pt.2, 121(1974).

[57] N.D. Lang and A.R. Williams, Phys. Rev. B16, 2408(1977).

[58] H. Ishida, N. Shima and M. Tsukada, Surf. Sci. 158, 438(1985).

[59] For example, K. Terakura, J. Phys. F7, 1773(1977).

[60] P. Hohenberg and W. Kohn, Phys. Rev. 136, B864(1964).

[61] W. Kohn and L.J. Sham, Phys. Rev. 140, A1133(1965).

[62] E.P. Wigner, Phys. Rev. 46, 1002(1938).

[63] G.B. Bachelet, D.R. Hamann and M. Schlüter, Phys. Rev.

B26, 4199(1982).

[64] J. Ihm, A. Zunger and M.L. Cohen, J. Phys. C12, 4409(1979).

[65] G. Lehmann and M. Taut, Phys. Stat. Sol. b54, 469(1972).

[66] J.O. Porteus, Surf. Sci. 41, 515(1974).

[67] M. Van Hove, S.Y. Tong and N. Stoner, Surf. Sci. 54, 259(1976).

[68] B.A. Hutchins, T.N. Rhodin and J.E. Demuth, Surf. Sci. 54, 419(1976).

[69] For example, H. Ibach and D.L. Mills, *Electron Energy Loss Spectroscopy and Surface Vibrations* (Academic Press, New York, 1982).

[70] T.K. Grepstad, P.O. Gartland and B.T. Slagsvold, Surf. Sci. 57, 348(1976).

[71] E. Wimmer, M. Weinart, A.J. Freeman and H. Krakauer, Phys, Rev. B24, 2292(1981).

[72] C.J. Todd and T.N. Rhodin, Surf. Sci. 42, 109(1974).

Figure Caption

Fig.1 Measured work function variations with the increasing adatom coverage (θ) for (a) Cs/Al(111), (b) Na/W(001) and (c) K/Cu(001).

Fig.2 Schematic energy diagram of the alkali-metal adatom s resonance originally given by Gurney [12] at (a) low θ and (b) high θ limit.

Fig.3 (a) charge transfer and (b) hybridization induced dipole moments as a function of the substrate Fermi level (E_F) relative to the center of the alkali-metal adatom s resonance.

Fig.4 Slab geometry used for the electronic structure calculation of the alkali-metal overlayers on the jellium surface.

Fig.5 The structures of the Na overlayers on Al(001). Na and top-layer Al atoms are indicated by larger and smaller circles, respectively. (a) c(2x2) (θ=1/2), (b) p(2x2) (θ=1/4) and (c) ($\sqrt{8}$x$\sqrt{8}$)R45° (θ=1/8).

Fig.6 Upper panels: calculated electron densities of the Na/jellium surfaces on a vertical cut plane passing Na atoms at every interval of $a_{//}$. The jellium edge and Na atoms are indicated by arrows and filled circles, respectively. Lower panels: corresponding difference

charges defined by eq.(4.1) on the same vertical cut plane. (a) θ=1, (b) θ=1/3.

Fig.7 Contour maps of the difference charge $\delta\rho(r)$ for the Na/jellium surfaces on the same vertical cut plane as in Fig.6. The shaded and hatched areas indicate the regions where $\delta\rho(r)\geqq 0.001(a.u.)$ and $\delta\rho(r)\leqq -0.0005(a.u.)$, respectively. The dash-dotted lines correspond to $\delta\rho(r)=0$. of $a_{//}$.

Fig.8 The change in the electrostatic potential $\delta\varphi_{ele}(r,\theta)$ due to the charge redistribution $\delta\rho(r,\theta)$ for the Na/jellium surfaces on the same vertical cut plane as in Fig.6. (a) θ=1, (b) θ=1/2, (c) θ=1/3 and (d) θ=1/5.

Fig.9 Contour maps of the difference charge $\delta\rho(r)$ for the Li/jellium surfaces on a vertical cut plane passing Li adatoms at every interval of $a_{//}$. The jellium edge and Li atoms are indicated by arrows and filled circles, respectively. The shaded and hatched areas indicate the regions where $\delta\rho(r)\geqq 0.001(a.u.)$ and $\delta\rho(r)\leqq -0.0005(a.u.)$, respectively. The dash-dotted lines correspond to $\delta\rho(r)=0$. of $a_{//}$.

Fig.10 The calculated work function and adatom dipole moment as a function of θ on the Na/jellium surface.

Fig.11 The planar average of the difference charge, $\delta\rho_{ave}(z,\theta)$

for the Na/jellium surfaces. (a) θ=1, (b) θ=1/2, (c) θ=1/3 and (d) θ=1/5.

Fig.12 The calculated adatom valence density of states $\rho_a(\varepsilon,\theta)$ for the Na/jellium surfaces. The origin of the energy is adjusted to the Fermi level (E_F) for all the coverages. (a) θ=1, (b) θ=1/2, (c) θ=1/3 and (d) θ=1/5. For the sake of comparison, $\rho_a(\varepsilon,\theta)$ at θ=1 is shown also in the panel (d) by dashed lines.

Fig.13 The calculated s partial density of states of a Na on the jellium surface. (a) θ=1, (b) θ=1/2, (c) θ=1/3 and (d) θ=1/5. The thick and dashed lines indicate the first and second terms of the right-hand side of eq.(4.9), respectively.

Fig.14 The calculated p_x partial density of states of a Na on the jellium surface. (a) θ=1, (b) θ=1/2, (c) θ=1/3 and (d) θ=1/5. The thick and dashed lines indicate the first and second terms of the right-hand side of eq.(4.9), respectively.

Fig.15 The calculated p_z partial density of states of a Na on the jellium surface. (a) θ=1, (b) θ=1/2, (c) θ=1/3 and (d) θ=1/5. The thick and dashed lines indicate the first and second terms of the right-hand side of eq.(4.9), respectively.

Fig.16 The calculated bond order density of the Na-jellium bond. (a) θ=1, (b) θ=3/4, (c) θ=1/2 and (d) θ=1/5.

Fig.17 The calculated bond order density of the nearest Na-Na bond. (a) θ=1, (b) θ=3/4, (c) θ=1/2 and (d) θ=1/5.

Fig.18 The calculated dipole density within a sphere centered at a Na site on the Na/jellium surfaces. (a) θ=1, (b) θ=3/4, (c) θ=1/2 and (d) θ=1/5. The dashed lines in panels (a)-(d) show the dipole density of the bare jellium surface (θ=0).

Fig.19 Contour maps of the difference charge $\delta\rho(r)$ for the Na/Al(001) surfaces on the vertical cut plane penetrating a Na and two of the nearest neighbor Al atoms. Al and Na atoms are indicated by filled circles. The shaded and hatched areas indicate the regions where $\delta\rho(r)\geq 0.001(a.u.)$ and $\delta\rho(r)\leq -0.0005(a.u.)$, respectively. The dash-dotted lines correspond to $\delta\rho(r)=0$. (a) c(2x2) (θ=1/2), (b) p(2x2) (θ=1/4) and (c) $(\sqrt{8}\times\sqrt{8})R45^{\circ}$ (θ=1/8 in units of Al(001) monolayers.)

Fig.20 The calculated work function and adatom dipole moment on the Na/Al(001) surface as a function of Na coverage.

Fig.21 The planar average of the difference charge, $\delta\rho_{ave}(z,\theta)$ for the Na/Al(001) surfaces at θ=1/2 (full lines) and θ=1/4

(dashed lines).

Fig.22 The planar average of the local part of the one electron potential for the Na/Al(001) surfaces at θ=1/2 (full lines) and θ=1/4 (dashed lines).

Fig.23 The calculated adatom valence density of states $\rho_a(\varepsilon,\theta)$ for the Na/Al(001) surfaces. The origin of the energy is adjusted to the Fermi level (E_F) for all the coverages. (a) θ=1/2, (b) θ=1/4, (c) θ=1/8. The dashed lines in panel (a) shows $\rho_a(\varepsilon,\theta)$ at θ=1/2 calculated with the plane wave cut-off energy 10Ry instead of 6.5Ry.

Fig.24 The change in the electrostatic potential $\delta\varphi_{ele}(r,\theta)$ due to the charge redistribution $\delta\rho(r,\theta)$ for the Na/Al(001) surfaces on the same vertical cut plane as in Fig.19.

Fig.25 The calculated s partial density of states of a Na on Al(001). (a) θ=1/2, (b) θ=1/4, and (c) θ=1/8. The thick and dashed lines indicate the first and second terms of the right-hand side of eq.(4.9), respectively.

Fig.26 The calculated p_x partial density of states of a Na on Al(001). (a) θ=12, (b) θ=1/4, (c) θ=1/8. The thick and dashed lines indicate the first and second terms of the right-hand side of eq.(4.9), respectively.

Fig.27 The calculated p_z partial density of states of a Na on Al(001). (a) θ=1/2, (b) θ=1/4, and (d) θ=1/8. The thick and dashed lines indicate the first and second terms of the right-hand side of eq.(4.9), respectively.

Fig.28 The calculated bond order density of the Na-Al bond on the Na/Al(001) surfaces. (a) θ=1/2, (b) θ=1/4, and (c) θ=1/8.

Fig.29 The calculated dipole density within a sphere centered at a Na site on the Na/Al(001) surfaces. (a) θ=1/2, (b) θ=1/4, and (c) θ=1/8.

Fig. 1

(a) Cs/Al(111)

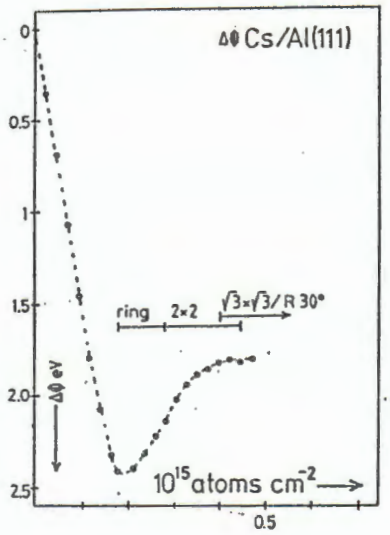

(b) Na/W(001)

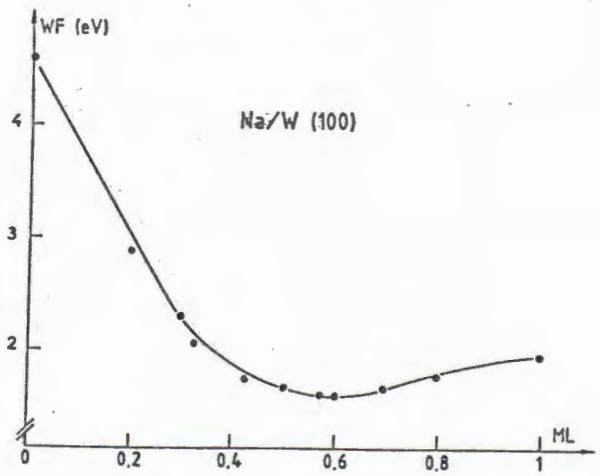

(c) K/Cu(001)

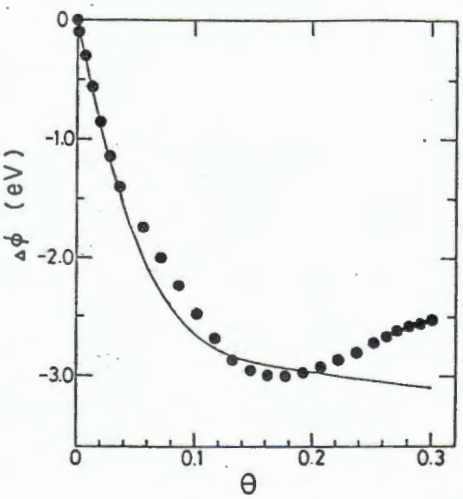

Fig. 2

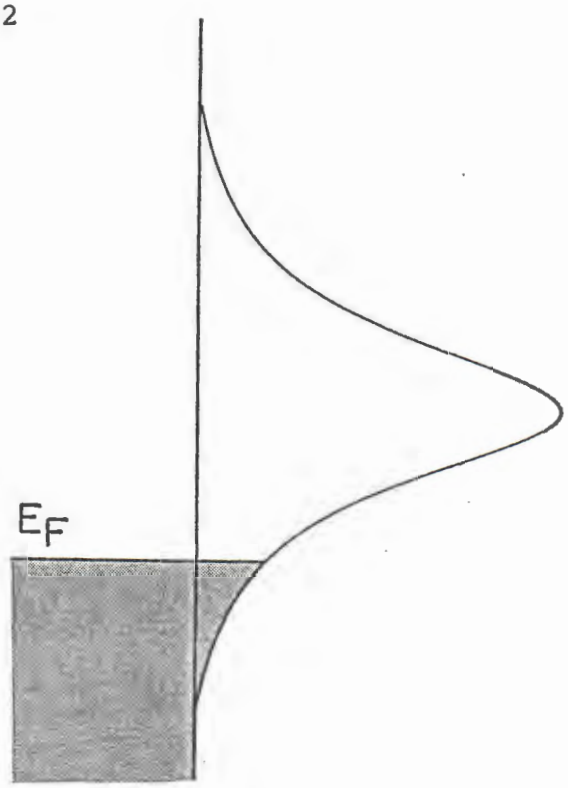

(a) $\theta \ll 1$

$n_s \ll 1$

ionic

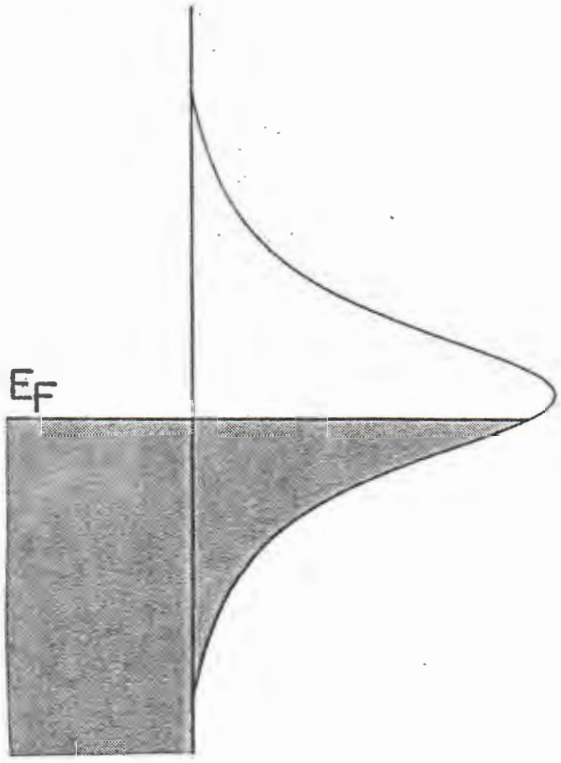

(b) $\theta \sim 1$

$n_s \sim 1$

neutral

Fig. 3

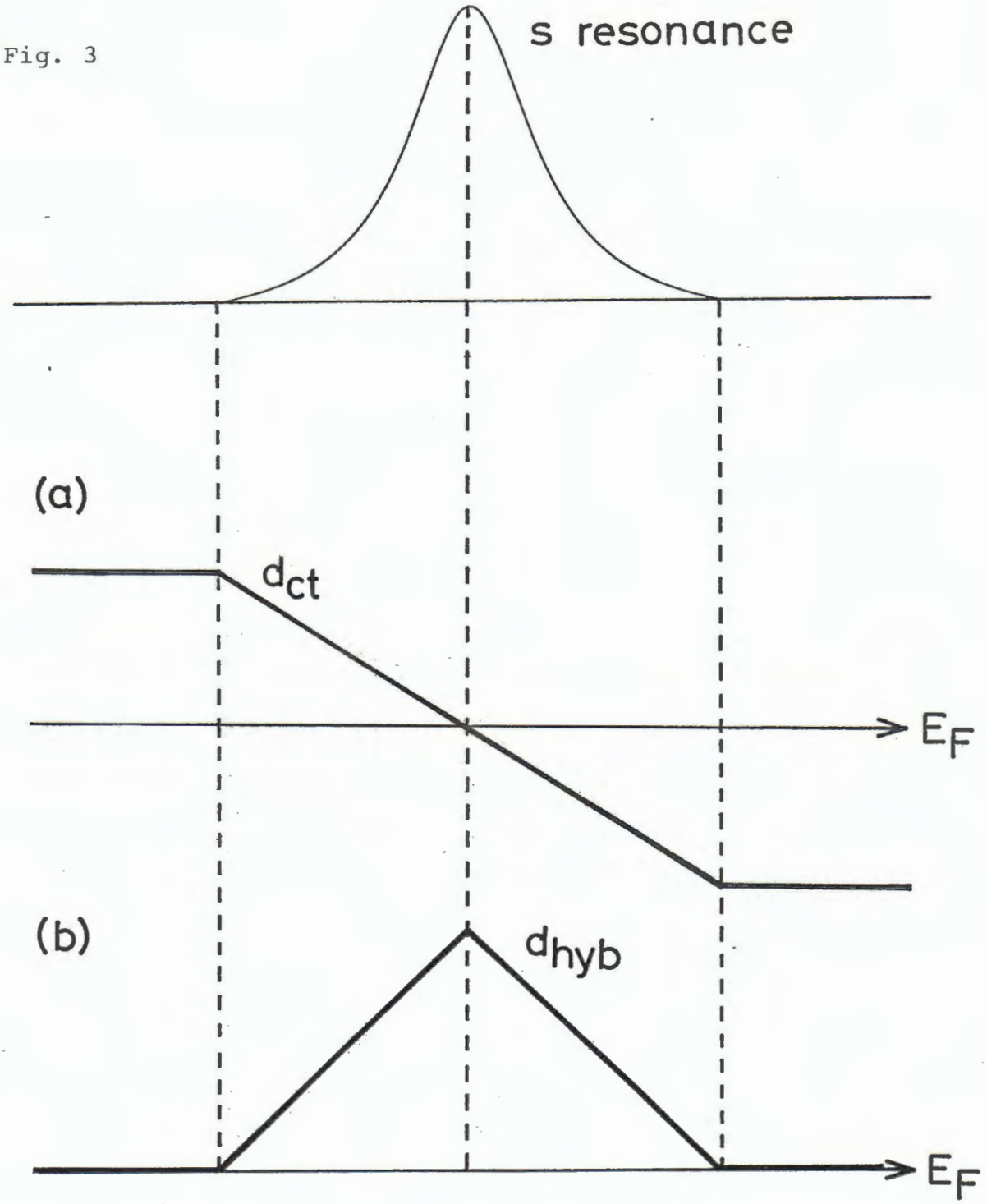

Fig. 4

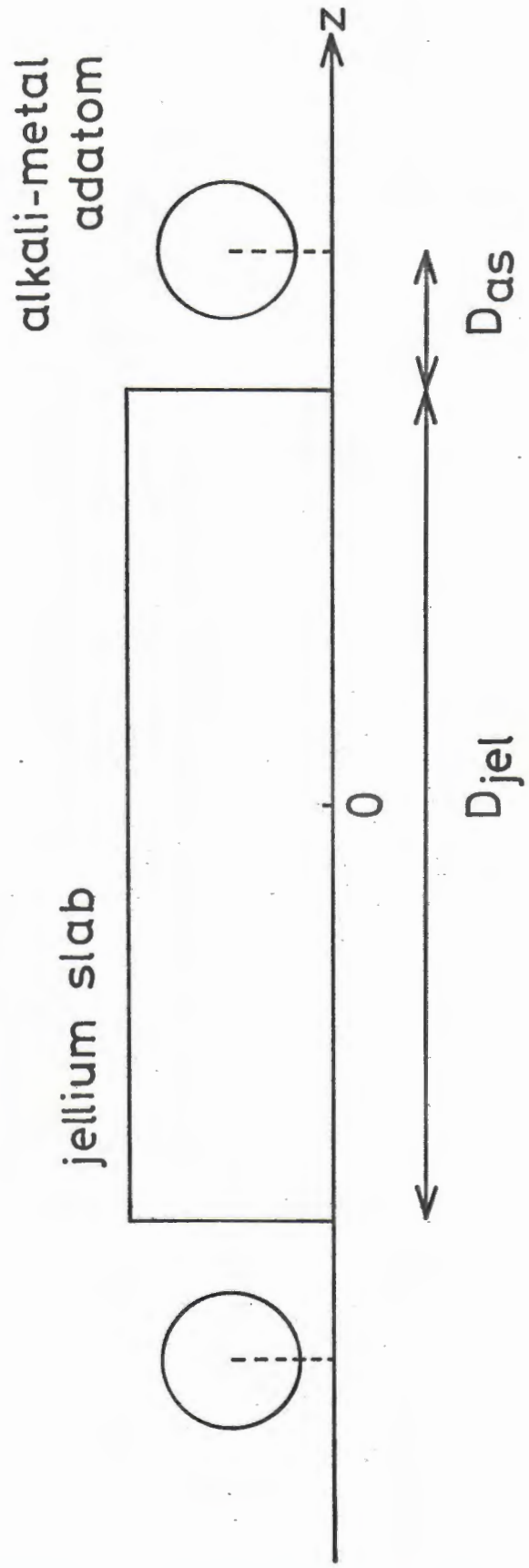

Fig. 5

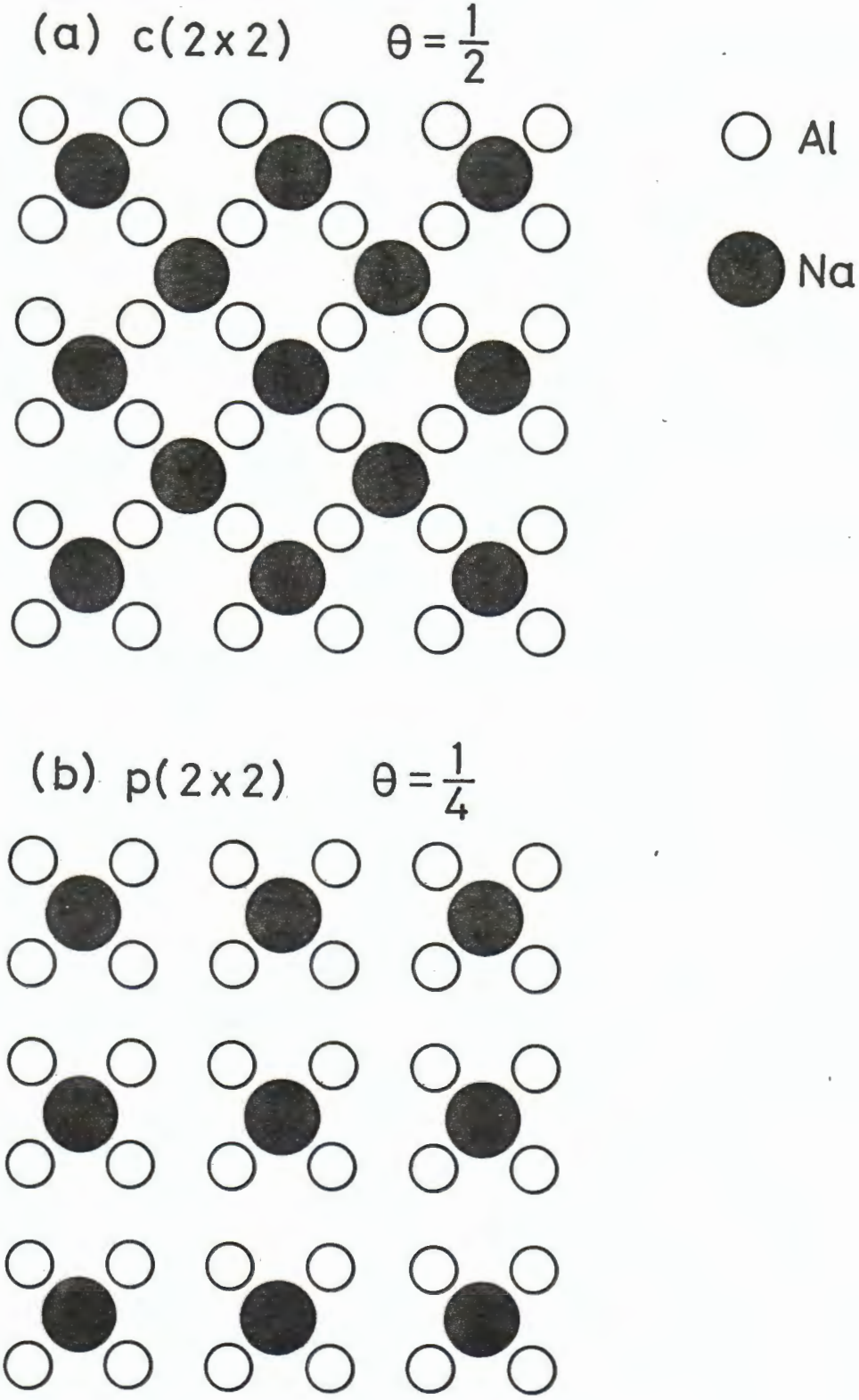

(c) $(\sqrt{8} \times \sqrt{8})R45^\circ$ $\theta = \frac{1}{8}$

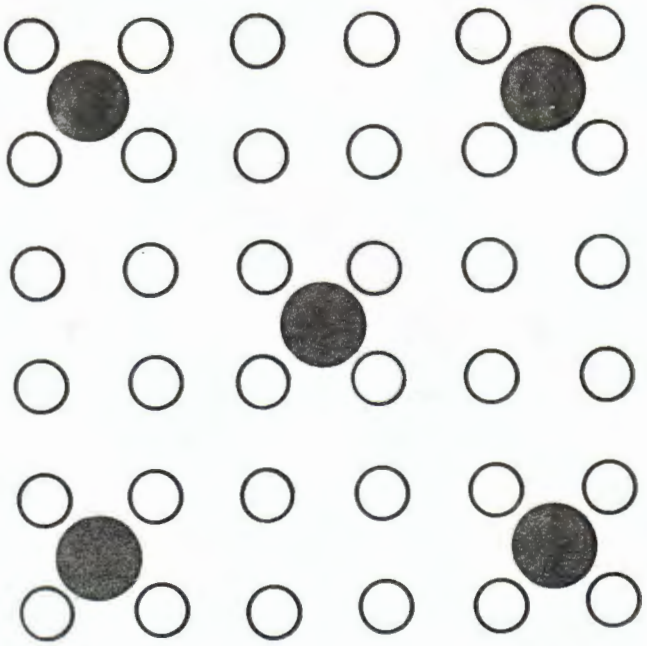

Fig. 6

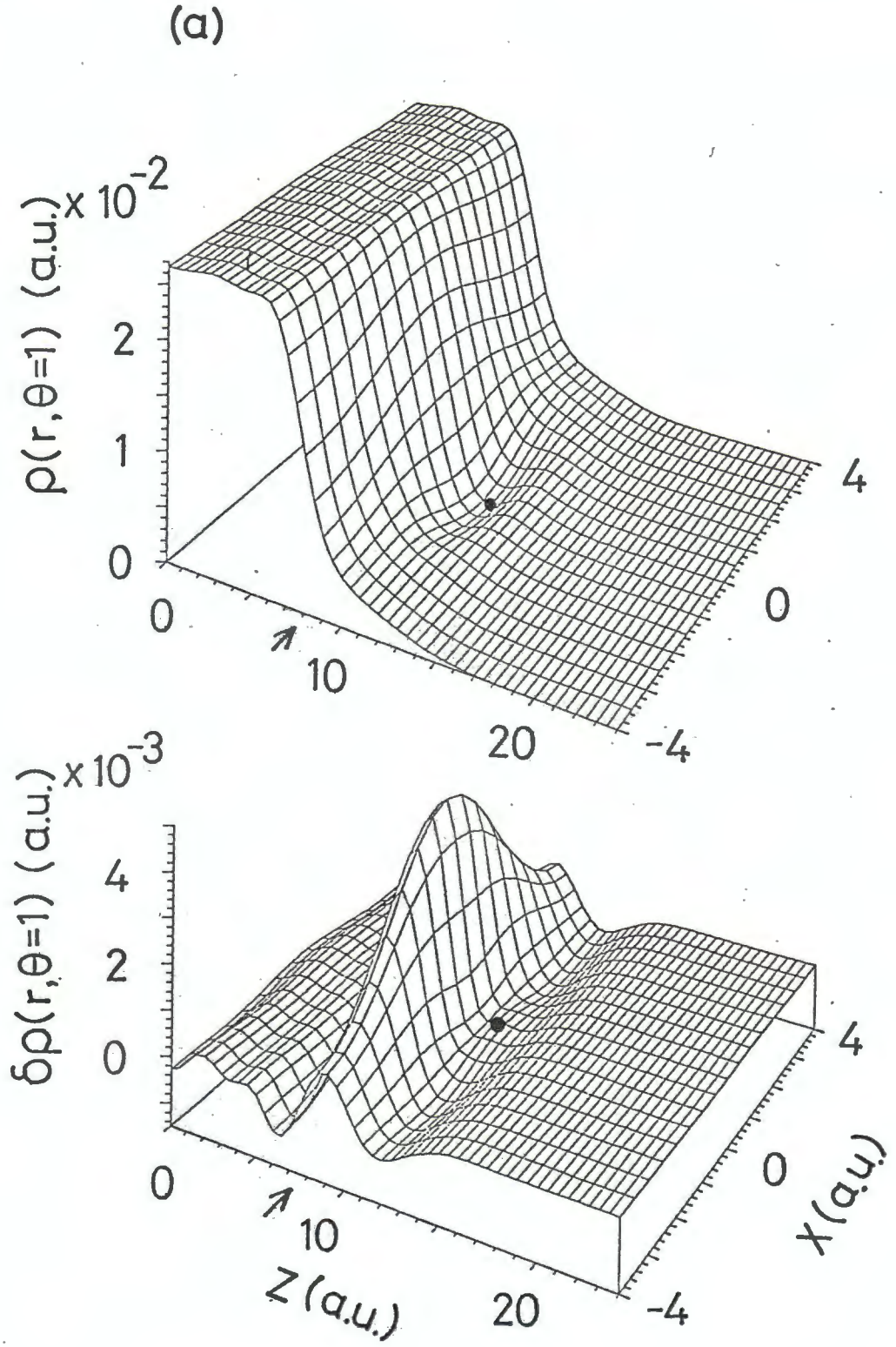
(a)
ρ(r,θ=1) (a.u.)
x 10^-2
2
1
0
0
10
20
4
0
-4
δρ(r,θ=1) (a.u.)
x 10^-3
4
2
0
0
10
Z (a.u.)
20
4
0
-4
X (a.u.)

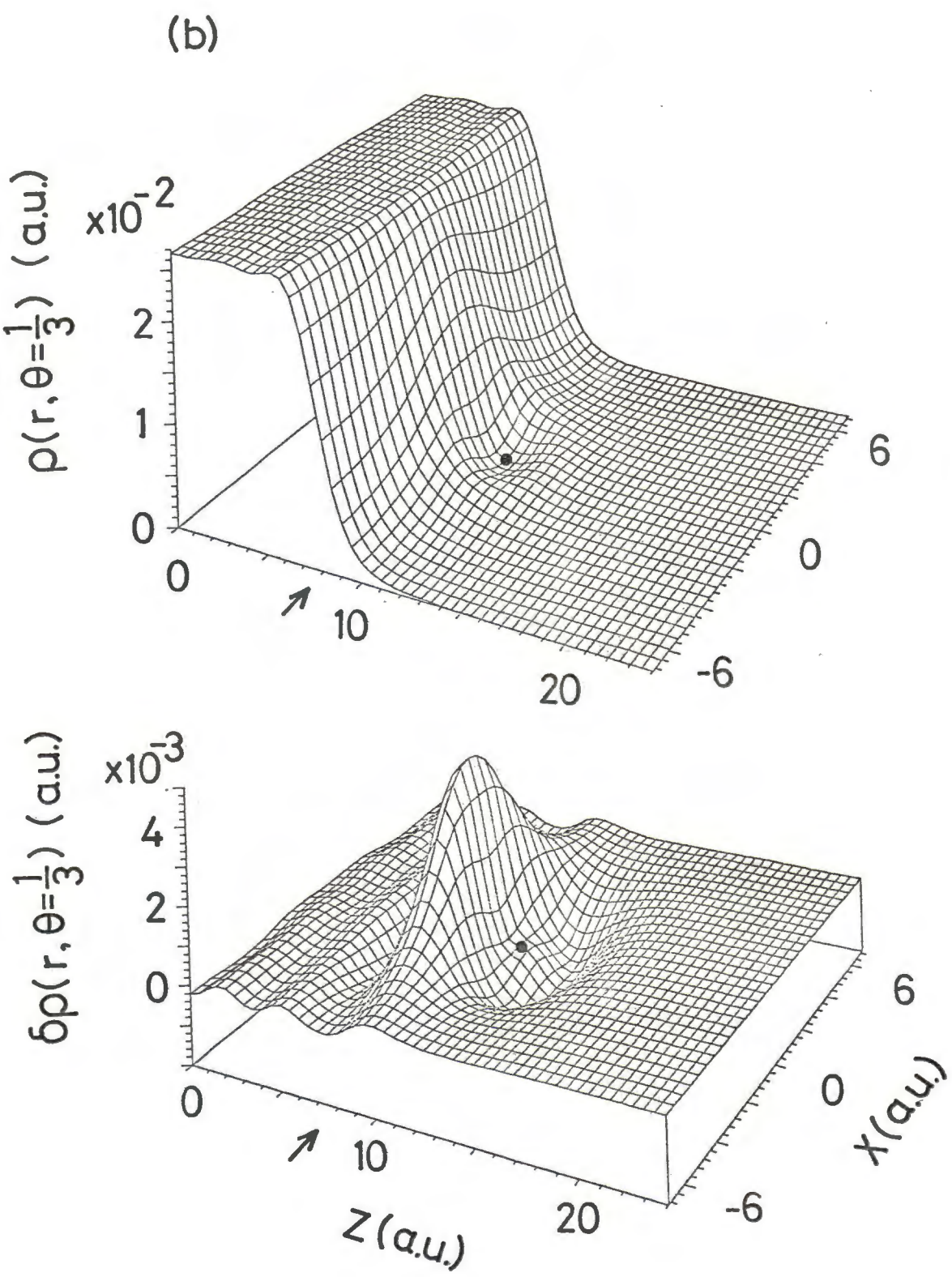
(b)
ρ(r, θ=1/3) (a.u.)
x10^-2
2
1
0
0
10
20
6
0
-6
δρ(r, θ=1/3) (a.u.)
x10^-3
4
2
0
0
10
20
Z(a.u.)
6
0
-6
X(a.u.)

Fig. 7

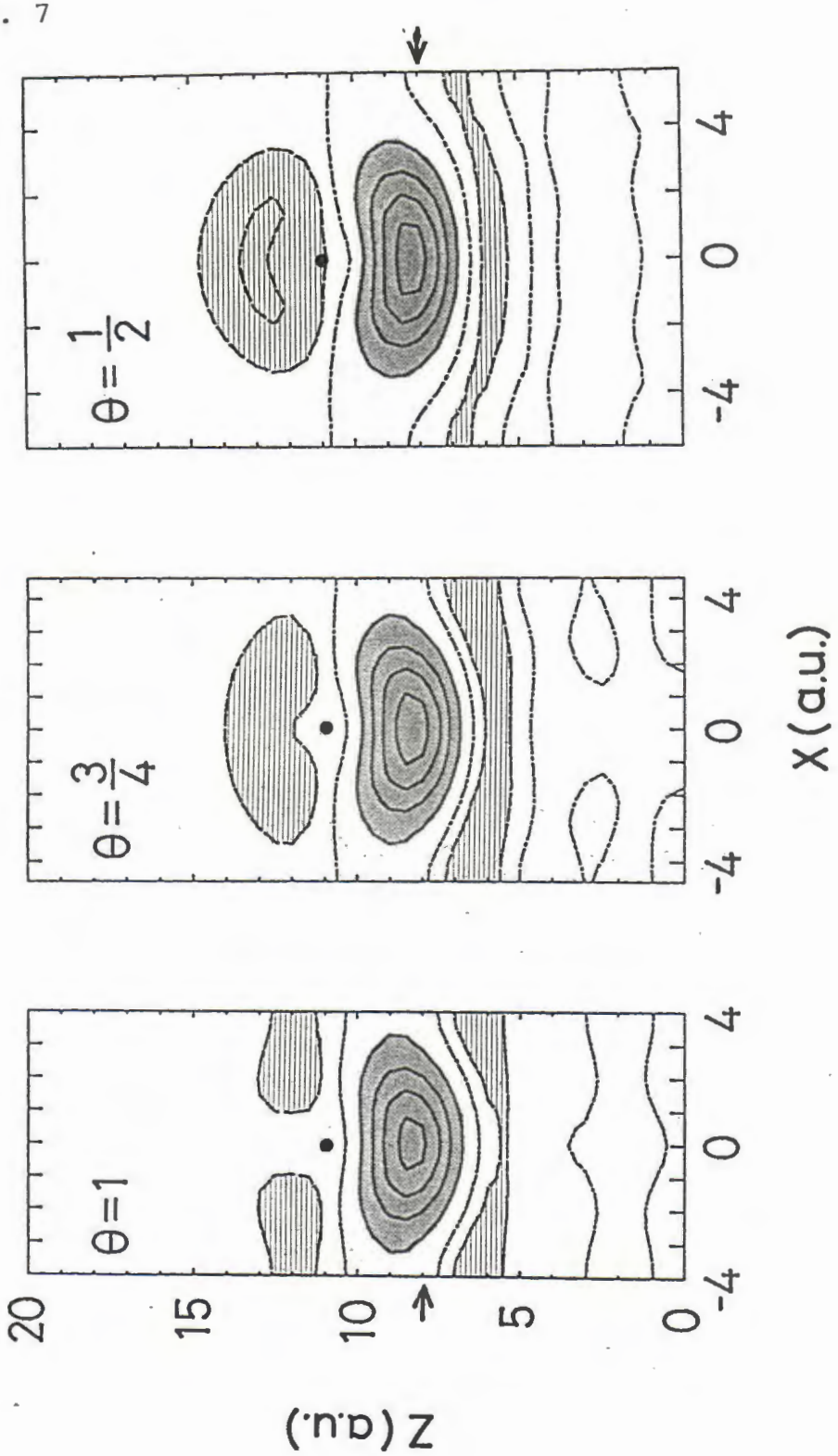

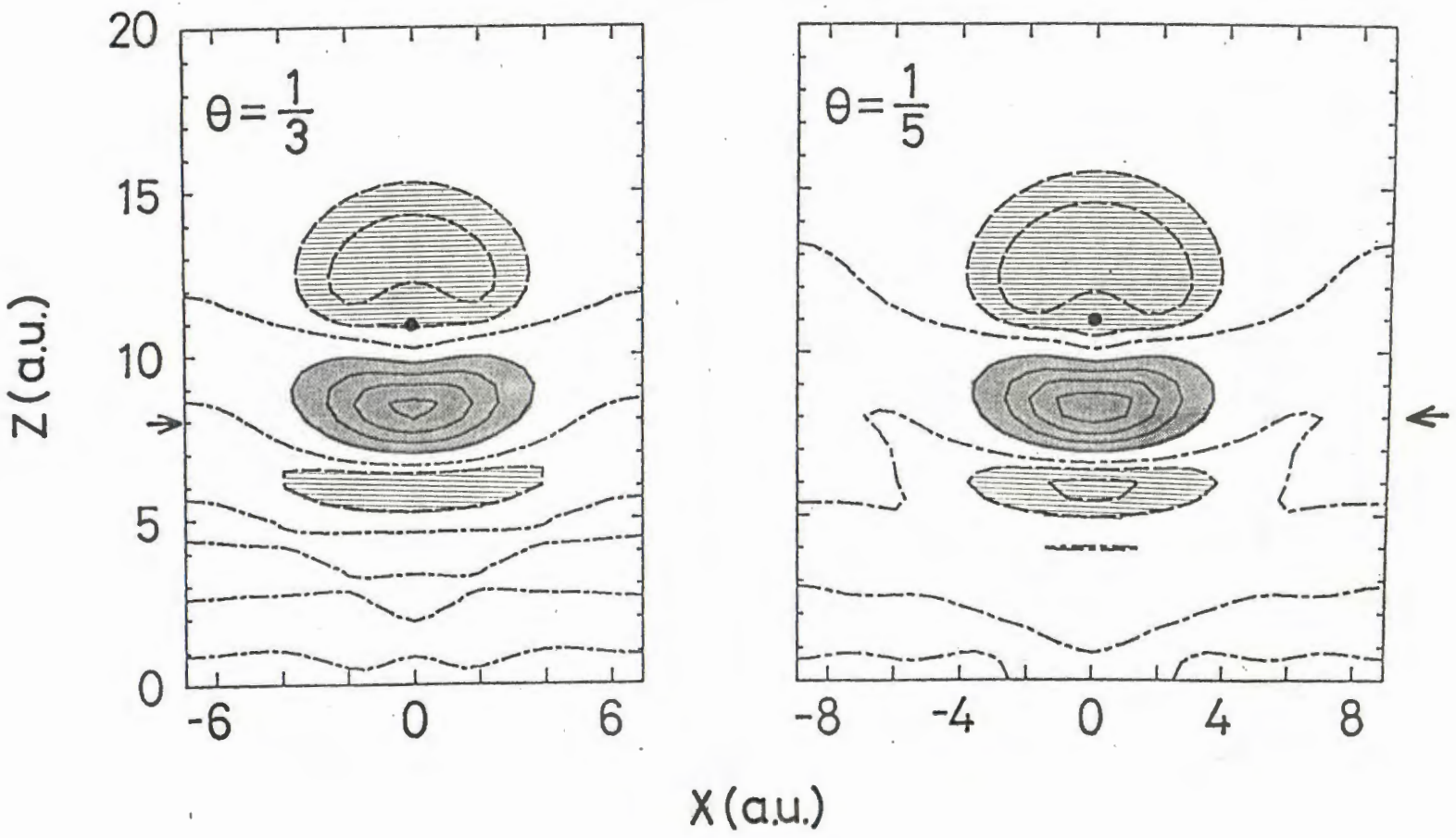
θ=1/3
θ=1/5
Z(a.u.)
X(a.u.)
20
15
10
5
0
-6
0
6
-8
-4
0
4
8

Fig. 8

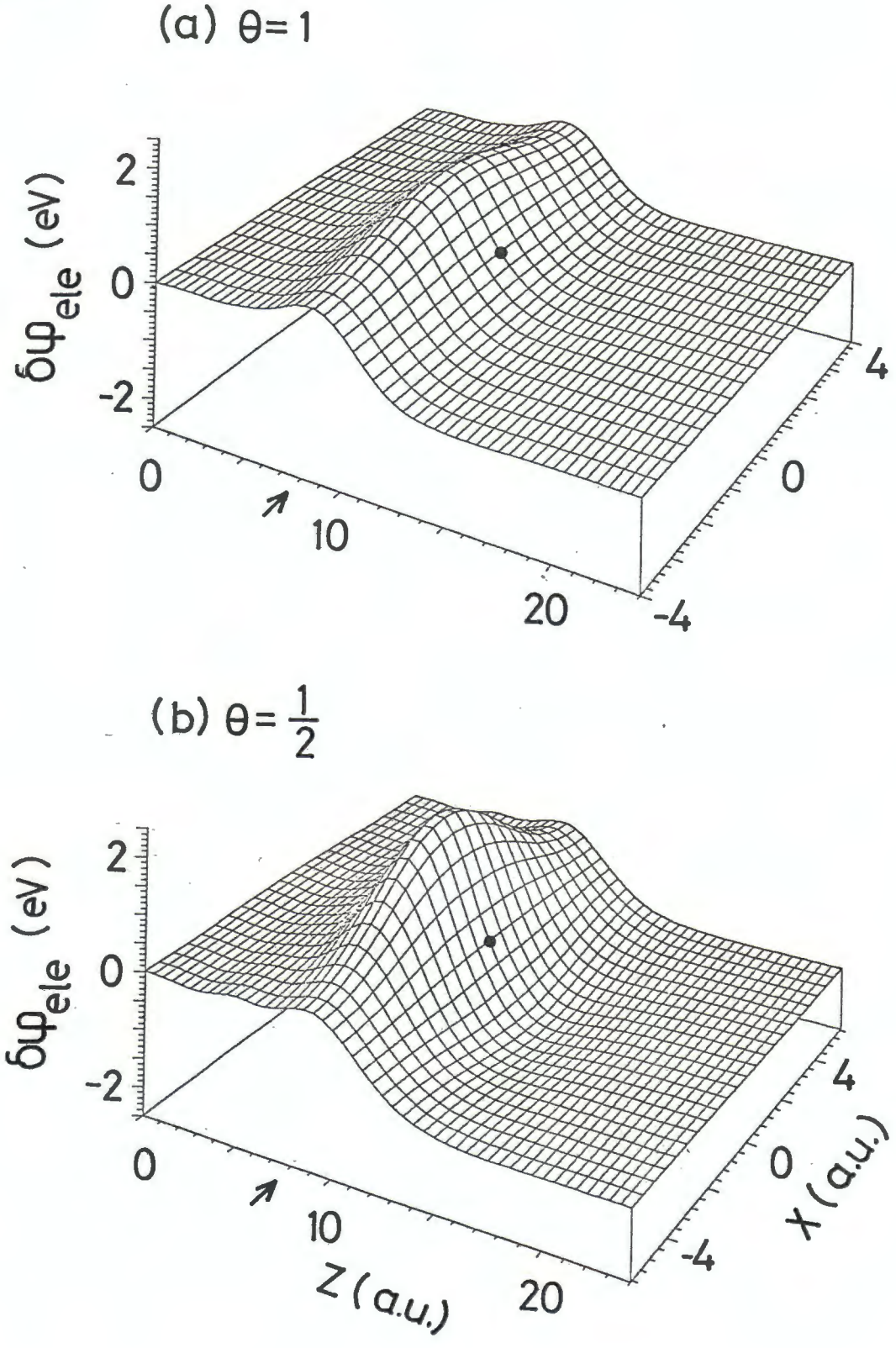

(c) $\theta = \frac{1}{3}$

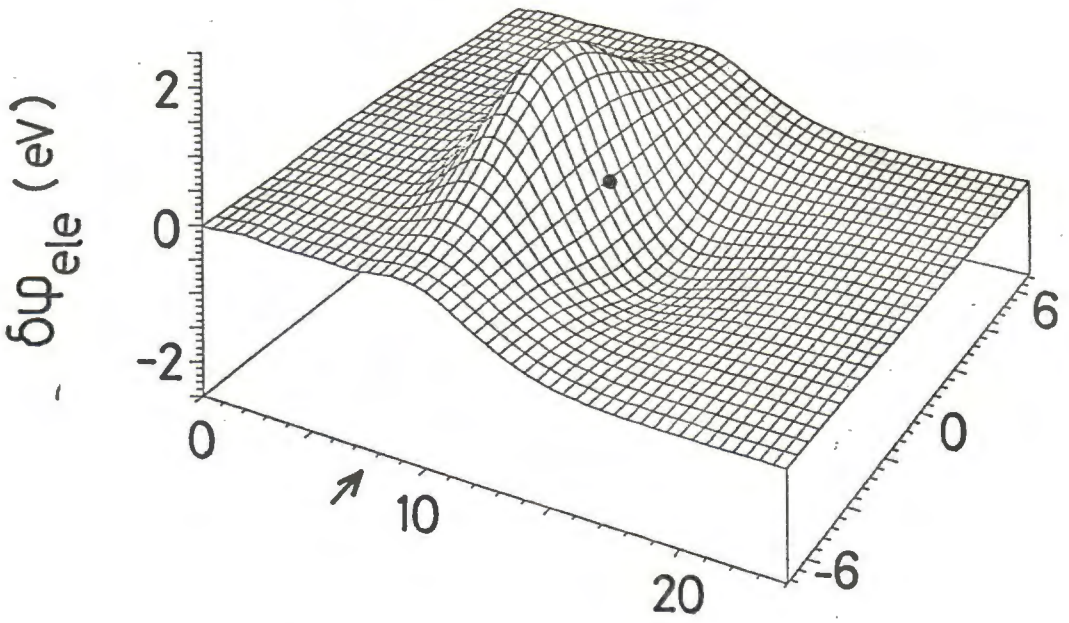

(d) $\theta = \frac{1}{5}$

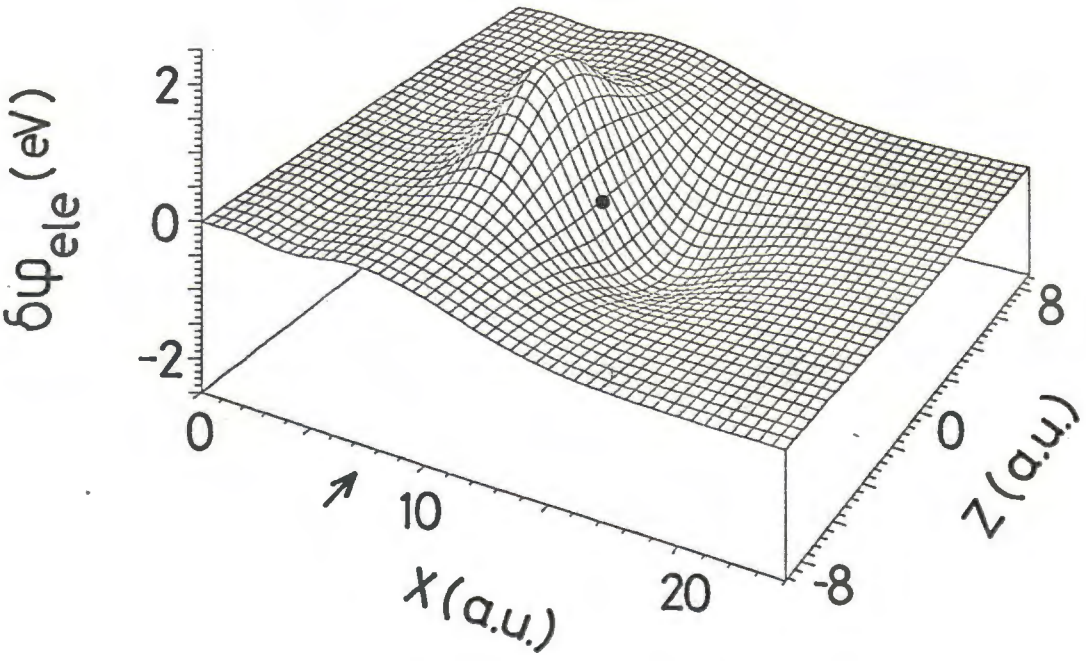

Fig. 9

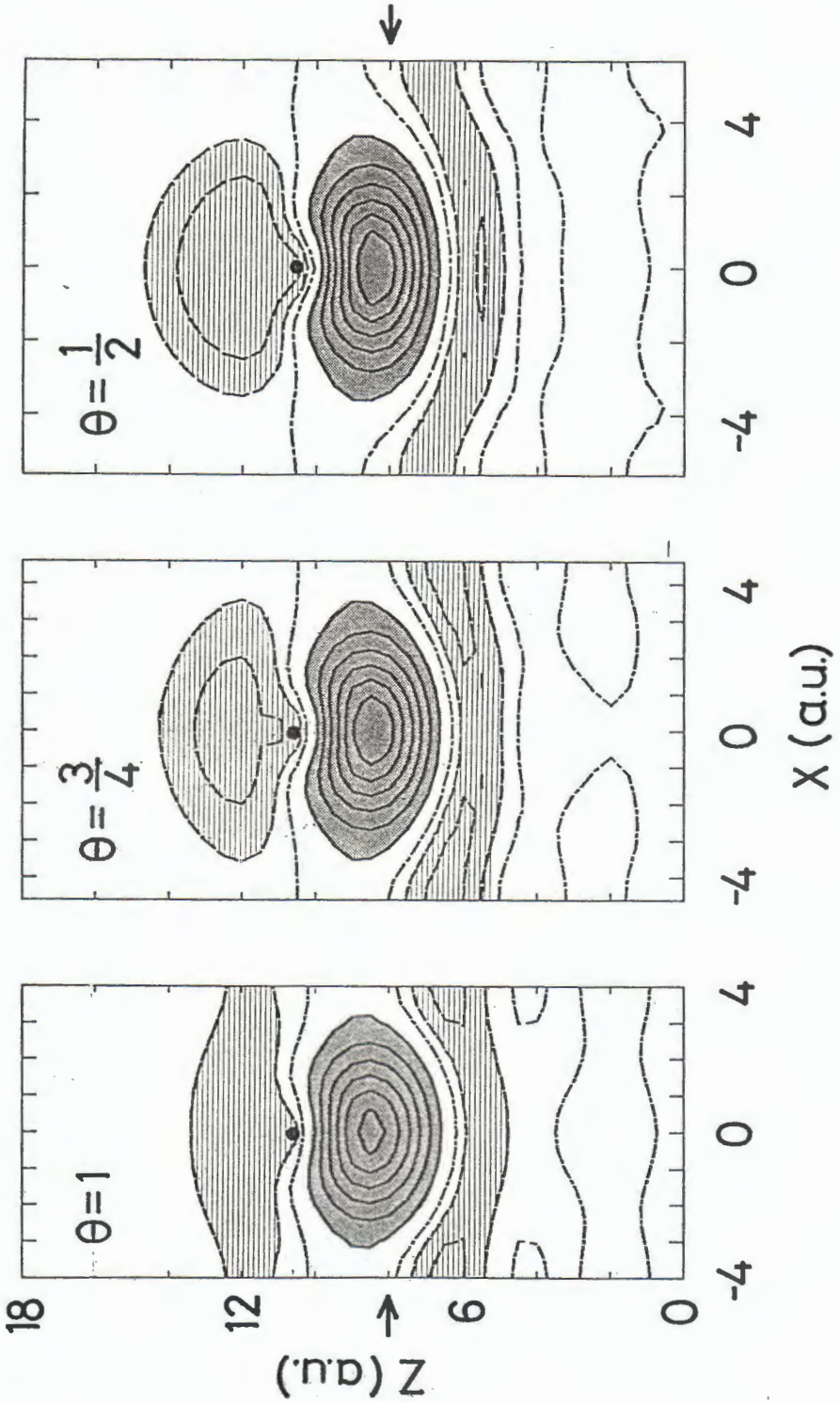

Fig. 10

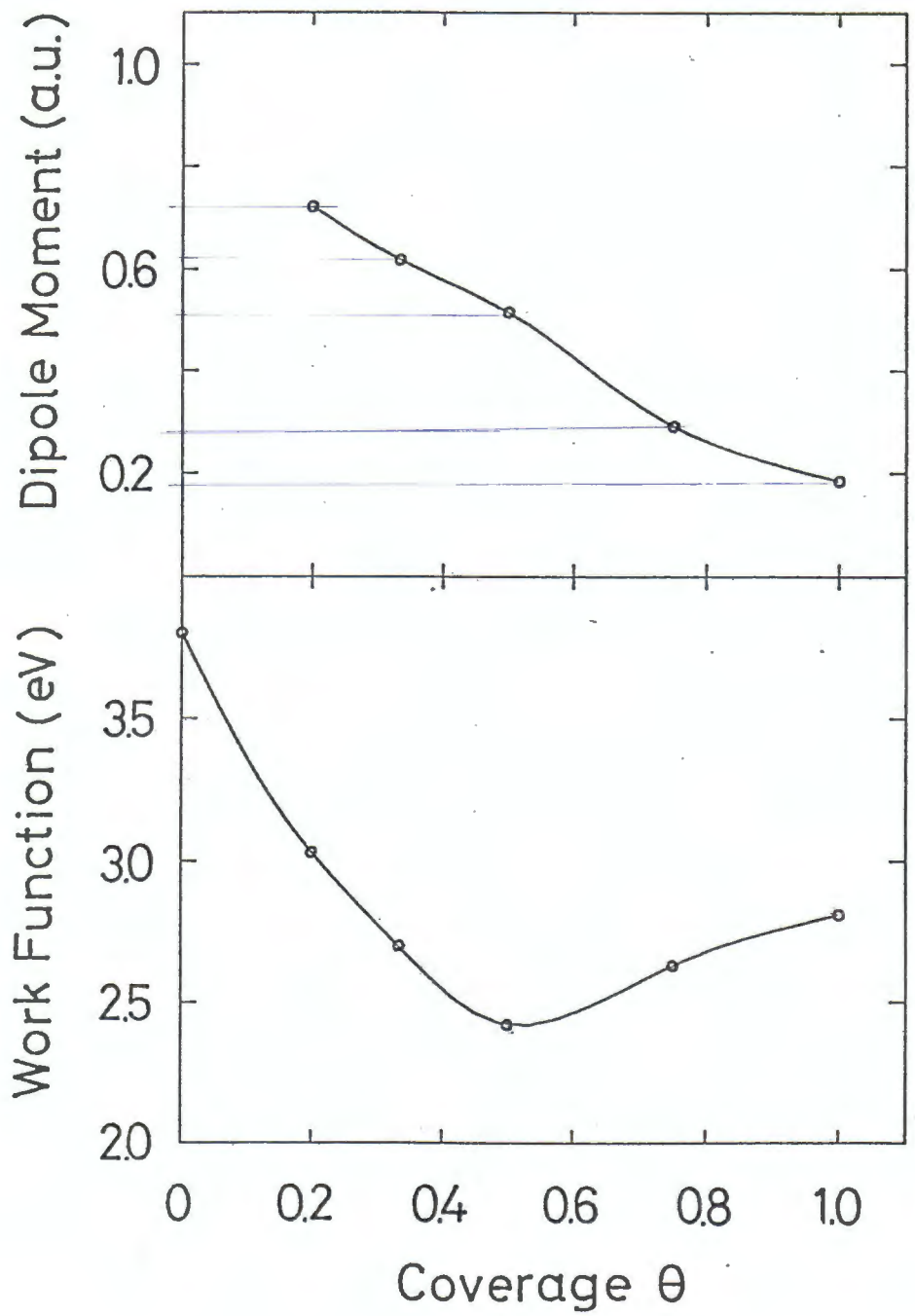
Dipole Moment (a.u.)
1.0
0.6
0.2
Work Function (eV)
3.5
3.0
2.5
2.0
0
0.2
0.4
0.6
0.8
1.0
Coverage θ

Fig. 11

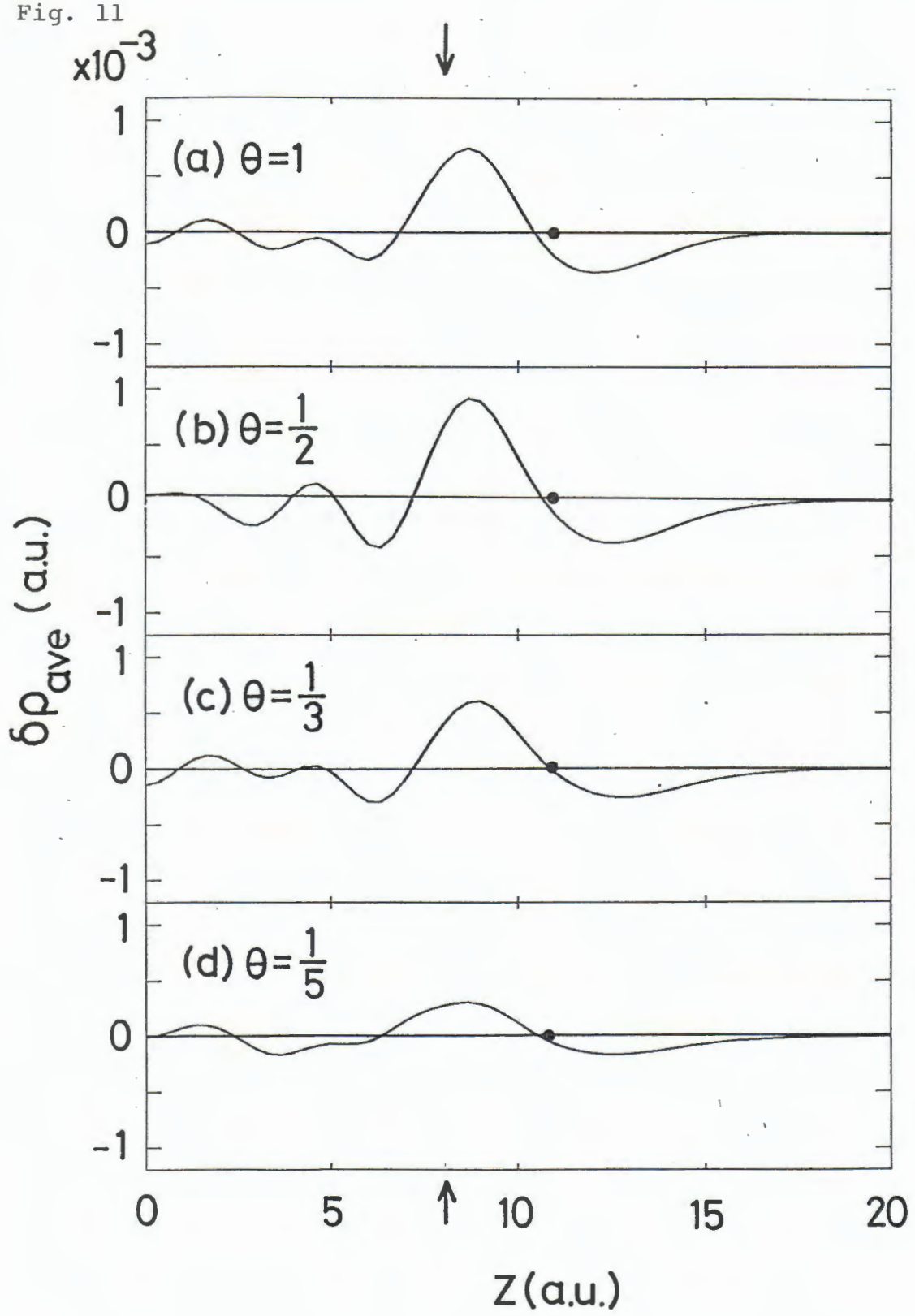

Fig. 12

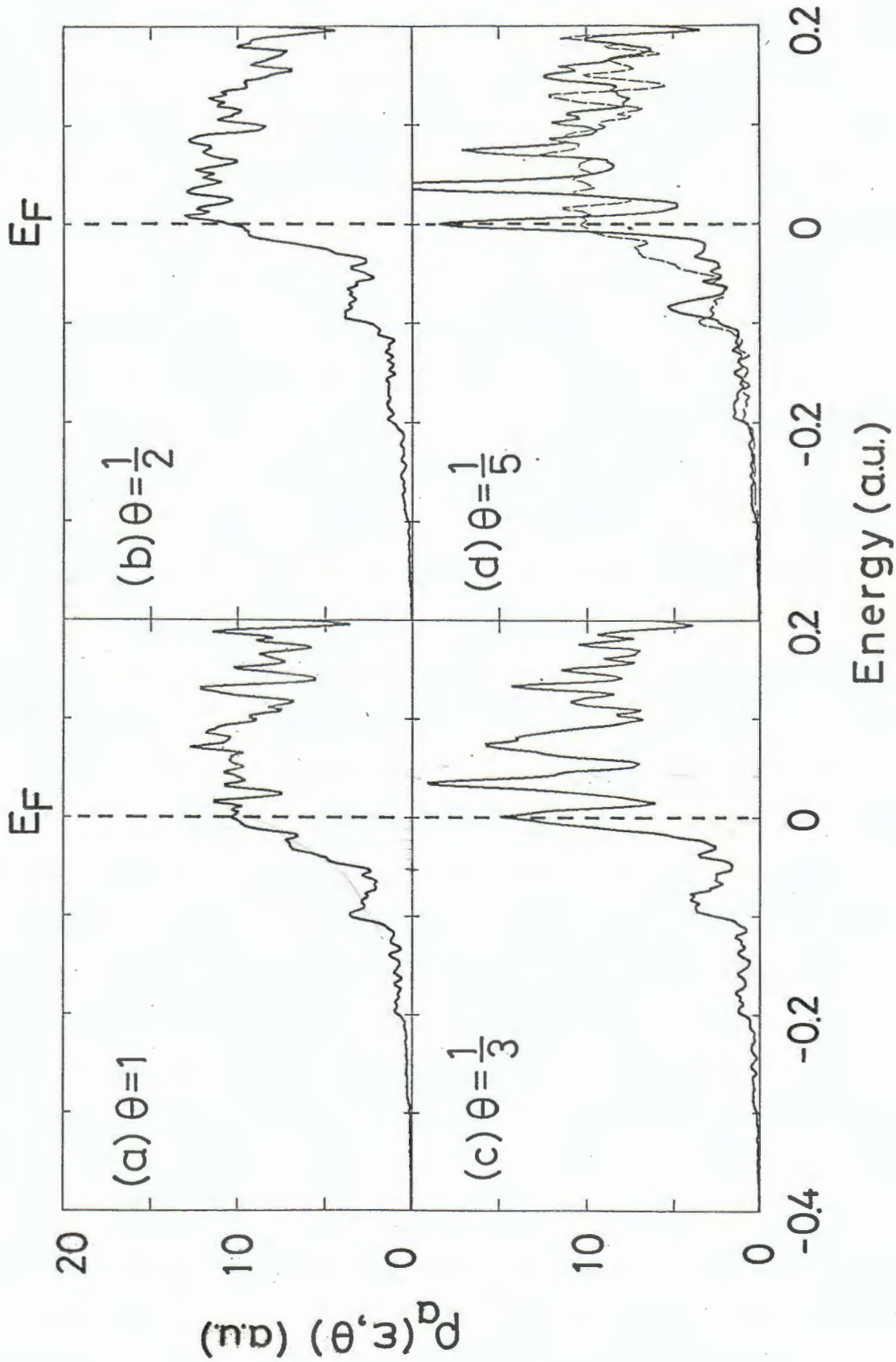
(a) θ=1
(b) θ=1/2
(c) θ=1/3
(d) θ=1/5
E_F
E_F
ρ_Q(ε,θ) (a.u.)
Energy (a.u.)
20
10
0
10
0
-0.4
-0.2
0
0.2
-0.2
0
0.2

Fig. 13

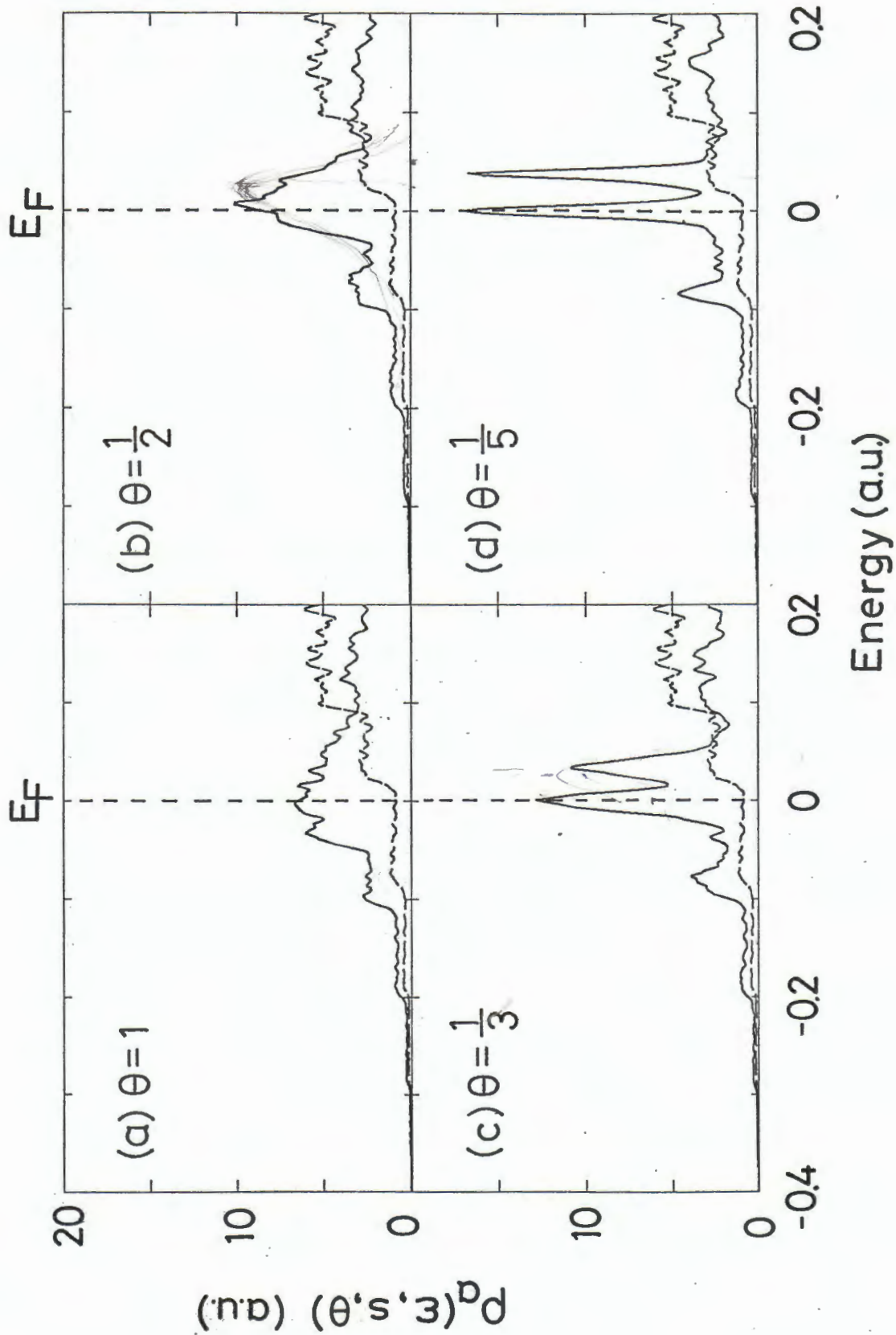
(a) θ=1
(b) θ=1/2
(c) θ=1/3
(d) θ=1/5
E_F
E_F
20
10
0
10
0
-0.4
-0.2
0
0.2
-0.2
0
0.2
ρ_α(ε, s, θ) (a.u.)
Energy (a.u.)

Fig. 14

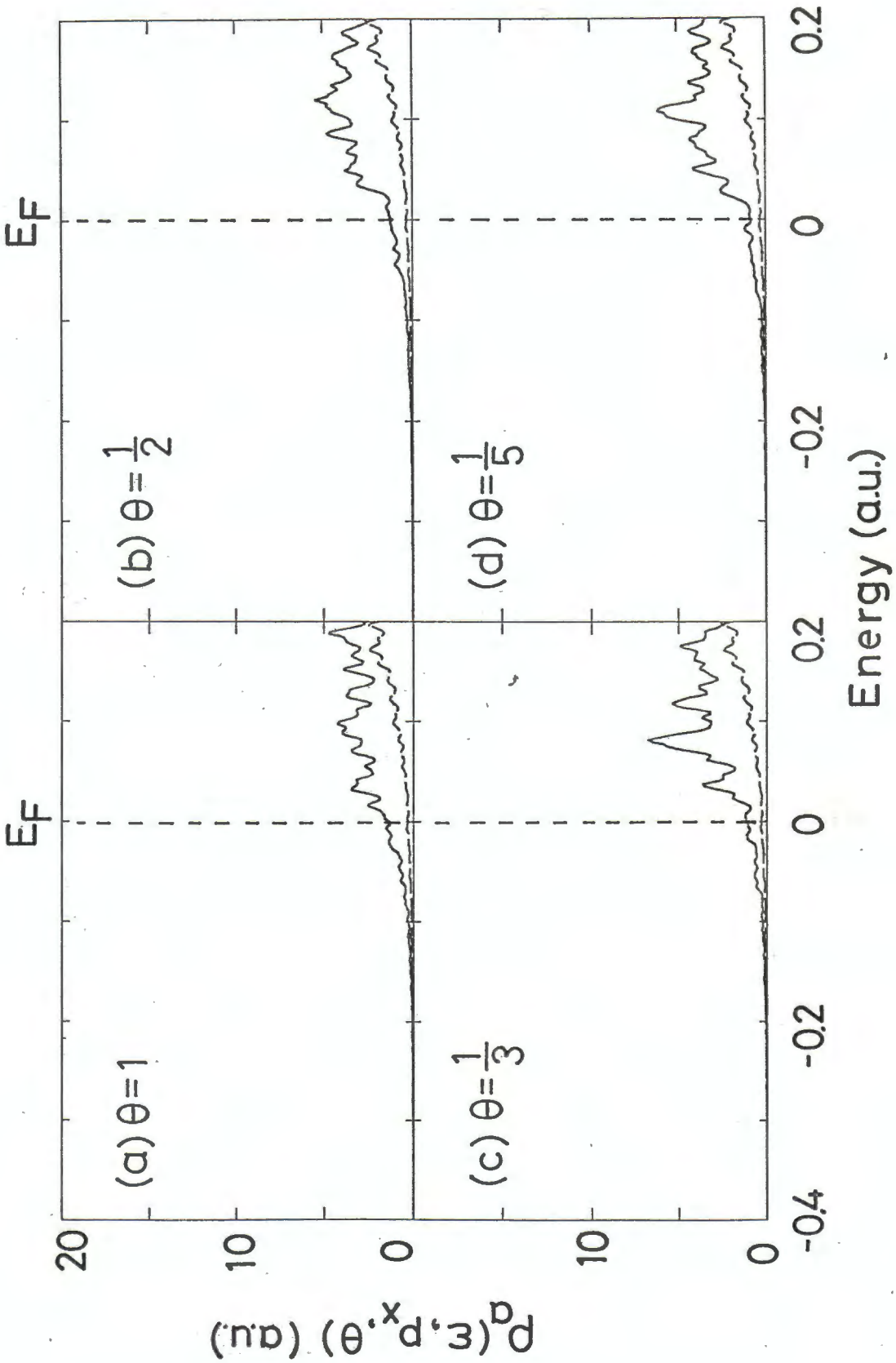
(a) θ=1
(b) θ=1/2
(c) θ=1/3
(d) θ=1/5
E_F
E_F
20
10
0
10
0
0.2
0
-0.2
0.2
0
-0.2
-0.4
Energy (a.u.)
ρ_α(ε, p_x, θ) (a.u.)

Fig. 15

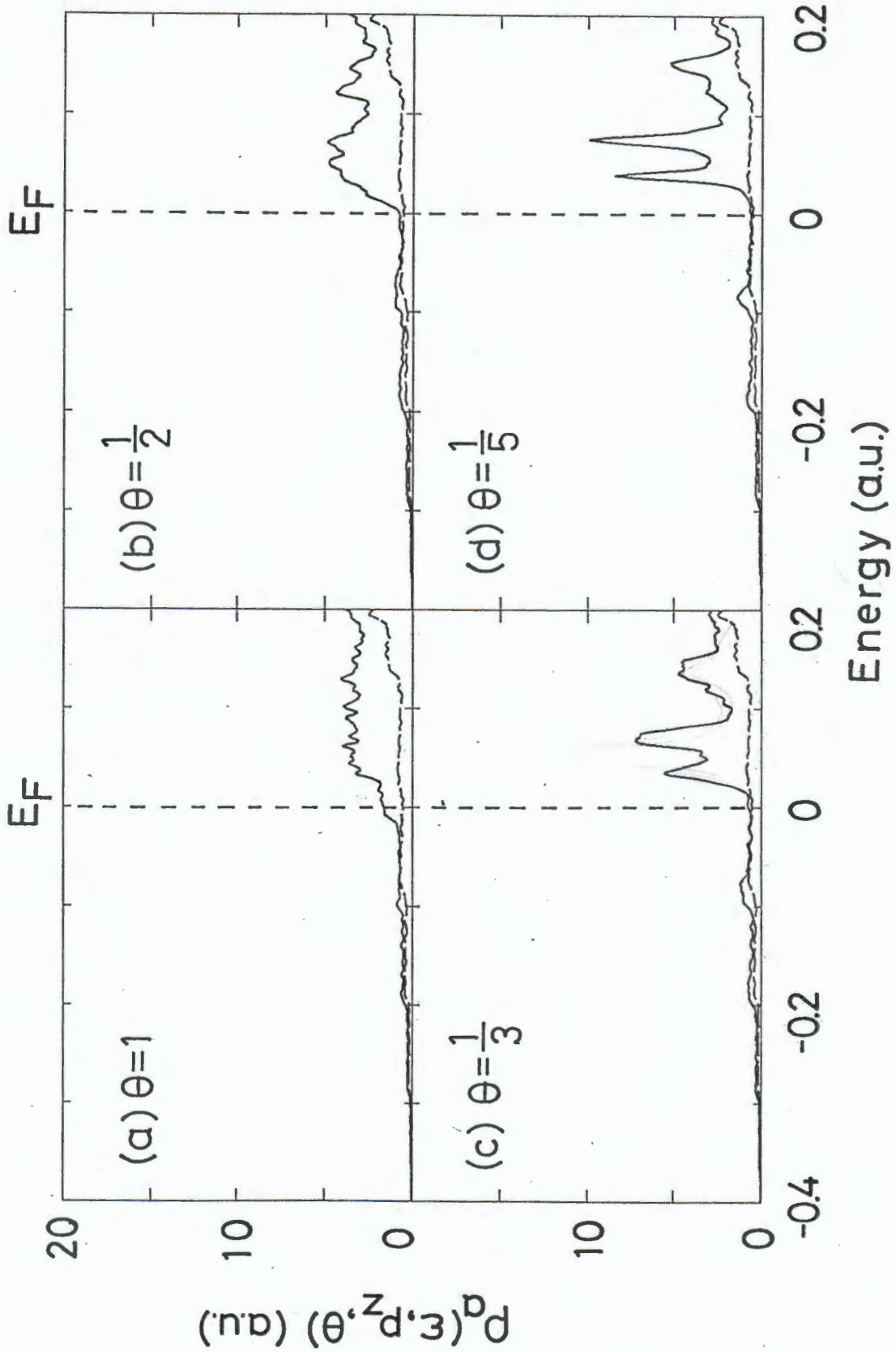
(a) θ=1
(b) θ=1/2
(c) θ=1/3
(d) θ=1/5
E_F
E_F
20
10
0
10
0
-0.4
-0.2
0
0.2
-0.2
0
0.2
Energy (a.u.)
P_α(ε,p_z,θ) (a.u.)

Fig. 16

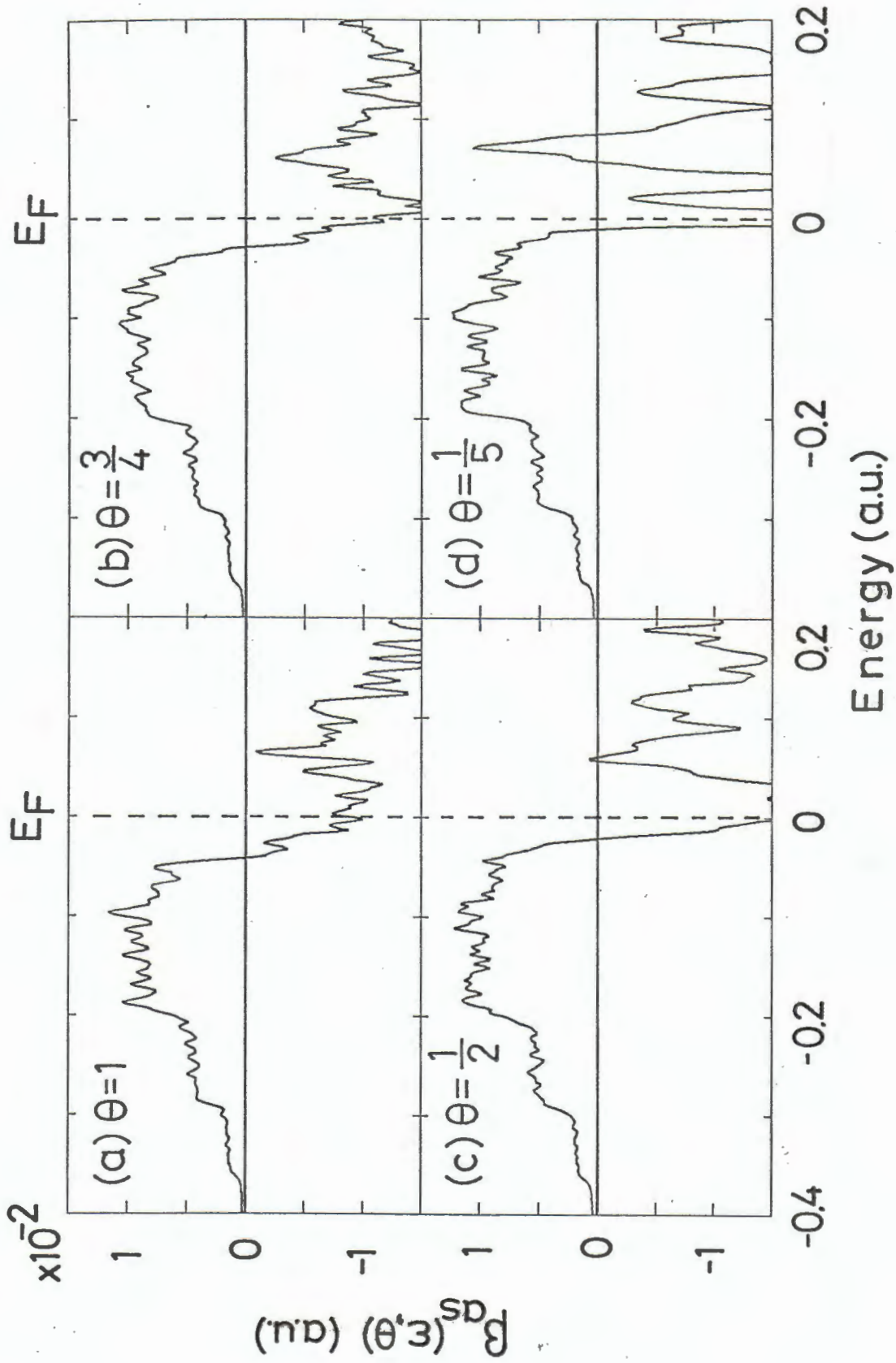
(a) θ=1
(b) θ=3/4
(c) θ=1/2
(d) θ=1/5
E_F
E_F
x10^-2
1
0
-1
1
0
-1
-0.4
-0.2
0
0.2
-0.2
0
0.2
Energy (a.u.)
ρ_as(ε,θ) (a.u.)

Fig. 17

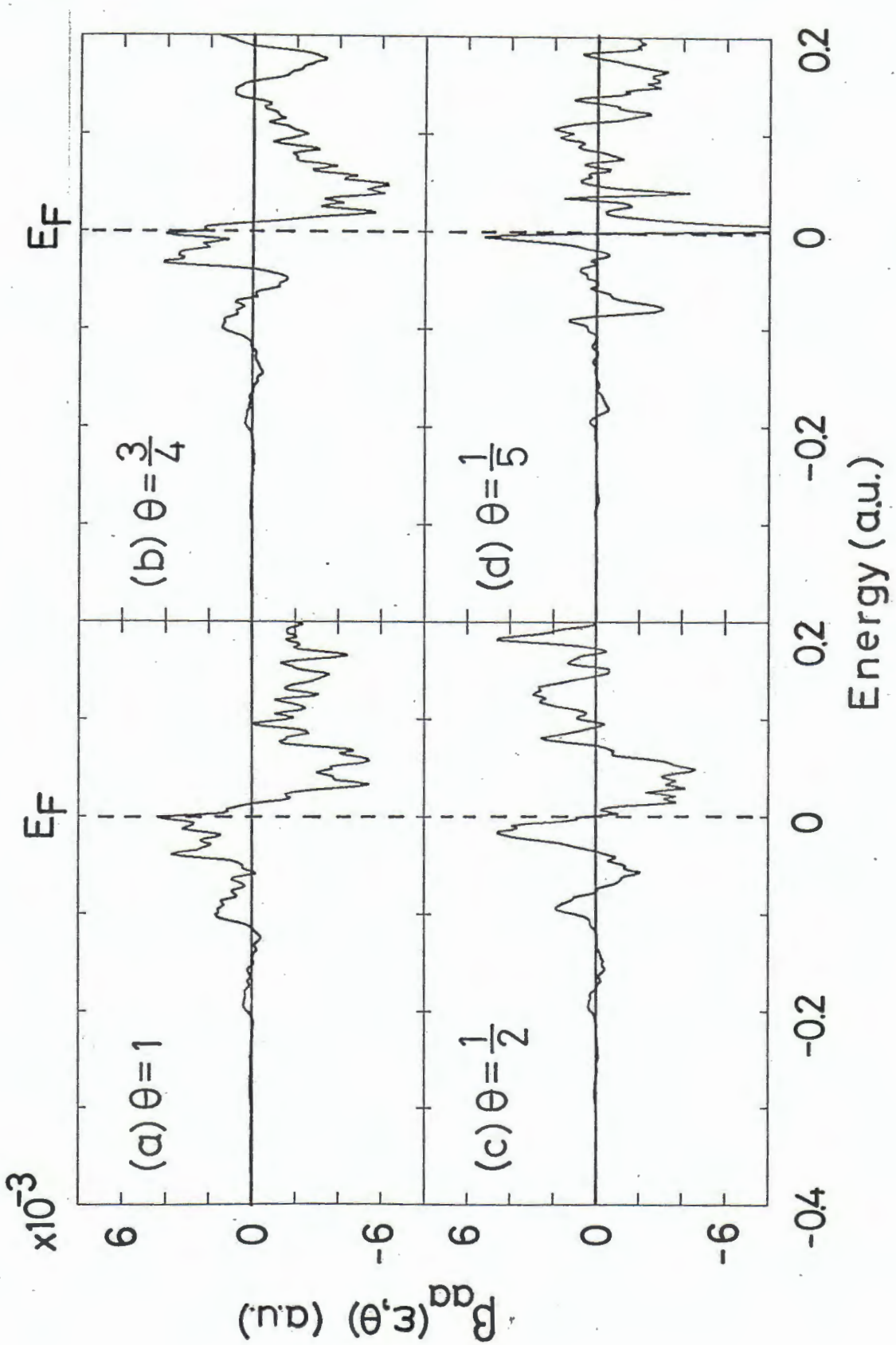
$\rho_{aa}(\varepsilon,\theta)$ (a.u.)
$\times 10^{-3}$
6
0
-6
E_F
(a) $\theta = 1$
(b) $\theta = \frac{3}{4}$
(c) $\theta = \frac{1}{2}$
(d) $\theta = \frac{1}{5}$
0.2
0
-0.2
-0.4
Energy (a.u.)

Fig. 18

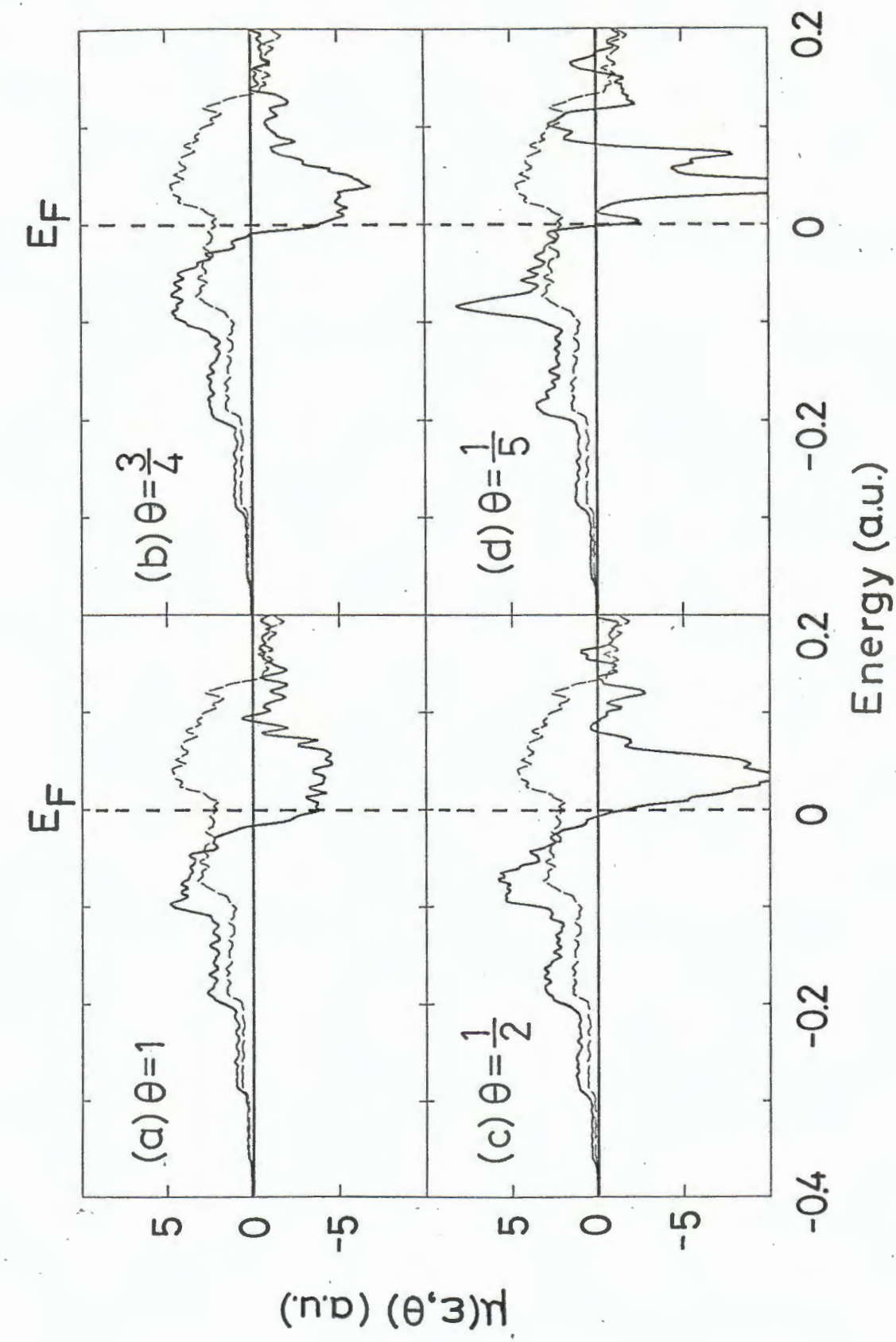

Fig. 19

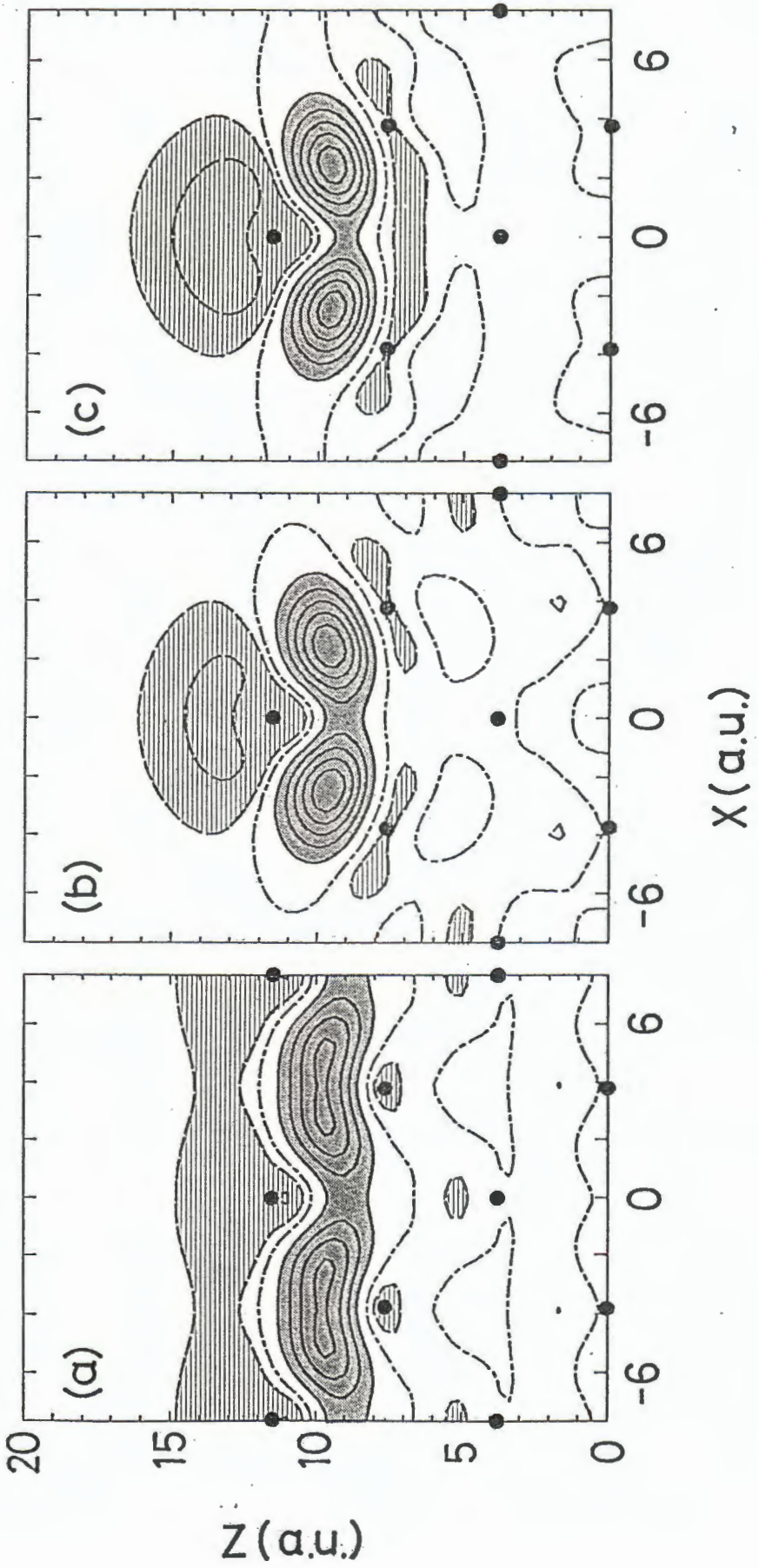

Fig. 20

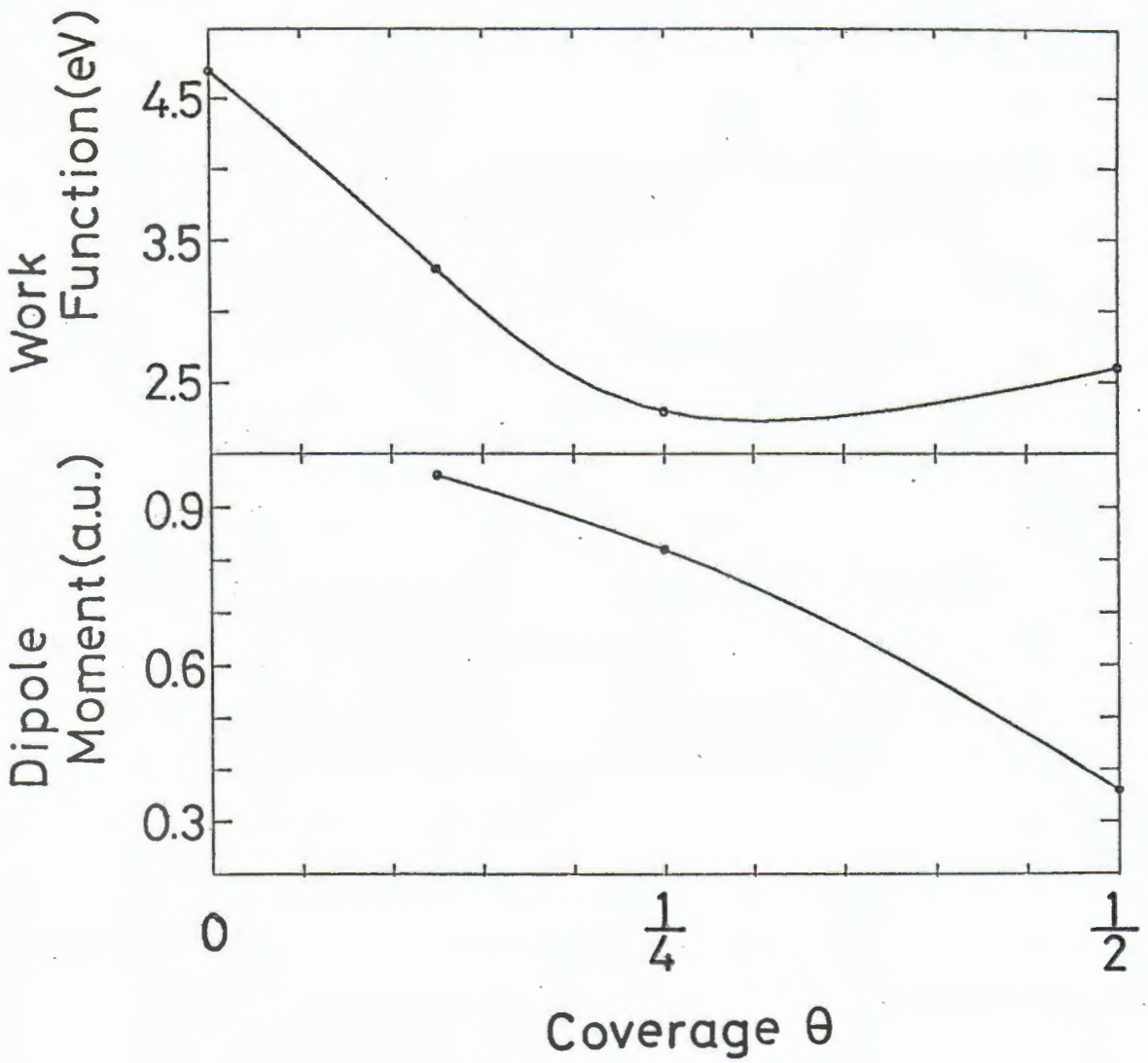
Work Function(eV)
4.5
3.5
2.5
Dipole Moment(a.u.)
0.9
0.6
0.3
0
1/4
1/2
Coverage θ

Fig. 21

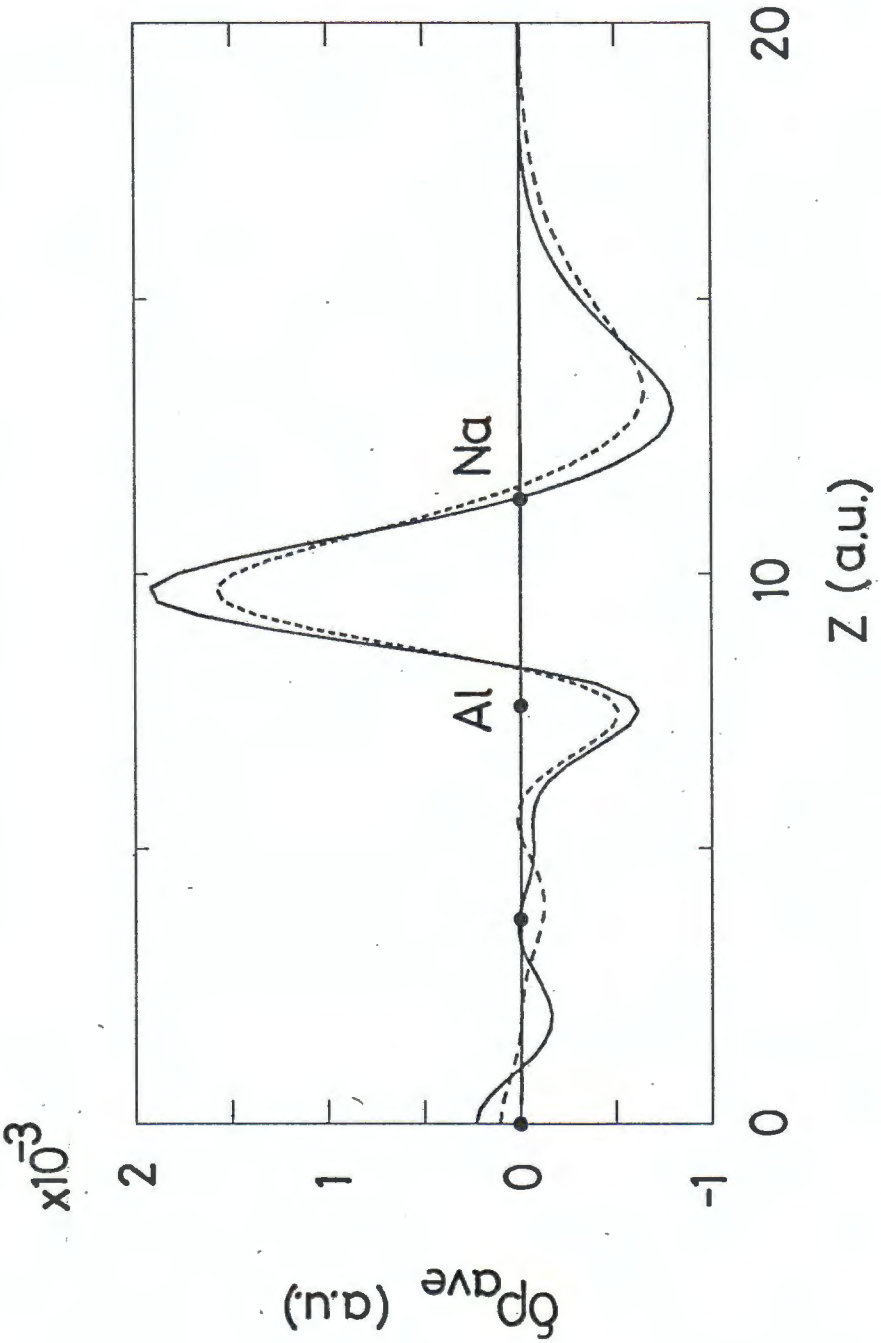

Fig. 22

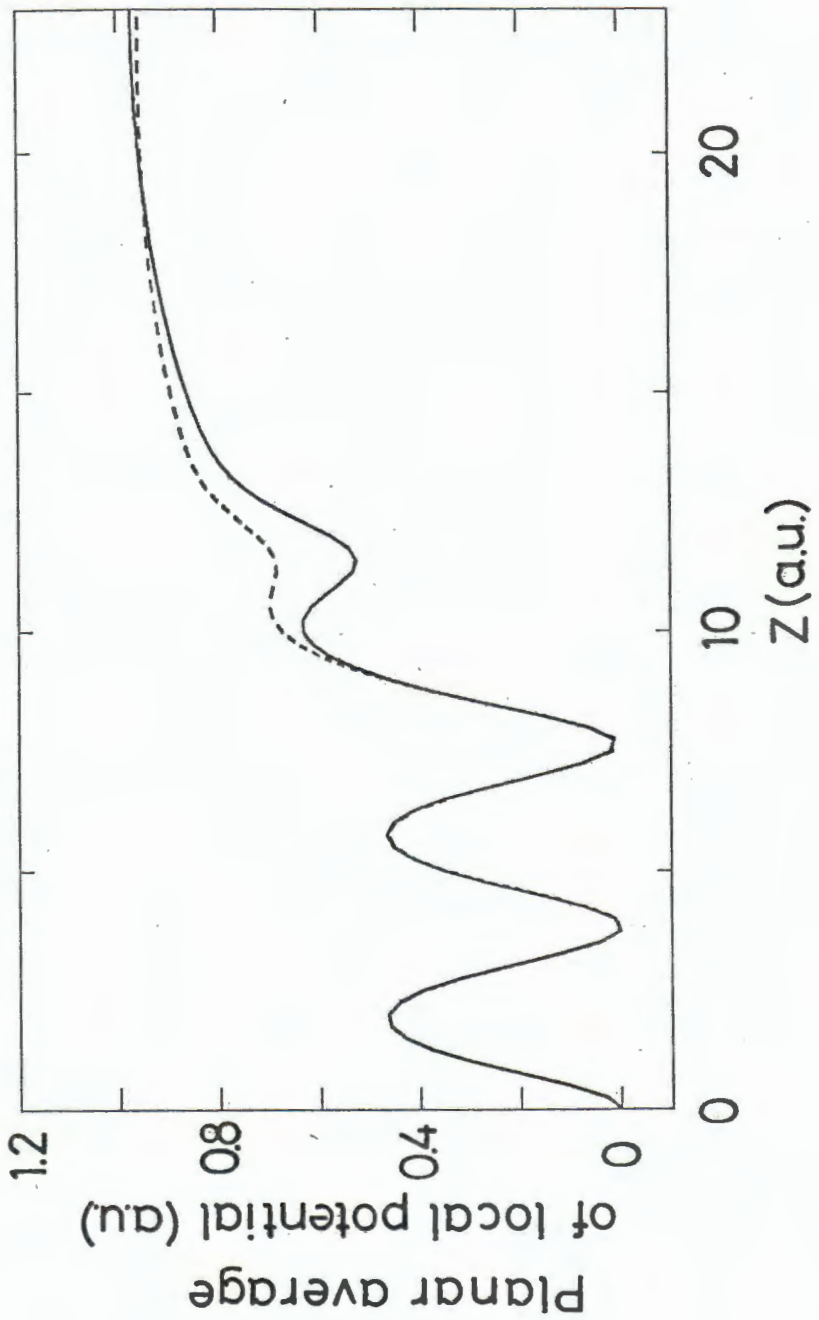

Fig. 23

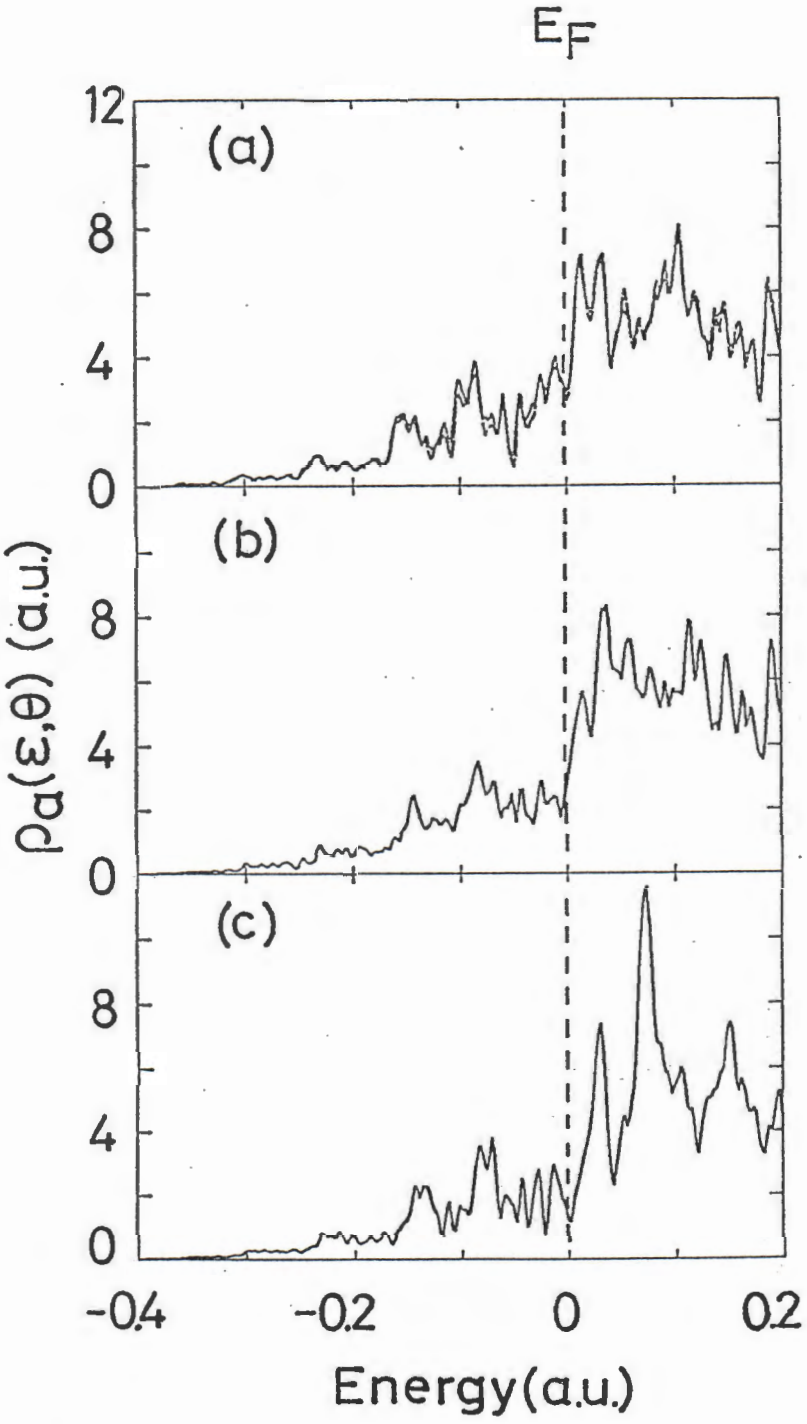

Fig. 24

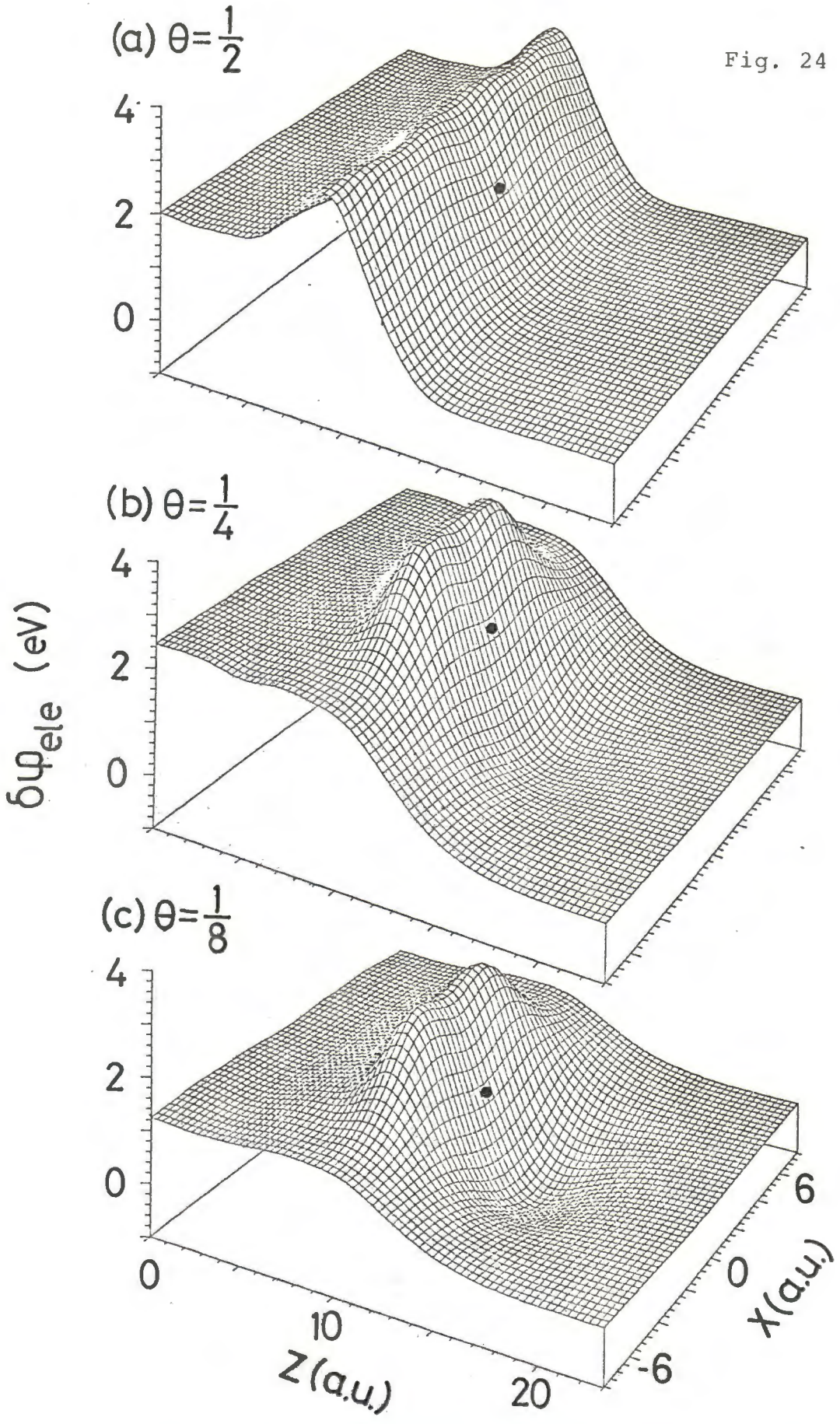

Fig. 25

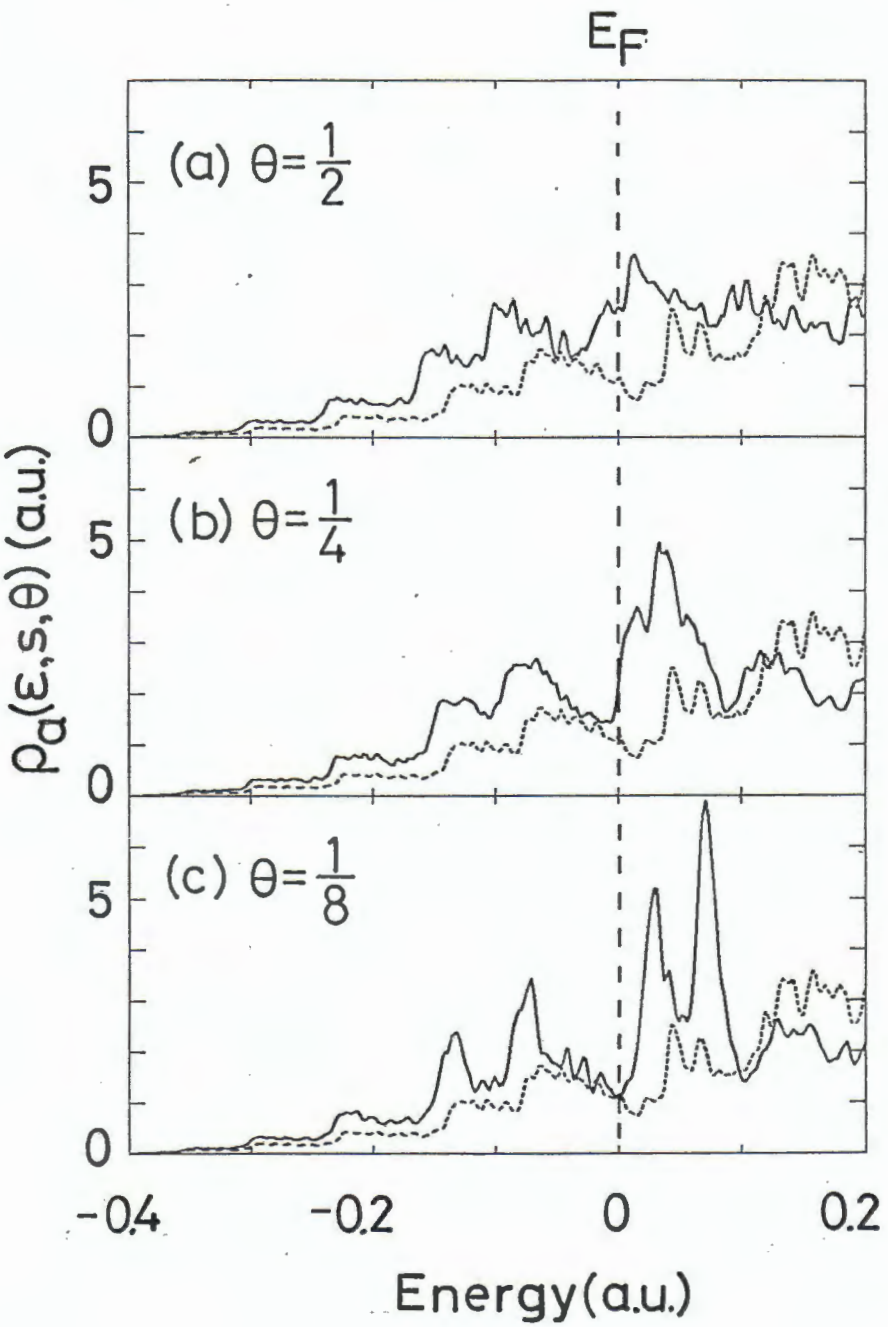
E_F
(a) $\theta=\frac{1}{2}$
(b) $\theta=\frac{1}{4}$
(c) $\theta=\frac{1}{8}$
5
0
$\rho_\alpha(\varepsilon,s,\theta)$ (a.u.)
-0.4
-0.2
0
0.2
Energy(a.u.)

Fig. 26

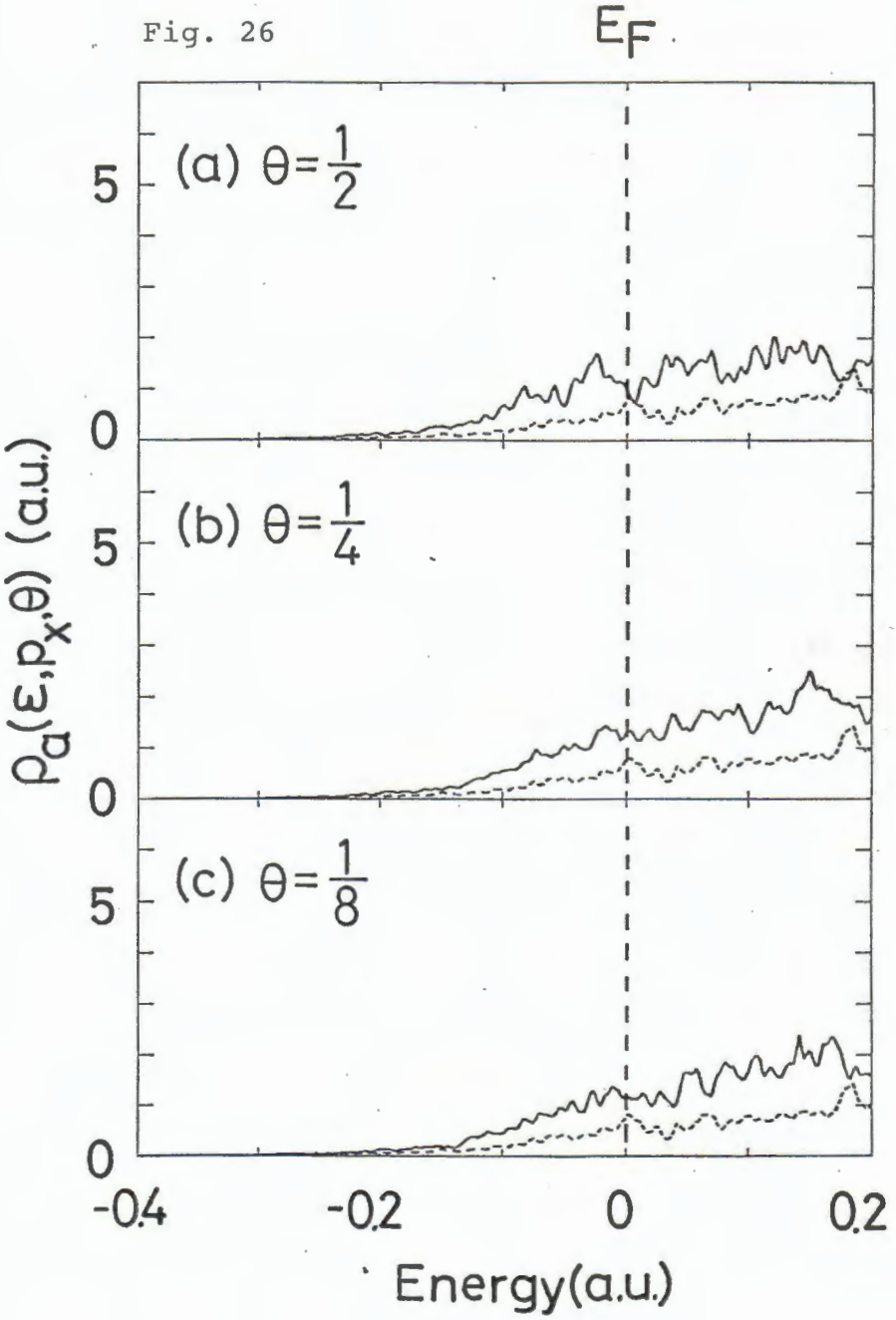
E_F
(a) $\theta=\frac{1}{2}$
(b) $\theta=\frac{1}{4}$
(c) $\theta=\frac{1}{8}$
5
0
5
0
5
0
$\rho_a(\varepsilon,p_x,\theta)$ (a.u.)
-0.4
-0.2
0
0.2
Energy(a.u.)

Fig. 27

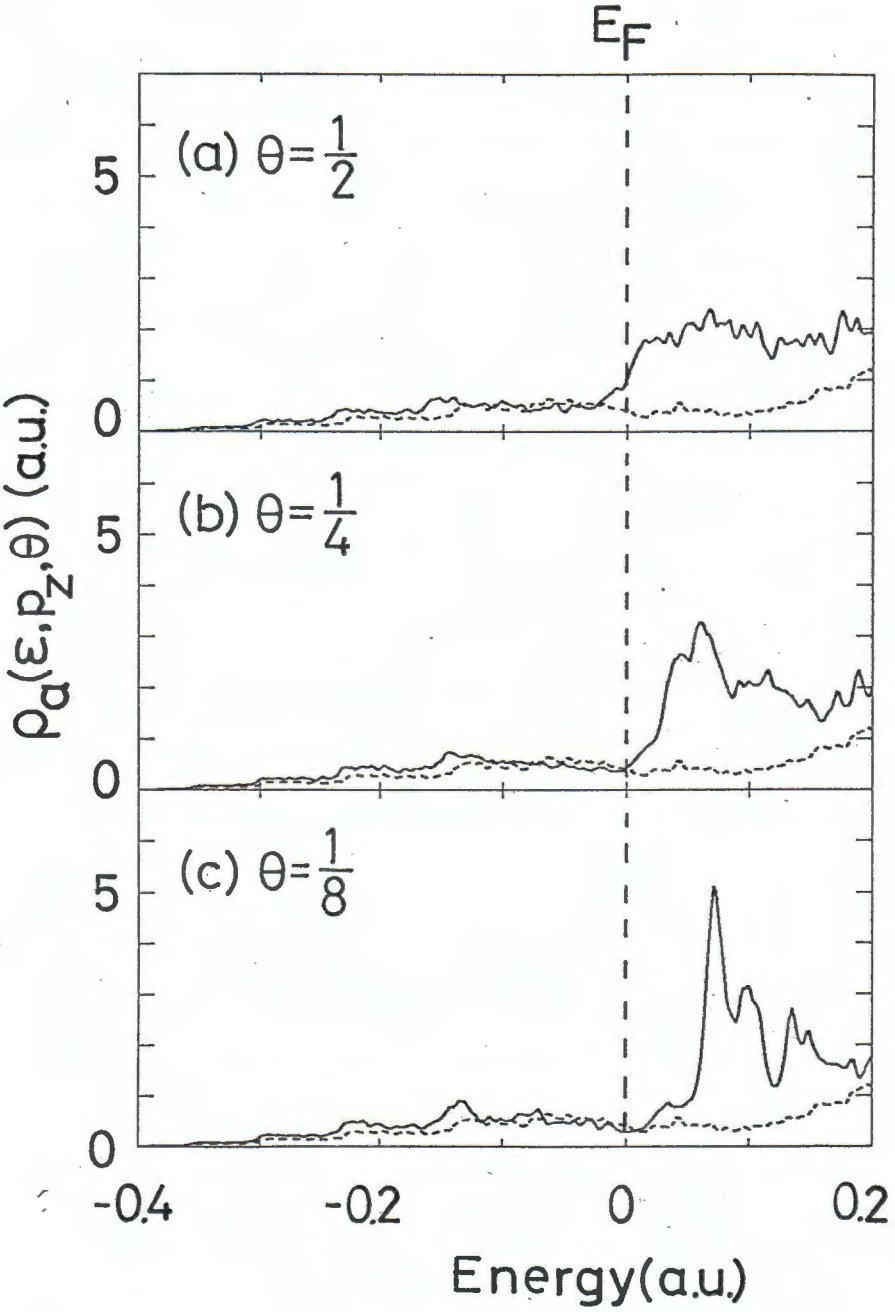
E_F
(a) $\theta=\frac{1}{2}$
(b) $\theta=\frac{1}{4}$
(c) $\theta=\frac{1}{8}$
5
0
5
0
5
0
$\rho_a(\varepsilon,p_z,\theta)$ (a.u.)
-0.4
-0.2
0
0.2
Energy(a.u.)

Fig. 28

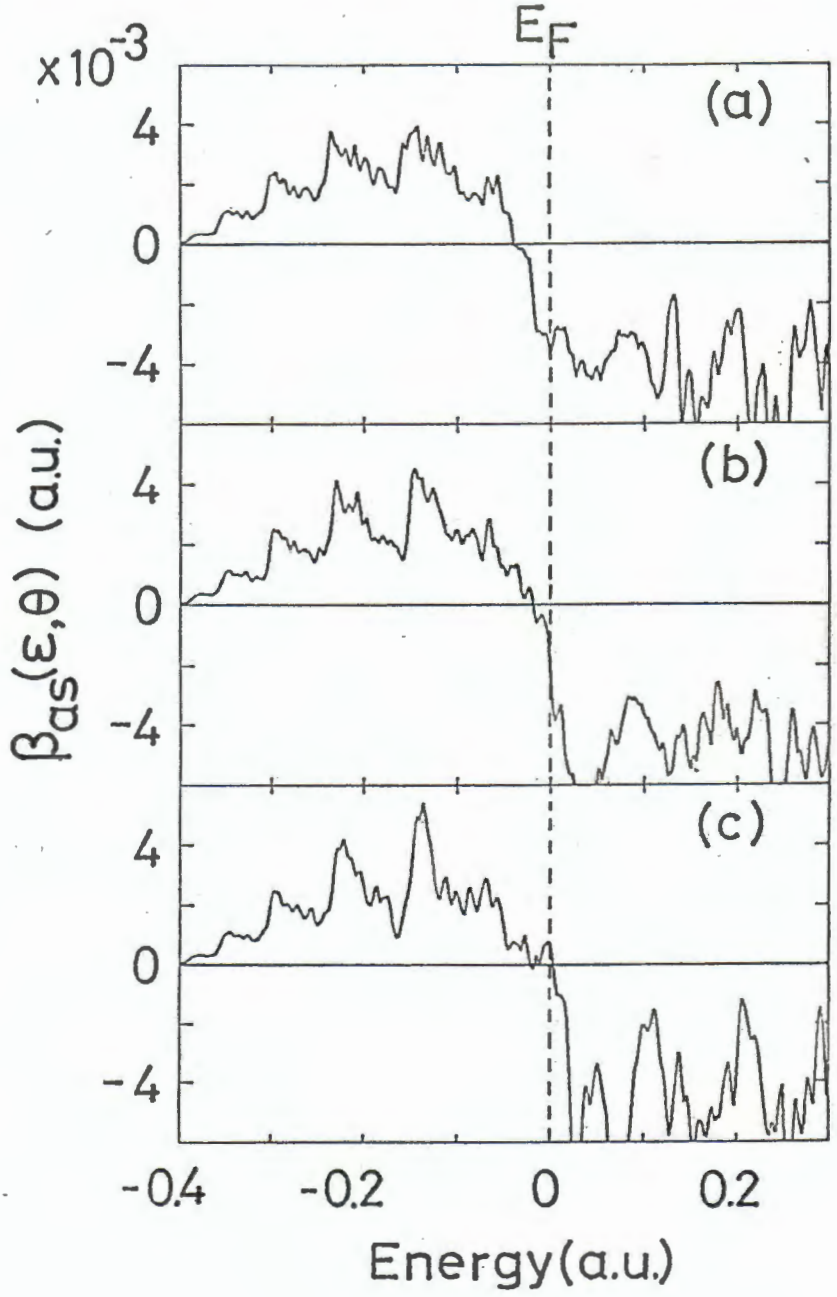

Fig. 29

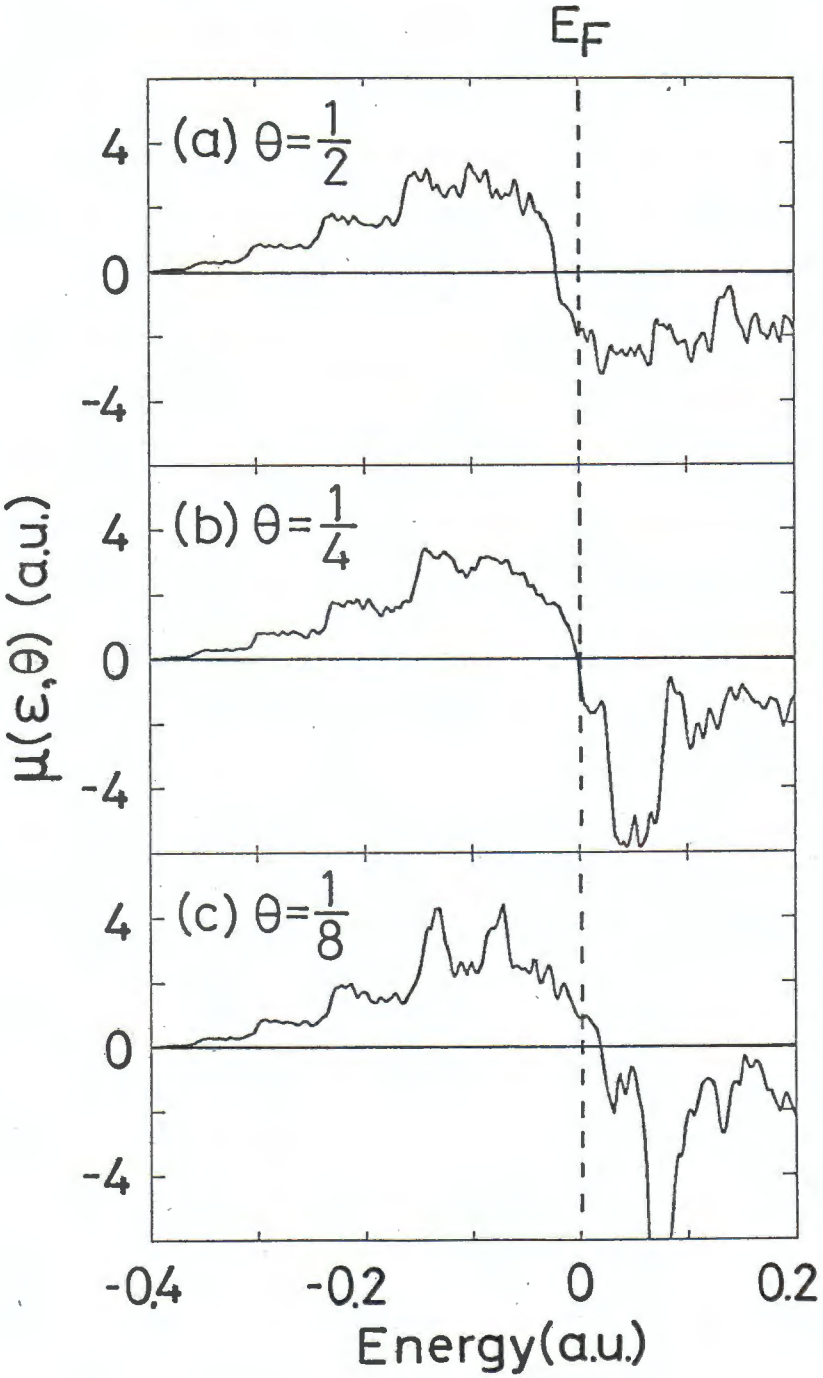
E_F
(a) $\theta=\frac{1}{2}$
(b) $\theta=\frac{1}{4}$
(c) $\theta=\frac{1}{8}$
4
0
-4
$\mu(\varepsilon,\theta)$ (a.u.)
-0.4
-0.2
0
0.2
Energy(a.u.)